IMMUNOMODULATORY BIOMATERIALS FOR SKELETAL MUSCLE REPAIR

A Dissertation
Presented to
The Academic Faculty

By

Cheryl Lau San Emeterio

In Partial Fulfillment
of the Requirements for the Degree
Doctor of Philosophy in the
Wallace H. Coulter Department of Biomedical Engineering

Georgia Institute of Technology and Emory University

May 2018

IMMUNOMODULATORY BIOMATERIALS FOR SKELETAL MUSCLE REPAIR

Approved by:

Dr. Edward A. Botchwey, Advisor
Wallace H. Coulter Department of Biomedical Engineering
Georgia Institute of Technology

Dr. Gabe A. Kwong
Wallace H. Coulter Department of Biomedical Engineering
Georgia Institute of Technology

Dr. Andrés J. García
Woodruff School of Mechanical Engineering
Georgia Institute of Technology

Dr. Gordon L. Warren
Department of Physical Therapy
Georgia State University

Dr. Young C. Jang
School of Biological Sciences
Georgia Institute of Technology

Date Approved: December 1, 2017

ACKNOWLEDGEMENTS

I would like to thank my thesis advisor, Dr. Edward A. Botchwey, for giving me the intellectual guidance, creative freedom, and resources that enabled me to pursue this research. Ed has always challenged me to move past my tunnel vision and expand my creativity and though at times it has been uncomfortable, I know that I am a better scientist and engineer for it. I admire Ed for constantly thinking about different ways to interpret and present scientific findings and to never undervalue or discount an experiment. Because of Ed's mentorship, I have an improved view of the "big picture" goal, what to prioritize to get to that point, and to not get caught up in the minutiae. I am so grateful that Ed has always believed in me, in the road from taking this muscle project from just an idea, to where it is now. In turn, I believe in my ability to take any problem, think it over carefully, and come up with creative solutions that will elevate the research to the next level.

I would like to thank each of my committee members who have given insight, support and time over the course of my degree. I have admired Dr. Garcia's candor since being his student in Advanced Biomaterials my first year of graduate school and am thankful to have had his experienced eye on my research as part of my committee. I remember attending Dr. Jang's faculty candidate seminar before he formally came to Georgia Tech and am so lucky that I have had the opportunity to collaborate with him and his lab. He has been beyond generous with providing time, advice, and resources. I want to thank Dr. Kwong for his evaluation of my work and for fostering a collaboration between our labs focusing on the photothermal control of macrophages. Finally, I want to thank Dr. Warren, who walked over from Georgia State University countless times to meet with me

and help me with experiments. I am humbled that all my committee members gave their valuable time and expertise in helping me progress as a researcher.

I've always thought of my labmates as my second family. We have spent 5 years together, through the thick and thin, and I can't imagine getting to where I am now without them. Dr. Molly Ogle has been an outstanding mentor to me. She taught me how to do western blots my first year of graduate school and since then has continued to show me techniques, critique my writing, suggest clever phrasing for presentations, and everything in between. I look up to her as both a professional and personal role model and am so thankful for everything she has taught me. Secondly, I want to thank Dr. Claire Olingy for being the best friend both in lab and in life these past 5 years. She is thoughtful, considerate, and always speaks from her heart and I will forever treasure the friendship we built from seeing each other every day, from lunches and gchats, from planning our weddings together, and exciting trips to Europe and Charleston. I also want to thank Dr. Jack Krieger and Caitlin Sok for rounding out the unofficial innate immunity arm of our laboratory. It has been so rewarding to be able to discuss experimental ideas and details with them. Thank you to Nathan Chiappa for teaching me Mass Spectrometry techniques, helping me run samples and for always having a positive attitude. Thank you to the newest member of our lab, Thomas Turner, who is taking over this muscle work – I have every confidence that he will be extremely successful. Thank you to Dr. Hannah Song, Dr. Tony Awojoodu, Tiffany Wang, and Jada Selma for being great labmates.

In addition to having a great lab, my friends outside of lab (plus Claire!) have been the greatest support system I could have ever hoped for. I remember first meeting Betsy Campbell during orientation and immediately gravitating towards her and hoping she

would like me, and that we would become friends. We have come a long way from that first encounter – from pool days, happy hours, fitness classes, girls' trips, tough times, and being the maid of honor at my wedding, Betsy has always made her best effort to be an amazing friend and make me feel loved and special. Dr. Candice Hovell and I bonded over our love for Harry Potter, and cats (mostly cats). I will always appreciate her sense of humor and resilient spirit. I invited Giuli Salazar-Noratto out with us when she first got to Georgia Tech and since then she's always been good for getting us girls together and providing sympathy and support.

I would like to thank the many Georgia Tech support staff, both technical and administrative, who have helped me out over the course of my PhD. In particular, I want to thank Andrew Shaw for his unending patience and expertise in microscopy. I would not have been able to accomplish this work without him. I also want to thank Nadia Boguslavsky for her expertise in running the flow cytometry core, and for her constant flexibility and patience. The staff in the IBB PRL have been so helpful in making sure we are well equipped to perform animal studies. I want to thank Dr. Richard Noel, and Dr. Laura O'Farrell, for their veterinary experience and Kim Benjamin for ensuring the PRL runs smoothly. I want to thank the other PRL staff, particularly Andrea Gibson, Altair Rivas, Josh Scarbrough, and Ogeda Blue, whom I have gotten to know over the course of the past several years. Their constant cheerfulness has made my countless trips to the PRL more enjoyable.

I want to thank our graduate coordinator, Shannon Sullivan, who carries the emotional weight of our program on her shoulders. I have shown up many times at her door in distress and without fail, she has always welcomed me in, listened patiently to my

worries, and given me great advice. I want to thank Sally Gerrish for providing excellent career advice, for connecting me to alumni in my new geographical location, and for being a great advocate for professional development.

With all my heart, I want to thank my family. My mom and dad came over to the United States from Hong Kong with no one but each other in the hopes of building a great life for themselves and eventually, for my brother and I. My dad was pursuing his PhD when I was growing up, and my mom held the reins of raising us. Because of them, I understand the value of higher education, of working hard, and dedicating your life to your family. I well up with pride every time I think of how much my mom and dad have accomplished, and how much they have built from nothing. My brother Eric is the true embodiment of my mom and dad's American dream – he graduated with top honors from MIT and is now pursuing a Masters degree at Stanford, and I am prouder of him that I can say. There is so much that I cannot put into words but I am thankful to my core that they are my family and have always been there for me my whole life.

Finally, I want to especially thank my husband, Juan, for his unending encouragement and support. We met my first year of graduate school and got married in 2016. He is my favorite person in the whole world and understands me better than anyone else. He has taught me to always be confident in what I am worth. Every day, I remember how lucky I am to have found Juan and I will forever treasure our love and commitment to each other. Our little family has grown over the course of the past few years to include 3 cats, Henry, Lily, and Charlie, who are our pride and joy. They are the most beautiful and loyal cats on earth and have carried us through many a tough time. I am so blessed to have them in my life and I cannot wait to continue life's adventures together with them.

TABLE OF CONTENTS

LIST OF TABLES

LIST OF FIGURES

LIST OF SYMBOLS AND ABBREVIATIONS

ANOVA	Analysis of variance
Ach	Acetylcholine
ADP	Adenosine di-phosphate
ATP	Adenosine tri-phosphate
$CaCl_2$	Calcium Chloride
CCL	CC-chemokine ligand
CCR	CC-chemokine receptor
CP	Creatine Phosphate
CD	Cluster of differentiation
CO_2	Carbon dioxide
CXCL	C-X-C ligand
CXCR4	C-X-C chemokine receptor 4
CX3CR1	C-X3-C chemokine receptor 1
$CX3CR1^{GFP/+}$	B6.129P-Cx3cr1tm1Litt/J mice
DAMP	Damage Associated Molecular Patterns
DMEM	Dulbecco's Modified Eagle Media
DMD	Duchenne Muscular Dystrophy
DWC	Dorsal skinfold window chamber
ECM	Extracellular matrix
EGTA	ethylene glycol-bis(β-aminoethyl ether)-N,N,N',N'-tetraacetic acid
FACS	Fluorescence Activated Cell Sorting

FBS	Fetal bovine serum
FGF	Fibroblast growth factor
GFP	Green fluorescent protein
IACUC	Institutional Animal Care and Use Committee
IGF	Insulin-like growth factor
IHC	Immunohistochemistry
IL	Interleukin
iNOS	Inducible nitric oxide synthase
IFN	interferon
i.p.	Intraperitoneally
KOH	Potassium Hydroxide
LPS	Lipopolysaccharide
MCP-1	Monocyte chemoattractant protein-1
MerTK	Mer receptor tyrosine kinase
MHCII	Major histocompatibility complex II
$MgCl_2$	Magnesium Chloride
mg/kg	Milogram per kilogram
MMP	Matrix metalloproteinase
M1	Classically activated inflammatory macrophage
M2	Alternatively activated macrophages
NIH	National Institutes of Health
PBS	Phosphate buffered saline
PLGA	Poly(lactic-co-glycolic acid)
PDGF	Platelet-derived growth factor
SSC	Side scatter

SDF-1	Stromal cell-derived factor-1
S.E.M.	Standard error of the mean
S1P	Sphingosine-1-phosphate
S1PR	Sphingosine-1-phosphate receptor
TGF-ß	Transforming growth factor-beta
TLR7	Toll-like receptor 7
TNF- α	Tumor necrosis factor-alpha
VEGF	Vascular endothelial growth factor
VML	Volumetric Muscle Loss
WT	Wildtype
3D	Three-dimensional
2D	Two-dimensional

SUMMARY

Severe skeletal muscle trauma resulting from ischemic damage, nerve transection injuries, or volumetric defects is an intractable problem. Dysfunction and disability owing to the latter are an increasingly significant clinical burden. Though skeletal muscle possesses robust potential for healing after injury, large volumetric wounds that occur during combat, accidents or surgical resection often do not heal completely, resulting in fibrotic scarring and limited range of motion. Current standard of care involves the autologous transfer of tissue but exhibits limited success and complications at both the donor and injury site. Moreover, extensive soft tissue injury and damage to collateral blood vessels prevents adequate vascularization and can result in muscle fibrosis and chronic muscle strength deficits. Even minor damage and or overuse of supporting connective tissues such as the rotator cuff tendon, and associated mechanical unloading, results in disorganized muscle fiber remodeling, gradual fatty/fibrous degeneration and muscle mass loss. And, as the sequelae of muscle injuries increases at a disproportionate rate with advancing age, the burden of muscle injury on an aging domestic population is increasingly severe.

Microenvironmental cues within injured skeletal muscle dictate either regenerative or fibrotic healing outcomes. These cues include signals from blood vessels, extracellular matrix (ECM), immune cells, and motor neuron associations. Tightly coordinated interplay between these cues govern the endogenous muscle stem (satellite) cell niche and are critical determinants of muscle repair success. Most notably during muscle injury recovery, monocytes and macrophages release mitogenic growth factors that protect muscle

progenitor cells from apoptosis, stimulate myogenic processes, and enhance revascularization. However, monocytes and macrophages are markedly heterogeneous *in vivo,* displaying both inflammatory and anti-inflammatory phenotypes, which enable a wide range of functions in varied tissue-specific contexts. Thus, identifying key monocyte subsets and their differentiated functions within the injury niche is critical to harnessing function of these cells in directing repair. To address this challenge, we developed novel biomaterial drug-delivery systems that leverage the pro-regenerative functions of recruited blood monocytes to enhance muscle healing outcomes.

Using cell tracking techniques, we identified anti-inflammatory, non-classical monocytes as biased progenitors of CD206+ alternatively-activated macrophages in injured skin. We demonstrated that we could achieve local enrichment of non-classical, monocytes within sites of volumetric muscle loss via the local delivery of FTY720 from a bulk polymer thin film. Redirection of these non-classical monocytes from circulation into injured muscle occurred concomitantly with increased accumulation of alternatively-activated macrophages, coinciding with enhanced vascularization, collagen matrix deposition, and muscle regeneration. We then further explored how incorporating FTY720 into an electrospun polymer fiber mesh would impact parenchymal and immune cell behavior in a larger volumetric defect. We found that FTY720 delivery from a nanoscale fiber scaffold (FTY720-NF) resulted in acute lymphopenia and decreased lymphocytes in the muscle tissue. Interestingly, FTY720-NF treated animals exhibited increased live cellularity in peri-defect tissue, which were attributed to increases in both muscle stem cell (satellite cell), non-classical monocyte, and alternatively-activated macrophage numbers. Regenerated muscle fibers exposed to FTY720 cues displayed higher diameter and notably,

increased alignment to the pre-injury fiber axis. These findings represent an improved understand of the role that pro-regenerative subsets of immune cells play in promoting endogenous mechanisms of tissue repair after traumatic muscle injuries.

1. INTRODUCTION AND SPECIFIC AIMS

Repair of injured skeletal muscle requires the coordinated activities of innate and adaptive immune cells that orchestrate the progression of inflammation and guide healing outcome. Circulating monocytes exist in at least two subsets in blood: classical monocytes, which are broadly considered as inflammatory cells, mature within peripheral blood under homeostasis to non-classical, anti-inflammatory monocytes. During inflammation, monocytes are rapidly mobilized from blood to enter the injured tissue space where they may persist as monocytes or differentiate into macrophages. Macrophages within tissue injury also display marked heterogeneity, but may be broadly classified as classically-activated (M1) or alternatively-activated (M2). Monocytes and macrophages of both subtypes have been shown to accumulate in toxin-induced muscle injury, but the roles these cells play in a volumetric injury context in which all tissue microcompartments must be regenerated *de novo* remains unknown. The *overall objective* of this work is to improve understanding of the roles that immune cells subsets play in the regeneration of volumetric muscle defect injuries and to engineer biomaterial therapies that tune their recruitment and function. This objective will be explored via the following three specific aims:

Aim 1: To investigate the contributions of classical and non-classical monocyte populations to the alternatively activated macrophage pool within traumatic soft tissue injury.

We *hypothesized* that anti-inflammatory, non-classical monocytes recruited from circulation during traumatic soft tissue injury preferentially give rise to alternatively activated macrophages. To test this hypothesis, we tracked the fate of blood-derived

monocyte subsets within excisional skin injury via latex bead-based labeling techniques and adoptive transfer of sorted monocyte subpopulations. Loss of function studies in which non-classical monocytes were depleted by clodronate liposomes, and gain of function studies in which the small molecule FTY720 was used to selectively recruit non-classical monocytes, were used to confirm findings from fate tracking experiments.

Aim 2: To characterize immune cell kinetics in the murine spinotrapezius volumetric muscle loss model and investigate effects of modulating myeloid cell recruitment on skeletal muscle healing

A novel model of full-thickness, volumetric muscle injury was established in the murine spinotrapezius to enable visual inspection of healing progression. Immune cell accumulation kinetics were assessed via flow cytometry and whole-mount immunofluorescence. We *hypothesized* that locally enriching non-classical monocytes would enhance the accumulation of alternatively-activated macrophages and promote muscle defect healing. We employed FTY720 delivery from polymer thin films as a tool to redirect non-classical monocytes from peripheral blood into injured skeletal tissue. Muscle healing parameters were assessed via whole-mount immunofluorescence imaging of injured spinotrapezius muscles with or without FTY720 treatment.

Aim 3: To assess the impact of local delivery of FTY720 via electrospun microfibers to volumetric skeletal muscle injury on innate and adaptive immune cell accumulation and regeneration in a non-healing volumetric defect.

We expanded the spinotrapezius volumetric muscle loss model to encompass a defect size that does not regain full functional recovery over the experimental time course.

We *hypothesized* that nanofiber based delivery of FTY720 to a non-healing muscle defect would positively impact muscle healing metrics such as fiber diameter and alignment. Flow cytometry was used to examine changes in lymphoid, myeloid, and muscle stem cell (satellite cell) accumulation in response to FTY720 nanofiber treatment. Muscle healing parameters were again assessed via whole-mount immunofluorescence imaging of injured spinotrapezius muscles.

Significance:

The current gold-standard of therapy for volumetric muscle loss involves the autologous transfer tissue which exhibits limited success and donor site morbidity. Strategies for treating volumetric muscle injuries will require the capability of initiating and promoting endogenous repair programs. Alternatively-activated, wound-healing macrophages drive differentiation of satellite cells in injured muscle and likely promote repair of other damaged microcompartments such as vasculature and motor neurons. The work presented represent the first studies to show that Ly6C^{lo} non-classical monocytes are key contributors to the pool of wound healing macrophages. We have demonstrated that locally enriching pro-regenerative monocytes and macrophages within volumetric muscle injury via biomaterial-based delivery of FTY720 results in favorable healing outcomes such as increased vascularization, attenuation of fibrotic tissue deposition, and improved alignment of regenerated muscle fibers. Taken together, we have gained an improved understand of the role that pro-regenerative subsets of immune cells play in the promotion of endogenous mechanisms of tissue repair after traumatic injuries.

2. THE INFLAMMATORY CASCADE WITHIN SKELETAL MUSCLE HEALING: INFORMING THE DESIGN OF IMMUNOMODULATORY BIOMATERIAL THERAPEUTICS[1]

2.1 Skeletal Muscle at Homeostasis and Injury

2.1.1 Skeletal Muscle Function and Physiology

Skeletal muscle is a hierarchically organized tissue comprising around 40% of total body weight [1]. The main function of skeletal muscle is to generate force to maintain posture and facilitate body movement. There are three main types of muscle action: isometric, dynamic concentric, and dynamic eccentric. Isometric action within a muscle generates force but is not accompanied by movement (such as holding a plank). Conversely, both dynamic actions involve force generation and joint movement, with dynamic concentric actions involving the shortening of the muscle, and dynamic eccentric motions resulting in the lengthening of a muscle from its original position.

In addition to motion production, there are other, less obvious, roles that muscle tissue plays as well. Skeletal muscle serves as storage for important biomolecules such as amino acids and carbohydrates that may be needed by other vitally important tissues such as the skin, brain, or heart when nutrient supply is insufficient[2]. The release of amino acids from muscle stores also aids in maintaining blood glucose levels during insufficient

[1] Portions of this chapter adapted from: Olingy CE, San Emeterio CL, Ogle ME, Krieger JR, Bruce AC, Pfau DD, et al. Non-classical monocytes are biased progenitors of wound healing macrophages during soft tissue injury. Sci Rep. 2017;7:447. Published under Creative Commons license.

nutrient intake. Skeletal muscle also contributes to basal energy metabolism and the production of heat for homeothermic thermoregulation [1]. Consequently, reduced muscle mass hinders the body's response to stress and chronic illness.

Muscle fibers, or myofibers, constitute the basic cellular building block of skeletal muscle and are multinucleated, post-mitotic cells that are arranged in bundles to form whole muscles. Each muscle fiber is composed of thousands of myofibrils and billions of myofilaments – the main myofilaments being the thick filament composed of myosin and the thin filament composed of actin, troponin, and tropomyosin[1]. Myofilaments are assembled in a characteristic, striated pattern to form sarcomeres, in which the thick and thin filaments slide past each other in response to calcium release from the sarcoplasmic reticulum. Upon neural stimulus from the motor neuron, the sarcoplasmic reticulum releases calcium ions that bind to troponin on the thin filament. This binding displaces tropomyosin to reveal myosin binding sites on the actin molecules within the thin filament. In the presence of adenosine tri-phosphate (ATP), the myosin within the thick filaments is able to then bind to actin, and hydrolysis of ATP to adenosine di-phosphate (ADP) causes the myosin to actively pull the actin towards the middle of the sarcomere (M line), thus shortening the sarcomere (known as the "sliding filament theory")[1]. The simultaneous shortening of many sarcomeres within a muscle fiber is what causes the muscle fibers to contract, and multiple muscle fibers contracting together enables a muscle to produce force and movement.

Muscle movement requires energy in the form of ATP. There are three energy pathways that are utilized within the muscle fiber: reserve stores of ATP and creatine phosphate (CP), anaerobic glycolysis, and oxidative phosphorylation. The muscle usage of

a specific metabolic energy pathway to use is based on the duration and intensity requirements of the activity at hand. Due to the highly limited reserves of ATP and CP in the muscle, this mechanism supports high intensity muscle activities for short durations of a few seconds[1]. The second mechanism, anaerobic glycolysis, produces ATP very rapidly (about 100 times faster than oxidative phosphorylation) and is utilized for muscle activity lasting a few minutes. However, anaerobic glycolysis quickly becomes detrimental to muscle function due to the production and buildup of the end-product, lactate, which causes muscle fatigue[1]. Lastly, oxidative phosphorylation, which occurs in the muscle mitochrondria, sustains muscle activity for minutes to hours. The dense network of capillaries within muscle (Figure 1) supplies oxygen to the muscle fibers to power the oxidative phosphorylation pathway, and interestingly, the extent of the capillary network is correlated with the metabolic demand of the muscle fiber to which it is coupled[1]. During a session of muscle activity, all three of these pathways may be activated at certain points depending on the intensity of the exercise

Somewhat counterintuitively, the main fuels utilized by the muscle to produce ATP are carbohydrates (glucose from plasma and glycogen from muscle stores) and fats (free fatty acids from plasma and triglycerides from muscle.)[1] During intense muscle activity, muscle glycogen is the preferred fuel substrate whereas lower intensity (and longer duration) of exercise favors free fatty acid metabolism for energy [1]. As with utilizing the metabolic pathways however, the muscle will select and combine which fuels to use for ATP production depending on the type of muscle activity being performed.

Human skeletal muscle exhibits heterogeneity in the individual muscle fibers that comprise a single muscle. There are two main categories of muscle fibers: type I, which

are slower to shorten during a single twitch (a contraction in a single muscle fiber) and are also known as “slow twitch” fibers, and type II, which shorten fast during a single twitch and are known as “fast twitch” fibers. Type I and type II fibers possess their twitch speed based on two key characteristics: the type of myosin protein that is present, and the degree of dependence of the fiber on oxidative phosphorylation[1]. Myosin heavy chain I is present in type I, slow twitch fibers, whereas myosin heavy chain II is present in in type II, fast-twitch fibers [3]. Slow twitch fibers rely heavily on oxidative phosphorylation (which is slower to generate ATP compared to other metabolism mechanisms) and consequently, have more mitochondria per fiber than fast-twitch fibers. Slow-twitch fibers are slower to fatigue, however, and thus are more highly represented in muscles that maintain body posture, whereas fast twitch fibers are more highly represented in muscles that produce movement[4].

2.1.2 Satellite Cells

Satellite cells are adult muscle stem cells that reside on the outside of muscle fibers, located in between the sarcolemma and the basal lamina. While quiescent during tissue homeostasis, satellite cells rapidly activate, proliferate, and differentiate into mature muscle cells in response to injury stimuli[5]. These newly formed muscle cells can fuse with existing damaged muscle fibers to repair traumatically injured tissue. Activated satellite cells can also give rise to new satellite cells that repopulate and maintain the quiescent satellite cell compartment[5]. Quiescent and activated satellite cells can be distinguished via differential expression of canonical transcription factors. Quiescent satellite cells express the transcription factor PAX7 but not the transcription factor myoblast determination protein 1 (MyoD), whereas activated satellite cells express both

PAX7 and MyoD[5]. Activated satellite cells that proliferate and commit to differentiating into myotubes then express the transcription factor myogenin. Detection of quiescent satellite cells histologically has been technically challenging, but recent advances in making transgenic mice with a fluorescent reporter under the PAX7 promoter has made tracking the behavior of both endogenous and transplanted satellite cells more feasible. Satellite cells can also be detected and isolated by Fluorescence-Activated Cell Sorting (FACS) techniques using defined surface marker profiles[6]. A common scheme for identifying satellite cells via FACS involves the exclusion of hematopoietic and stromal cells by negative selective of lineage markers (lin-), Sca1, and CD31, then positive selection of satellite cells via dual expression of CXCR4 and beta-1 integrin (CD29) [7].

2.1.3 Skeletal Muscle during Injury, Pathology, and Aging

Healthy skeletal muscle is able to regenerate very quickly after injury, and the healing process follows a specific sequence of events that ultimately result in restoration of tissue function. This sequence of events can be divided into roughly three phases. The first phase is the destruction and inflammatory phase in which damaged muscle fibers undergo necrosis and release damage-associate molecular patterns (DAMPs) that trigger an inflammatory response and the arrival of immune cells such as neutrophils, and inflammatory monocytes, and macrophages[8]. The second phase is the repair phase, in which the muscle fiber detritus is cleared by immune cells, and satellite cells activate, proliferate and fuse to form new muscle fibers. During the repair phase, a provisional extracellular matrix scar is formed as a scaffold for infiltrating immune and parenchymal cells[9]. The third phase is the remodeling phase in which newly regenerated muscle fibers are reorganized and the provisional scar tissue is remodeled, thus restoring tissue function.

Failure to progress through this healing sequence results in fibrosis and decrease in muscle function[9].

There are many types of myopathies that stem from varied causes such as gene mutations, microscopic structural defects, metabolic/mitochondrial dysfunction, and autoimmunity[10]. Muscular dystrophy is a form of myopathy that is characterized by chronic cycles of muscle fiber degeneration and regeneration, fatty tissue infiltration and fibrosis, ultimately resulting in severe muscle weakness, with most patients being unable to walk by the age of 12. Duchenne Muscular Dystrophy (DMD) is the most common form of muscular dystrophy that is caused by a mutation in the dystrophin gene that leads to impaired function within both mature muscle fibers and satellite cells[11]. Lack of dystrophin within muscle fibers renders them incapable of attaching to the extracellular matrix, and leads to cyclic cycles of muscle degeneration, inflammatory response, and regeneration over the patient's lifetime. Satellite cells in dystrophic mice exhibit an inability to establish cellular polarity, resulting in failure to undergo asymmetric cell division and initiation of myogenic programs. Thus, DMD is both a disease of the muscle fibers themselves and also a disease of the stem cells that are responsible for regenerating muscle[11].

The loss of skeletal muscle mass and strength with advanced age is called sarcopenia, and is associated with a reduction in the number of satellite cells within the muscle compartment. Interestingly, there is a particular decrease in the number of satellite cells that are associated with type II, fast-twitch fibers which are the predominant type of fiber lost with advanced age[1]. Thus with any injury, the capacity to regenerate decreases with age, due in part to lower numbers of satellite cells. Changes within the muscle fiber

itself also contribute to the decrease in muscle function, such as alterations in the sarcoplasmic reticulum structure that isolate calcium stores to only certain areas of muscle, and diminished numbers of mitochondria per myofiber. The quality of the muscle fiber also decreases, with single fiber demonstrating reduced maximal force with age. This phenomenon has been attributed to a range of mechanism. For example, disruptions in myostatin gene transcription, or reductions in its translation to protein can account for diminished myosin content seen in aging. Additionally, post-translational modifications to myosin such as oxidation of the protein may interfere in the binding of actin to its binding site on myosin, resulting in lower cross-bridges and limiting force production[1].

2.2 Contributions of Immune Cells within Skeletal Muscle Injury and Repair

2.2.1 Systemic and Local Monocyte/Macrophage functions at homeostasis

The mononuclear phagocyte system plays a multi-faceted role in maintaining tissue homeostasis and responding to both acute injuries and pathological processes including autoimmune diseases, cancer, and aberrant wound healing. Monocytes circulate in the bloodstream during steady state and have been shown to patrol for endothelium integrity [12] as well as extravasate into resting tissues and travel to lymph nodes where they may present antigen[13]. The ontogeny of macrophages varies in different tissues, such that some tissue resident macrophages are seeded embryonically, such as microglia in the brain, and self-renew in a similar manner to stem cells. However, macrophages that reside in tissues such as the dermis or the gut are continuously exposed to outside microorganisms and may be subject to low-grade chronic inflammation that induces blood monocyte recruitment and subsequent differentiation to replenish resident macrophages [14-18].

Tissue-resident macrophages can perform a wide variety of functions at homeostasis that are tailored to the specific tissue in which they reside. For example, adipose-associated macrophages are involved in the control of insulin sensitivity and energy homestasis, alveolar macrophages clear surfactant in the lungs, and bone marrow macrophages support erythropoiesis and maintain hematopoietic stem cells within their niche[19]. When challenged with inflammatory insult, tissue macrophages can activate and release signals that drive robust recruitment of neutrophils and monocytes from blood to initiate the healing cascade[19].

2.2.2 Monocyte Heterogeneity

Two distinct subpopulations of monocytes have been identified in mouse and human blood, which can be distinguished by well-characterized surface protein expression profiles. Classical inflammatory monocytes are identified by $Ly6C^{hi}CX3CR1^{lo}CD43^{lo}$ expression in mice ($CD14^{hi}CD16^{-}$ in human), whereas non-classical alternative monocytes are $Ly6C^{lo}CX3CR1^{hi}CD43^{hi}$ in mice ($CD14^{+}CD16^{+}$ in human)[14]. A third population of intermediate monocytes characterized by intermediate expression of Ly6C in mice ($CD14^{hi}CD16^{+}$ in humans) are thought to complement the functions of non-classical monocytes and may preferentially differentiate into dendritic cells within inflamed tissues[20, 21]. Under homeostasis, classical $Ly6C^{hi}$ monocytes that are housed in the bone marrow are released diurnally into peripheral blood circulation under control of the circadian gene *Bmal1*[17]. Once in blood, the $Ly6C^{hi}$ monocyte population possess a relatively short half-life of 20 hours[17], whereupon they decrease Ly6C expression and become non-classical $Ly6C^{lo}$ monocytes[17, 22], which patrol the luminal side of resting endothelium[12]. If damaged endothelium is encountered, $Ly6C^{lo}$ monocytes may respond

to these danger signals via Toll-like receptor 7 (TLR7) and recruit neutrophils that elicit focal necrosis of the compromised endothelium. Ly6C^{lo} monocytes subsequently clear the cellular debris. In contrast, the role of classical monocytes at homeostasis is less well-studied, though it has been shown that classical monocytes also survey steady-state tissues and can traffic to lymph nodes to present antigen without differentiating into macrophages[13]. In response to injury stimuli, monocytes extravasate from the circulation into damaged tissues where they may persist as monocytes or differentiate into macrophages.

2.2.3 Macrophage Origin and Heterogeneity

Macrophages are highly responsive to cues within the injury niche, enabling them to dynamically modify their behavior in response to changes in the microenvironment and display extremely varied phenotypes. Classically activated ("M1") macrophages are primary players in pathogen destruction, secretion of inflammatory cytokines, and driving Th1-type responses[23]. Conversely, alternatively activated wound healing ("M2") macrophages (of which a number of subtypes have been described[23], where M2a subtypes induced by IL-4 stimulation may be pro-fibrotic, and M2c subtypes induced by IL-10 stimulation promote the proliferation of satellite cells[24]) are associated with pro-regenerative activities such as angiogenesis[25, 26], extracellular matrix remodeling[27], secretion of anti-inflammatory cytokines[23], and resolution of inflammation[28] (Figure 1.)

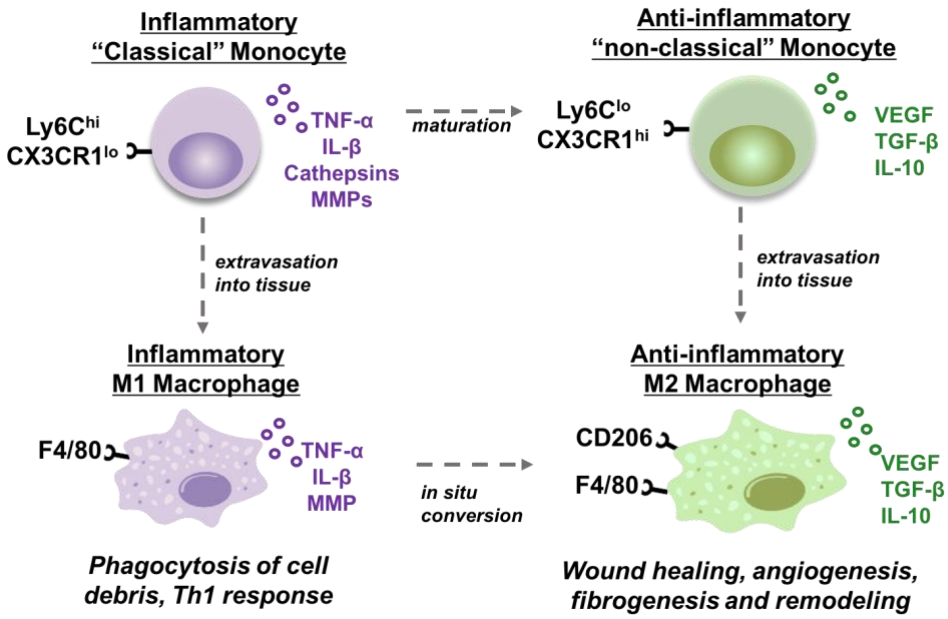

Figure 1. Monocyte and macrophage heterogeneity. Monocytes exist in two principal subsets in circulation and can be identified by defined surface marker profiles such as Ly6C and CX3CR1. Circulating classical monocytes secrete inflammatory factors, and patrol steady state tissue. Classical monocytes mature in the blood to become non-classical monocytes which secrete pro-regenerative factors and survey resting endothelium. Under injury conditions, these monocytes extravasate into tissue where they differentiate into macrophages. Wound macrophages display a wide range of phenotype broadly classified as either inflammatory or M1, or anti-inflammatory, M2. M1 macrophages can arise from classical monocyte differentiation, but M2 wound macrophages may arise from either in situ conversion of M1 macrophage to M2, or from direct differentiation of non-classical monocytes.

The highly complex and heterogeneous nature of inflamed tissue microenvironments has rendered a general description of macrophage origin and function challenging. Within toxin-induced muscle injury[29], liver fibrosis[30], infection[31], and autoimmune disease[32], classical Ly6C^{hi} monocytes are recruited from circulation and undergo *in situ* differentiation to be the primary contributors of injury Ly6C^{lo} monocytes/macrophages. In contrast, sequential recruitment of classical Ly6C^{hi} followed by non-classical Ly6C^{lo} monocyte subsets after myocardial infarction[33], and direct recruitment of adoptively transferred Ly6C^{lo} monocytes within excisional skin injury[34]

and during the development of inflammatory arthritis[35] have been reported. Recently, we demonstrated that circulation-derived Ly6C^{lo} monocytes that are directly recruited to injured skin are biased progenitors of CD206+ wound-healing macrophages[36]. Using latex bead labeling, we labeled Ly6C^{hi} and Ly6C^{lo} monocytes in the circulation and tracked their accumulation within the dorsal skinfold window chamber model of partial-thickness excisional skin injury. We observed that a significantly higher proportion of labeled Ly6C^{lo} monocytes within injured skin were immunophenotyped as CD206+F4/80+ alternatively-activated macrophages, whereas labeled Ly6C^{hi} monocytes did not display this differentiation bias. Adoptive transfer of Ly6C^{hi} or Ly6C^{lo} monocytes from CD45.1 mice into CD45.2 mice revealed that though the number of adoptively transferred cells per milligram of tissue did not vary between the two donor cell types, there was a higher frequency of CD206+CD301b+ wound healing macrophages derived from Ly6C^{lo} monocytes compared to Ly6C^{hi} monocytes.

2.2.4 Monocytes and Macrophages are required for Skeletal Muscle Repair

Macrophages govern nearly all stages of tissue repair and are required for effective healing, which has been demonstrated by depletion studies in a wide array of injured tissues such as skeletal muscle[29, 37], skin[38], myocardium[39], and cornea[40]. Depletion of macrophages in these studies by clodronate liposomes or diphtheria toxin administration to LysM-Cre/DTR mice restricted injured tissues to the acute and mid-phases of tissue healing, with failure to progress into the healing and resolution stages.

Monocyte/macrophage depletion studies within skeletal muscle injury models have highlighted the crucial role that these cells play at the onset of injury, with depletion

of all circulating monocytes before toxin-induced muscle injury resulting in incomplete healing and fibrotic muscle. Intramuscular depletion of macrophages in the later stages of healing severely impairs muscle regeneration indicating that macrophages present within the muscle are actively involved in reparative processes at this later stage of healing[29]. Depletion of CD11b-expressing cells via diphtheria toxin at days 1 or 2 post-cardiotoxin injury resulted in persistence of necrotic fibers and smaller regenerated fiber diameter, whereas depletion at 4 days did not result in any changes in muscle regeneration compared to control (of note, this depletion method depletes circulating CD11b+ cells, indicating that at day 4, myeloid cells already recruited to tissue are sufficient for complete regeneration) [29]. Interestingly, depletion at day 0 did not result in differences in regenerated fiber diameter but did result in elevated fat accumulation suggesting that the microenvironment at day 0 may be involved in adipogenic progenitor proliferation and differentiation[41]. In cryo-injured muscles, depletion of circulating monocytes resulted in persistent inflammation and necrosis of muscle, and at later time points, significantly higher fatty infiltration among regenerated fibers[37]. Taken together, these results highlight the critical role that monocytes play in resolving inflammation and initiating muscle repair.

2.2.5 Myeloid Cell Functions within Acute Muscle Injury

The progression of inflammation during muscle regeneration is tightly associated with stages of reparative myogenesis. Inflammatory monocytes and macrophages have been shown to promote the proliferation of activated satellite cells *in vitro* [42] whereas anti-inflammatory monocytes and macrophages govern satellite cell differentiation. *In vivo,* the range of cells that make up the immunological repertoire changes in accordance with the repair state of the injured muscle, and influences not only satellite cell proliferation

and differentiation, but also other required processes such as angiogenesis, nerve regeneration, and extracellular matrix deposition and remodeling.

Following muscle damage, the number of intramuscular leukocytes increases both rapidly and drastically. Within a few hours, neutrophils (commonly immunophenotyped as CD11b+SSC^{hi}Ly6G+) accumulate in the tissue, and reach peak numbers at around 24 hours. Acting as the "first responders" to injury, neutrophils phagocytose apoptotic cells and debris, and secrete cytokines such as interferon-gamma (IFNγ) and tumor necrosis factor-alpha (TNF) that shifts the injury microenvironment towards a pro-inflammatory state. Upon the arrival of monocytes and macrophages from both circulation and peri-muscular/vascular niches, the pre-conditioned, pro-inflammatory environment educates these cells to likewise adopt a pro-inflammatory state. Pro-inflammatory macrophages dominate for the first few days after injury (day 1-2), where they phagocytose cellular debris and exert a pro-proliferative, anti-differentiating effect on satellite cells via the secretion of TNF-α, IFN-γ and IL-6[43-47]. Conversely, anti-inflammatory monocytes/macrophages that dominate the later stages of healing (day 3 and onward) promote satellite cell differentiation, with IL-10 and IGF-1 identified as key molecules in the progression of late-stage myogenesis [24, 48]. In additional to soluble factors, cell-cell contacts between macrophages and myogenic progenitors have been shown to protect precursor cells from apoptosis [49]. Recent studies show that injection of pro-inflammatory human macrophages along with human myoblasts into immunocompromised mice enhanced the proliferative window of transplanted myoblasts, promoted their migration, and delayed differentiation, and ultimately resulted in more human-derived myofibers at 1

month post-transplantation, whereas co-injection of myoblasts with anti-inflammatory M2c-like macrophages enhanced myofiber number at an earlier day 5 timepoint[50].

Inflammatory "M1" macrophages are classified by their activation via Th1-type cytokines (such as the aforementioned IFNγ and TNF)[51], which distinguishes them from M2 alternatively-activated, repair macrophages which are activated by Th2-type cytokines (such as IL-4 and IL-10)[51]. However, the M1/M2 naming paradigm has been used to describe *in vitro* polarized macrophage states that often do not reflect the diverse and nuanced macrophage populations that are seen *in vivo* following muscle injury. Transcriptional profiling was performed on isolated muscle macrophages from injured CX3CR1-GFP transgenic mice that were sorted according to their Ly6C and CX3CR1 expression (with $Ly6C^{pos}CX3CR1^{lo}$ cells representing the "M1" class and $Ly6C^{neg}CX3CR1^{hi}$ representing the "M2" class of macrophages). Principle component analysis revealed that overall, macrophage populations segregated more by day (macrophages from days 1-2 clustered together, and macrophages from days 4-8 clustered together), than by their Ly6C immunophenotype. In vertical comparisons of macrophage subsets within each time point, canonical pro- and anti-inflammatory transcripts such as TNF-alpha, IL-1 beta (inflammatory) and TFG-beta and IL-10 (anti-inflammatory) were not significantly different between the $Ly6C^{pos}$ and $Ly6C^{neg}$ subsets. However, the modest differences in pro- and anti-inflammatory cytokines highlight the difficulty in defining *in vivo* macrophage phenotypes by conventional markers.

At day 2, $Ly6C^{pos}$ macrophages were upregulated in genes associated with innate immune response and cell motility, with IL1f9 being the top ranked inflammatory gene. Alarmins (molecules that are released upon tissue injury, eg. *S100a8 and S100a9*), and

acute (inflammation) phase protein (*Lcn2, Lrg1, Hp, and Saa3*) genes were also upregulated in day 2 Ly6C^{pos} macrophages compared to day 2 Ly6C^{neg} macrophages. Interestingly, the inflammatory profile of day 2 Ly6C^{pos} macrophages was driven independently of the IFN-γ-STAT signaling pathway, as several of the inflammatory genes (*Saa3, Il1f9, S100a9*) were not differentially expressed in day 2 CD45+ cells collected from STAT1 knockout mice compared to wild-type mice (though coinjection of LPS along with toxin did induce their expression, showing that these genes were expressed based on a pro-inflammatory muscle environment). Conversely, Ly6C^{neg} macrophages at day 2 and day 4 post injury were upregulated in genes that governed cell cycle progression and cell division, showing the proclivity of anti-inflammatory macrophages to proliferate. Importantly, there was an early upregulation of genes (between days 1 and 2) of genes associated with oxidative phosphorylation and TCA cycle, followed by subsequent downregulation of genes associated with glycolysis and glucose metabolism in both Ly6C^{pos} and Ly6C^{neg} macrophages, indicating that macrophages shift their metabolic profile from glycolysis to oxidative metabolism prior to shifting their inflammatory status from a pro-inflammatory to anti-inflammatory state.

Horizontal comparisons of the Ly6C^{pos} macrophage population along the timecourse of regeneration showed that the most important changes in gene expression happened between days 2 and 4 post-injury, right when inflammatory Ly6C^{pos} macrophages are undergoing the phenotypic switch to repair Ly6C^{neg} macrophages. Upregulated genes at day 4 compared to day 2 were molecules associated with macrophage interactions with the adaptive immune system (such as *Cd7, Ifng, Cd2, Ciita*, among others), whereas genes encoding both pro-inflammatory and anti-inflammatory secreted

effector molecules (*Il6, Il10, Itga1*) and genes involved in transcription, translation and lipid metabolism were downregulated.

Ly6C^{neg} macrophages first upregulate genes associated with cell proliferation and cell division up until day 4 post-injury, and downregulate chemotaxis and cell motility associated genes (e.g. *Itga1, Ccl2 Pecam1, Itgal*) within this acute phase. Later on in the regenerative process, genes associated with immune response and cell communication/cytokine production were upregulated (e.g *Il6, Il10, CD81, Ccl22, Pdgfb* for immune response, and *Itk, Map2k3, Dusp16* for signal transduction) while genes governing metabolism of ribosomes/RNA, glucose, and other macromolecules were downregulated at the late stages of regeneration. Molecules that are known to be secreted by macrophages and play roles in myogenesis such as insulin-like growth factors (IGF)[48], platelet derived growth factor-alpha, hepatocyte growth factor, and bone morphogenic protein 2, were shown to increase along the time course of regeneration within the Ly6C^{neg} macrophage subset in particular. Late-phase Ly6C^{neg} macrophages highly express genes that code for both extracellular matrix (ECM) proteins, as well as ECM remodeling proteins, indicating that these repair macrophages not only remodel the early ECM but directly contribute to ECM scaffolding network as well.

It is worth re-noting that this detailed information on muscle injury macrophages was only recently gathered from muscles that had underwent cardiotoxin induced muscle injury. More of experiments of this nature should be conducted on other types of muscle injury, such as nerve denervation injury and volumetric muscle loss, to more clearly understand the role that injury context plays in macrophage gene activation and subsequent functional behavior.

The diverse and time-dependent gene expression profiles (broadly, inflammatory, then anti-inflammatory) stemming from the sequentially dominant macrophage phenotypes likely affect other processes necessary for functional muscle healing including ECM deposition and reorganization, angiogenesis and vascular remodeling, and nerve regeneration. Knowledge of how different macrophage subsets affect the various tissue microcompartments within injured muscle is especially important in a volumetric defect context in which all tissue architecture must be regenerated *de novo*. We focus on the alternatively-activated macrophages that govern the later phases of healing as wounds tend to quickly switch from an inflammatory environment to an anti-inflammatory, pro-healing environment only a few days after injury [52].

ECM deposition and reorganization is crucial for the healing of tissue injuries in which the native matrix has been damaged or lost. During the proliferative phase of wound healing, fibroblasts can migrate into the defect space and initiate the deposition of a provisional ECM that is composed mostly of fibrin and fibronectin. This provisional ECM encourages fibroblast adhesion and migration into the damaged tissue space, where granulation tissue is formed and a vascular network is established [52]. Fibroblasts and myofibroblasts continue to secrete ECM, predominately collagen, that can either restore tissue mechanical properties, or lead to the formation of scar tissue (fibrosis). Alternatively-activated macrophages have been shown to control collagen fibril formation in regenerating skin[53] and promote the deposition of ECM by fibroblasts[54]. However, it has been shown that the unchecked production of TGF-β1 by macrophages present in chronic inflammation can promote the differentiation of fibroadipogenic progenitors into

robust matrix-producing fibroblasts that leads to unchecked deposition of collagen and ultimately, fibrosis [55].

Skeletal muscle is a heavy consumer of bioresources such as oxygen and nutrients, and consequently produces a lot of biowaste that must be cleared. To facilitate this rapid exchange of molecules, this tissue is highly vascularized, possessing larger blood vessels and an intricate network of capillaries. Restoration of an appropriate vascular network within regenerated muscle is crucial to proper functionality. Monocytes and macrophages appear to promote both angiogenic and arteriogenic expansion of the vasculature[56-58]. Macrophages are the primary source of angiogenic growth factors such as VEGF[59] and robust vascularization is associated with increased macrophage presence in and around biomaterial implants[60, 61]. M2-polarized macrophages (IL-4- or IL-10-stimulated) are considered pro-angiogenic both *in vitro* and *in vivo*[62-64], though recent studies have demonstrated that M1-polarized macrophages may also play key roles in angiogenesis [65, 66]. Promotion of both angiogenic expansion of vascular length and arteriogenic diameter network expansion in dorsal skin is correlated with the presence of $Ly6C^{lo}$ monocytes in higher proportion to $Ly6C^{hi}$ monocytes[67]. Hydrogel vascularization in response to growth factor delivery (platelet-derived growth factor and fibroblast growth factor) in the cornea was accompanied by accumulation of macrophages that produce both M1- and M2-associated mRNA transcripts, such as *Tnfa* and *Arg1*, respectively [60]. Matrigel implants rich in alternatively-activated (M(IL-4 or IL-10) macrophages show increased vascularization after subcutaneously implantation compared to implants supplemented with inflammatory macrophages (M(IFN-γ)) [63] . The robust difference in matrigel plug

vascularization was attributed to upregulated expression of fibroblast growth factor and placental growth factor within the M2 polarized macrophages.

Monocytes and macrophages have also been shown to interact closely with remodeling vasculature[57, 68, 69]. We have shown *in vitro* that anti-inflammatory CX3CR1^{hi} monocytes preferentially associated with endothelial cell networks and *in vivo,* exhibit closer homing to inflamed vasculature[36]. During development, M2-like macrophages serve as physical bridges between sprouting angiogenic tip cells, as if guiding them towards fusing together into a vascular intersection. Indeed, macrophages are seen to remain in close contact with these anastomoses even after formation of a vessel junction[57]. It has been suggested that vasculature can provide microenvironmental cues that educate non-classical monocytes to convert into alternatively activated macrophages via signaling with the endothelium[70], and consequently signal back to promote vessel remodeling. The importance of spatial positioning of monocytes and macrophages during healing is only beginning to be understood, but we have demonstrated that increased proximity of CD206+ cells to vasculature in ischemic tissues coincides with increased vessel density [36]. Thus, both the phenotype of monocytes and macrophages, as well as their spatial distribution is likely an important feature when assessing their function.

Skeletal muscle contracts in response to electrical stimulus from specialized nerves called motor neurons. In addition to facilitating movement, muscles must also be innervated simply to maintain muscle tone and avoid atrophy. Motor neurons branch throughout the muscle and connect with muscle fibers at the neuromuscular junction. The proper coupling of the pre-synaptic and post-synaptic junction is crucial for the transmission and translation of neural electrical signal (action potential) to the chemical

signal (acetylcholine - ACh) that crosses the synaptic cleft and binds to clusters of acetylcholine receptors on the muscle fiber [71]. Binding of ACh to the Ach receptors triggers an action potential within the muscle fiber, releasing calcium stores, and ultimately results in muscle contraction. Following injury, motor neurons undergo degeneration in the axonal portion distal to the injury site, a process known as Wallerian degeneration[72]. Within a few days, circulation-derived macrophages will enter the distal stump of the nerve and clear myelin debris[73]. Depletion of blood monocytes with clodronate liposomes in rats undergoing peripheral nerve transection resulted in significantly reduced macrophages within nerves and less myelin debris clearance, a process necessary to nerve regeneration[74]. Axons regenerate starting from the proximal stump, and macrophages promote axonal growth by secreting proteases, growth factors, and ECM remodeling proteins[75]. Macrophages at the site of nerve injury can be educated by molecules in the local microenvironment to polarize towards an anti-inflammatory M2 phenotype. Such molecules include apolipoprotein E, collagen VI, and CCL2/CCR2, which are all enhanced following peripheral nerve injury. Collagen VI and CCR2 knockout mice both display macrophage phenotypes skewed towards the M1 inflammatory phenotype. Several studies have investigated the therapeutic benefit of locally delivering macrophage polarizing cytokines to peripheral nerves. Locally delivering IFN-γ (a canonical M1-polarizing cytokine) from nerve guidance channels polarizes local macrophages to an M1 phenotype but did not result in increased Schwann cell infiltration or axonal growth. However, local delivery of IL-4 (canonical M2-polarizing cytokine) did promote increased Schwann cell infiltration and increased axonal growth, and the group showed that increased CD206+/CCR7+ (M1/M2) macrophage ratio is linearly correlated with improved axonal

growth [76]. Another group delivered IL-10 (canonical M2-polarizing cytokine) to intact peripheral nerves and saw increased M2 polarization by immunofluorescence staining for Arginase 1 and CD206, however they did not look at the benefits in a nerve injury model[77].

Taken together, it is evident that monocytes and macrophages are able to influence repair processes in skeletal muscle and the various sub-tissue compartments within. Thus, therapies that leverage the pro-regenerative activities of myeloid cells represent a promising strategy to promote the regeneration of not only muscle tissue, but also motor neurons and vasculature crucial to the proper function of skeletal muscle as a whole.

2.2.6 Contributions of Macrophages within Muscle Pathology and Aging

Though macrophages are required for muscle regeneration after acute injuries, their unchecked activity within muscle pathologies can lead to tissue destruction and fibrosis. In Duchenne Muscular Dystrophy, there is constant infiltration of CD4+, CD8+ T-lymphocytes, macrophages, eosinophils, and natural killer T-cells[78]. Depletion of F4/80+ macrophages in dystrophic mice result in significant reductions in muscle membrane lesions characteristic of dystrophic muscle[79]. However, knockout of the inflammatory cytokine IFN-γ polarized macrophages in dystrophic muscle to a more anti-inflammatory phenotype and improved gross motor function in the later stages of disease. Macrophages extracted from dystrophic muscle can display either a canonical inflammatory ($Ly6C^{hi,}$, tumor necrosis factor-alpha/TNF-α^{hi}) or anti-inflammatory ($Ly6C^{lo}$, transforming growth factor-beta/TGF-β^{hi}) phenotype, or interestingly, a mixed phenotype in which macrophages express both TNF-α and TGF-β[55]. However, the dual

presence of these cytokines, and in particular TGF-β, was shown to impair apoptosis of fibroadipogenic progenitors that promote fibrosis in dystrophic mice. Thus, it appears that anti-inflammatory macrophages can be either beneficial or deleterious within the context of muscular dystrophies and further studies to more closely categorize these macrophages and their contributions to the severity of muscular dystrophy are needed.

Aged muscle displays similar characteristics to dystrophic muscle, and the role of the immune system in sarcopenia is equally less understood. Studies in geriatric mice (22-24 months) have shown increases in anti-inflammatory M2 macrophages within skeletal muscle that can promote the fibrosis seen in resting aged skeletal muscle[80]. F4/80+MHCII- monocytes/macrophages were decreased in aged muscles damaged with cardiotoxin, and studies in humans show decreased macrophage infiltration in exercise-induced muscle injury in older patients vs younger patients. Indeed, unpublished data from our lab in aged mice (14-16 months) show decreased infiltration of both inflammatory (Ly6C+,CD206-) and anti-inflammatory (Ly6C-,CD206+) macrophages after volumetric muscle injury. Though it is clear that immune homeostasis and inflammatory response to muscle injury is dysregulated with age, further exploration of key altered aspects and how their modulation can reduce muscle wasting and/or improve regeneration is needed.

2.2.7 Lymphocytes within Skeletal Muscle Repair

Though the contributions of monocytes and macrophages to skeletal muscle repair have been well established in recent years, the role that the adaptive immune system plays in muscle healing is less understood. Recently, a population of regulatory T-cells (Tregs) was identified within regenerating skeletal muscle that displayed a transcriptome unique to

the injury niche compared with Tregs isolated from lymphoid organs such as the spleen [81]. The transcriptomic analysis revealed that muscle Tregs overexpress the chemokine IL-10, as well as the growth factors platelet-derived growth factor (PDGF) and Amphiregulin (Areg), compared to splenic Tregs and conventional T-cells (Tconv) from either injured muscle or spleen. Tregs accumulate in toxin-injured muscle at around 4 days, coinciding with the time frame around which accumulated myeloid cells undergo an inflammatory to anti-inflammatory phenotypic switch. Depletion of Tregs in Foxp3-diptheria toxin receptor mice resulted in failure for inflammatory, $Ly6C^{hi}$ cells within the injured muscle to undergo a proper phenotypic switch to the more anti-inflammatory $Ly6C^{lo}$ stage[81]. Concomitant with this stalled inflammatory phase was impaired muscle regeneration as detected by lower numbers of centrally nucleated, regenerating muscle fibers, and increased fibrotic collagen deposition. Indeed, aged mice that are impaired in muscle regeneration exhibit decreased Treg recruitment[82].

CD8+ T-cells have been shown to exert a positive impact on muscle regeneration through the secretion of monocyte chemoattractant protein-1 (MCP-1) that recruits inflammatory macrophages at the initial phase of muscle regeneration, promoting satellite cell proliferation[83]. However, depletion of CD8+ and CD4+ T-cells in dystrophic mice significantly reduces the skeletal muscle pathology seen in these animals[84]. Overall, the role of CD8+ cytotoxic T-cells and CD4+ helper T-cells within muscle injury and regeneration largely remains unknown.

2.2.8 Harnessing immune cells for the treatment of skeletal muscle injuries

Immunologically smart interventions that exploit the division of labor between different monocyte, macrophage, and lymphocyte populations require an understanding of the roles that these cells play in promoting repair. Though significant advances have been made in elucidating the immunobiology within toxin-induced skeletal muscle repair (Figure 2), further exploration of the role these immune cells play within volumetric skeletal muscle injury is required.

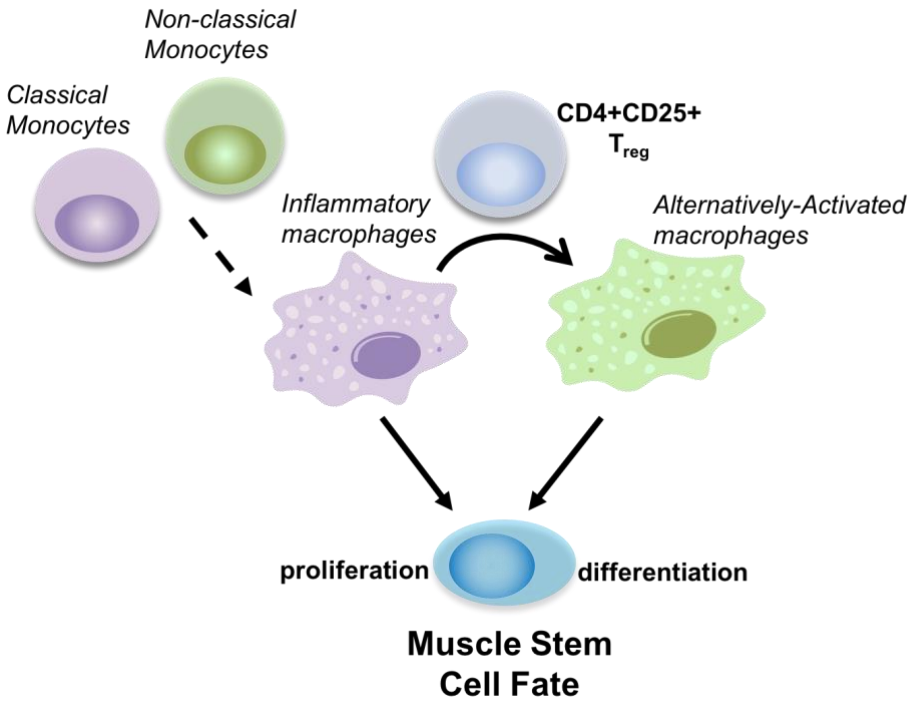

Figure 2. Immuno-biology within skeletal muscle injury. Within muscle injury, monocytes are recruited from circulation and become macrophages over a spectrum of phenotypes. In the acute phases of injury, inflammatory myeloid subsets promote the proliferation of muscle stem cells or satellite cells. Towards the midstages of repair, myeloid subsets undergo a switch from the inflammatory phenotype to the anti-inflammatory or repair phenotype, which then promote satellite cell differentiation. This phenotypic switch is thought to be governed at least in part by the activity of recruited regulatory T-cells.

A fine balance exists within successfully regenerated, from the subtypes of immune cells that are present, to the time at which they exert functional activity. The present work

will improve our understanding of the role that myeloid and lymphoid cells play in promoting endogenous mechanisms of tissue repair after traumatic injuries. In Chapter 3, we track the fate of circulating classical and non-classical monocyte subsets and identify non-classical Ly6C^{lo} monocytes as biased progenitors of alternatively-activated CD206+ macrophages. In Chapter 4, we establish a novel model of volumetric muscle injury (VML) in the murine spinotrapezius, which enables the whole-mount visualization of cell populations and tissue microstructures critical in muscle repair (Figure 3). We demonstrate for the first time that non-classical monocytes are directly recruited to volumetric muscle injury. We use the knowledge that non-classical monocytes are biased progenitors of alternatively activated macrophages as motivation to locally enrich their frequency in injured muscle tissue. We show that selective recruitment of non-classical monocytes to injured muscle coincides with increased CD206+ alternatively-activated macrophages in peri-defect tissue and improves muscle healing. In Chapter 5, we expand the spinotrapezius model to encompass a non-healing defect and demonstrate that implantation of FTY720 nanofibers over 2mm diameter muscle defects induces acute changes in lymphoid and myeloid cell subset accumulation. Assessment of muscle healing metrics reveal that increased alignment of regenerated muscle fibers to the pre-injury fiber axis was observed in animals treated with FTY720 nanofibers. Taken together, we will demonstrate an improved understand of the role that pro-regenerative subsets of immune cells play in the promotion of endogenous mechanisms of tissue repair after traumatic soft-tissue injuries.

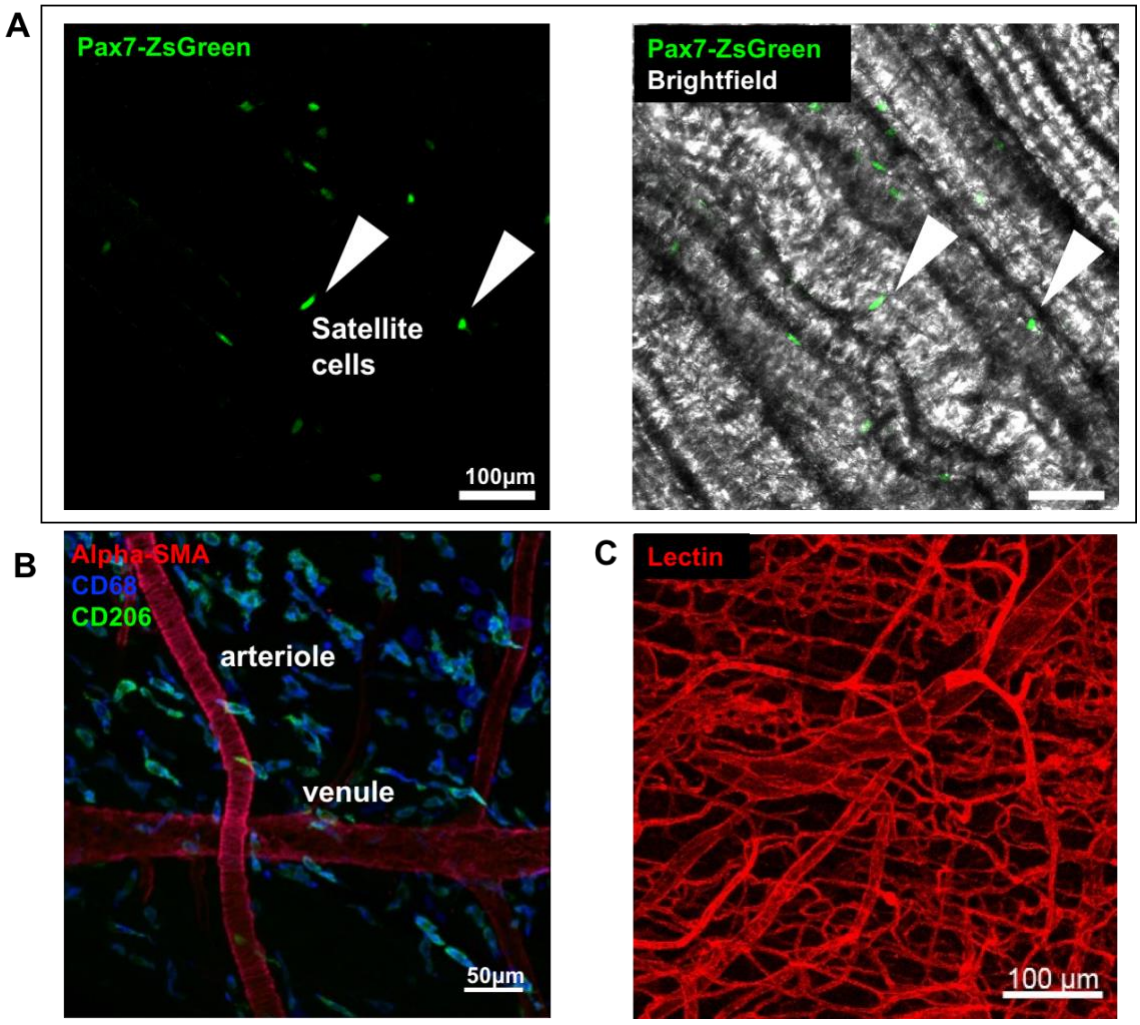

Figure 3. Whole mount confocal images of uninjured spinotrapezius muscle. A) Pax7-ZsGreen satellite cells lie along the basal lamina of muscle fibers. B) CD68+CD206+ cells in resting spinotrapezius muscle associate with blood vessels. C) Skeletal muscle possesses a dense network of larger blood vessels, and smaller capillaries.

3. NON-CLASSICAL MONOCYTES ARE BIASED PROGENITORS OF WOUND HEALING MACROPHAGES[2]

3.1 Abstract

Successful tissue repair requires the activities of myeloid cells such as monocytes and macrophages that guide the progression of inflammation and healing outcome. Immunoregenerative materials leverage the function of endogenous immune cells to orchestrate complex mechanisms of repair; however, a deeper understanding of innate immune cell function in inflamed tissues and their subsequent interactions with implanted materials is necessary to guide the design of these materials. Blood monocytes exist in two primary subpopulations, characterized as classical inflammatory or non-classical. While classical monocytes extravasate into inflamed tissue and give rise to macrophages, the recruitment kinetics and functional role of non-classical monocytes remains unclear. Here, we demonstrate that circulating non-classical monocytes are directly recruited to polymer films within skin injuries, where they home to a perivascular niche and generate alternatively activated, wound healing macrophages. Selective labeling of blood monocyte subsets indicates that non-classical monocytes are biased progenitors of alternatively activated macrophages. On-site delivery of the immunomodulatory small molecule FTY720 recruits S1PR3-expressing non-classical monocytes that support vascular remodeling after injury. These results elucidate a previously unknown role for blood-

[2] Portions of this chapter adapted from: Olingy CE, San Emeterio CL, Ogle ME, Krieger JR, Bruce AC, Pfau DD, et al. Non-classical monocytes are biased progenitors of wound healing macrophages during soft tissue injury. Sci Rep. 2017;7:447. Published under Creative Commons license.

derived non-classical monocytes as contributors to alternatively activated macrophages, highlighting them as key regulators of inflammatory response and regenerative outcome.

3.2 Introduction

The mononuclear phagocyte system plays a multi-faceted role in maintaining tissue homeostasis and responding to pathological processes such as autoimmune diseases, cancer, and aberrant wound healing. Monocytes circulate in the bloodstream during steady state and are robustly recruited to sites of inflammation, where they exert functions that include clearance of cellular debris, promotion of angiogenesis, and restoration of tissue integrity[85]. The ontogeny of macrophages varies in different tissues, such that some tissue resident macrophages are seeded embryonically and self-renew in a similar manner to stem cells, whereas other macrophages (such as in the dermis or gut) are continually replenished by blood-derived monocytes[14-18]. Consequently, circulating blood monocytes are considered a highly plastic and dynamic system of innate immune cells that initiate processes of organ and tissue remodeling[85-87].

Two distinct subpopulations of monocytes have been identified in mouse and human blood, which can be distinguished by well-characterized surface protein expression profiles. Classical inflammatory monocytes are identified by $Ly6C^{hi}CX3CR1^{lo}CD43^{lo}$ expression in mice ($CD14^{hi}CD16^{-}$ in human), whereas non-classical alternative monocytes are $Ly6C^{lo}CX3CR1^{hi}CD43^{hi}$ in mice ($CD14^{+}CD16^{+}$ in human)[14]. A third population of intermediate monocytes characterized by intermediate expression of Ly6C in mice ($CD14^{hi}CD16^{+}$ in humans) are thought to complement the functions of non-classical monocytes and may preferentially differentiate into dendritic cells within inflamed

tissues[20, 21]. Under homeostasis, classical monocytes in blood decrease Ly6C expression and become non-classical Ly6C^{lo} monocytes[17, 22], which patrol the luminal side of resting endothelium[12]. Classical monocytes also survey steady-state tissues and can traffic to lymph nodes without differentiating into macrophages[13]. During inflammation, monocytes exit peripheral blood and extravasate into tissue, where they may transiently persist as monocytes without differentiation and exert a host of functions within the damaged tissue[13, 56, 88-90]. Classical inflammatory monocytes present in the acute phases of injury secrete pro-inflammatory cytokines such as IL-6, iNOS, and TNFα[90] and exhibit high levels of matrix metalloproteinase and cathepsin production[33]. Conversely, Ly6C^{lo} monocytes present later during inflammation secrete high levels of vascular endothelial growth factor (VEGF) and IL-10 and can induce endothelial cell proliferation to promote arteriogenesis[29, 33, 56]. We have previously shown that strategies that enhance the early recruitment of Ly6C^{lo} monocytes couple with later increases in arteriolar expansion and angiogenic activity[34, 67]. Recruited monocytes primarily differentiate into macrophages, serving as an alternative source of wound macrophages to those derived from *in situ* proliferation of tissue resident populations[91].

Macrophages are highly responsive to cues within the injury niche, enabling them to dynamically modify their behavior in response to changes in the microenvironment and display extremely varied phenotypes. Classically activated ("M1") macrophages are primary players in pathogen destruction, secretion of inflammatory cytokines, and driving Th1-type responses[23]. Conversely, alternatively activated wound healing ("M2") macrophages (of which a number of subtypes have been described[23]) are associated with pro-regenerative activities such as angiogenesis[25, 26], extracellular matrix

remodeling[27], secretion of anti-inflammatory cytokines[23], and resolution of inflammation[28]. The highly complex and heterogeneous nature of inflamed tissue microenvironments has rendered a general description of macrophage origin and function challenging. Within toxin-induced muscle injury[29], liver fibrosis[30], infection[31], and autoimmune disease[32], classical Ly6C^{hi} monocytes are recruited from circulation and undergo *in situ* differentiation to be the primary contributors of injury Ly6C^{lo} monocytes/macrophages. In contrast, sequential recruitment of classical Ly6C^{hi} followed by non-classical Ly6C^{lo} monocyte subsets after myocardial infarction[33], and direct recruitment of adoptively transferred Ly6C^{lo} monocytes within excisional skin injury[34] and during the development of inflammatory arthritis[35] have been reported. However, whether specific populations of blood monocytes give rise to defined macrophage phenotypes surrounding implanted materials remains unknown.

Harnessing myeloid cell functions for regenerative medicine applications requires an understanding of the cues that direct the localization and fate of these cells. Immunoregenerative materials seek to leverage the function of endogenous immune cells to guide the progression of inflammation and repair damaged tissue[92]. For example, local delivery of stromal-derived factor-1 (SDF-1) from desulfated heparin-containing poly(ethylene glycol) (PEG) hydrogels increases the frequency of CXCR4^{hi}Ly6C^{lo} monocytes, which promotes capillary network expansion[67]. Moreover, co-delivery of macrophage colony-stimulating factor (M-CSF) with VEGF from PEG hydrogels increases the density and maturity of corneal blood vessels compared to VEGF alone[60]. Recently, our lab demonstrated that poly(lactic-*co*-glycolic acid) (PLGA)-based delivery of the small molecule FTY720, an agonist of sphingosine-1-phosphate receptor (S1PR) 3, recruits non-

classical monocytes to inflamed tissues and promotes arteriogenesis[34]. In the present study, we utilize cell labeling strategies to selectively track the fate of either classical $Ly6C^{hi}$ or non-classical $Ly6C^{lo}$ monocytes in response to biomaterial implantation within cutaneous wounds. We demonstrate that classical monocytes are able to give rise to both CD206- and CD206+ macrophages following monocyte depletion with clodronate liposomes, but labeled non-classical monocytes preferentially give rise to CD206+ M2-like macrophages. On-site delivery of the immunomodulatory small molecule FTY720 induces homing of extravasated non-classical monocytes to peri-implant vasculature. Subsequently, FTY720 promotes *in situ* generation of wound healing macrophages and vascular remodeling within ischemic skeletal muscle. These results shed light on the fate of specific monocyte populations following biomaterial implantation after injury and indicate that non-classical monocytes are a promising therapeutic target for harnessing pro-regenerative inflammation to promote repair.

3.3 Materials and Methods

3.3.1 Material fabrication

Films were fabricated as previously described[34]. Briefly, 350 mg PLGA (50:50 DLG 5E – Evonik Industries) was dissolved in 2ml dichloromethane in a glass scintillation vial via high-speed vortexing. For drug-loaded films, 1.75 mg of FTY720 (Cayman Chemical) was added at a 1:200 drug:polymer weight ratio, and mixed until completely incorporated. Polymer solutions were poured into Teflon-coated petri dishes and allowed to dry at -20°C for 7 days. Before use, films were lyophilized overnight to remove any traces of solvent.

3.3.2 Dorsal skinfold window chamber surgery

All animal procedures were conducted according to protocols approved by the Georgia Institute of Technology or University of Virginia Institutional Animal Care and Use Committee. Male C57BL/6J or B6.129P-Cx3cr1tm1Litt/J mice ($CX3CR1^{GFP/+}$) mice (8-12 weeks) were fitted with sterile dorsal skinfold window chambers (APJ Trading Co) as previously described[34]. Briefly, mice were anesthetized with an intraperitoneal (i.p.) injection of ketamine/xylanzine (100/10 mg/kg) in sterile saline. Dorsal skin was shaved, depilated, and sterilized with three alternating washes of 70% ethanol and chlorhexidine. A double-layered skin fold was elevated off the back of the mouse and fitted with the titanium frame of the window chamber on the underside. The epidermis and dermis were removed from the top side of the skinfold in a ~12mm diameter circular area via surgical microscissors to reveal underlying vasculature. Exposed tissue was superfused with sterile saline to prevent desiccation. The titanium frame was then mounted on the top side of the skinfold, attached to the underlying frame counterpart, and sutured to the surrounding tissue. Two films were placed on top of the exposed subreticular dermis layer immediately after surgery (day 0) and exposed tissue was sealed with a sterile glass window. Mice were euthanized 72 hours after surgery via CO_2 asphyxiation. The vasculature was immediately flushed with intracardiac infusion of saline follow by an intracardiac infusion of 4% paraformaldehdyde, prior to whole mounting of tissue and immunohistochemistry.

3.3.3 Spinotrapezius ischemia model

Mice were anesthetized with an i.p. injection of ketamine⁄xylazine⁄atropine (60⁄4⁄0.2 mg⁄kg). Ligation surgeries were performed as previously described[68]. Briefly,

a small incision was made on the dorsum above the lateral edge of the right spinotrapezius at the edge of the fat pad. The fascia was separated from the top of the muscle and the fat pad moved before isolating an anatomically reproducible feeding arteriole entering the muscle from below. This feeding arteriole was ligated with 10-0 nonabsorbable suture in two places and cut. The fat pad and fascia were moved back into position and the skin was closed with 8-0 nonabsorbable suture. To allow visualization of vascular endothelium of arterioles in CX3CR1$^{GFP/+}$ mice, anesthetized mice were administered an intra-jugular injection of labeled isolectin (IB4-Alexa Fluor 568; Life Technologies), which was allowed to circulate for 10 minutes. Anesthetized mice were euthanized via CO_2 asphyxiation 72 hours post-surgery. The vasculature was immediately flushed with an intracardiac infusion of adenosine (70 mg/L) in Ringer's solution followed by an intracardiac infusion of 4% paraformaldehyde.

3.3.4 Flow cytometry

Peripheral blood was collected via cardiac puncture and bone marrow was collected via centrifugation (1000g for 5 mins) of isolated tibiae. The dorsal tissue circumscribing films was punched out with 6mm biopsy punches and pooled from both films within one animal for most studies. For adoptive transfer studies, all inflamed dorsal tissue was collected for analysis. Tissue was digested with collagenase (1mg/ml) at 37°C for 30 minutes and further disaggregated with a cell strainer to create a single cell suspension. Single cell suspensions of tissues were stained for flow cytometry analysis according to standard procedures and analyzed on a FACS-AriaIIIu flow cytometer (BD Biosciences). The following antibodies were used for cell phenotyping: APC-Cy7- or BV421-conjugated anti-CD11b (BioLegend), APC- or BV510-conjugated anti-Ly6C (BioLegend), PerCP-

Cy5.5-conjugated CD43 (Biolegend), PE-Cy7-conjugated anti-GR-1 (BioLegend), APC-Cy7-conjugated anti-Ly6G (Biolegend), APC-conjugated anti-F4/80 (BioLegend), PE-Cy7- or FITC-conjugated anti-CD206 BioLegend), PE-Cy7-conjugated anti-CD301b, BV711-conjugated anti-CD64 (BioLegend), PE-conjugated anti-MerTK (Biolegend), BV605-conjugated anti-CD45.1, BV785-conjugated anti-CD45.2, or PerCP-eFluor710 conjugated anti-CD115 (eBioscience). Dead cells were excluded by staining with Zombie NIR^{TM} (Biolegend) in protein-free buffer prior to antibody staining. Staining using BV dyes was performed in the presence of Brilliant Stain Buffer (BD Biosciences). Positivity was determined by gating on fluorescence minus one controls. Absolute quantification of cell numbers in blood and tissue was performed by adding 25μL of AccuCheck counting beads to flow cytometry samples (Thermo Fisher Scientific). S1PR3 flow cytometry was performed by first performing Fc block (Biolegend), followed by staining cells with primary unconjugated anti-S1PR3 antibody (Alomone Labs) and secondary staining with DyLight 650 anti-rabbit IgG (Abcam). Positivity was determined by staining CX3CR1$^{GFP/+}$ cells with the secondary body only (no primary S1PR3 antibody). Gating for tissue monocytes and macrophages is shown in Figure 4.

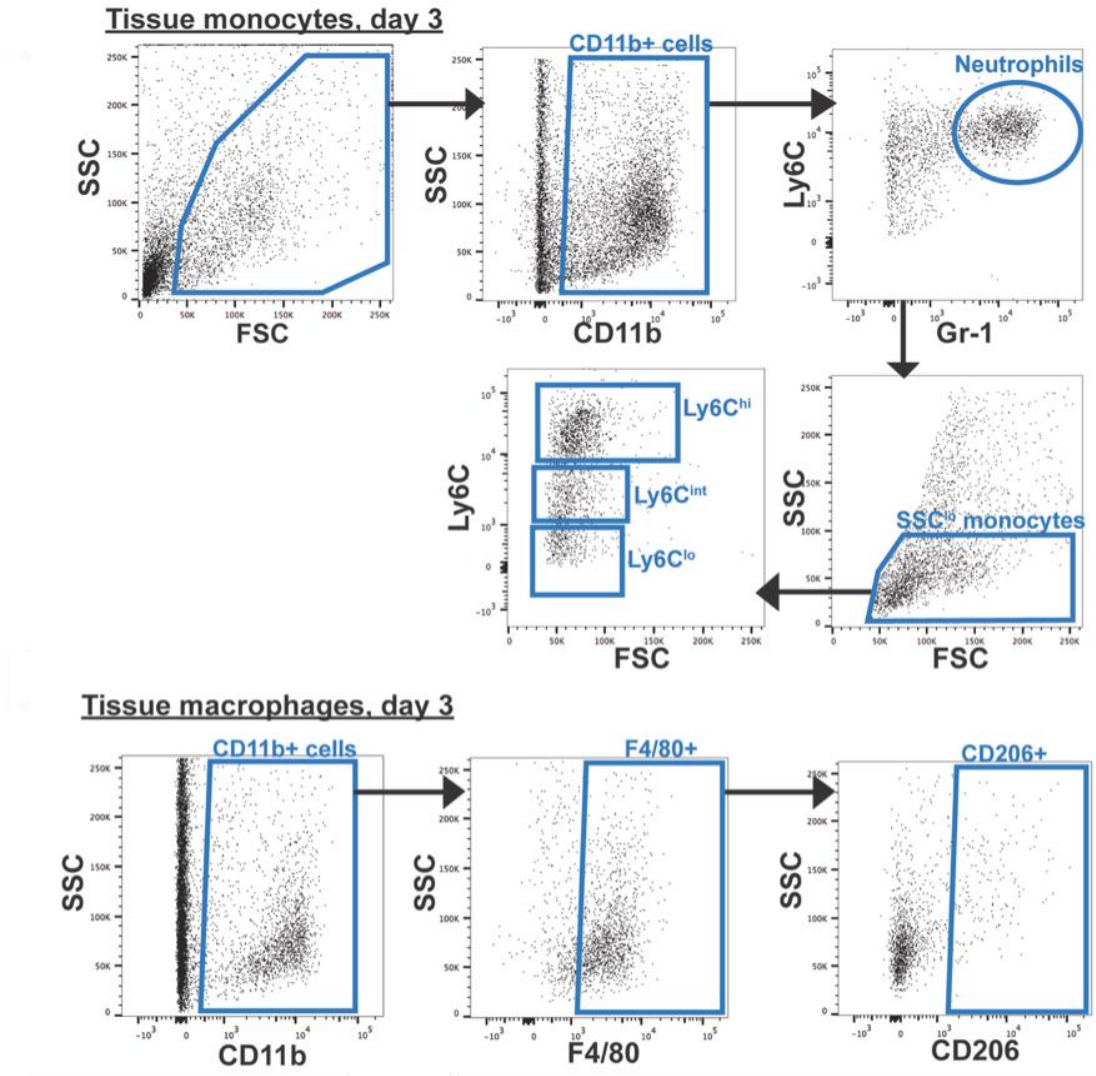

Figure 4. Gating strategy for dorsal skin tissue monocytes and macrophages. Classical monocytes are immunophenotyped as CD11b+, SSC^{lo}, and $Ly6C^{hi}$. Non-classical monocytes are immunophenotyped as CD11b+, SSC^{lo}, and $Ly6C^{lo}$. Alternatively-activated macrophages are identified as CD11b+F4/80+CD206+.

3.3.6 Whole mount immunohistochemistry

Dorsal tissue and spinotrapezius muscles were explanted and permeabilized overnight with 0.1-02% saponin. The tissues were blocked overnight in 5-10% mouse serum. Tissues were incubated at 4˚C overnight in solution containing 0.1% saponin, 5%

mouse serum, 0.5% bovine serum albumin, and the following conjugated fluorescent antibodies: Alexa Fluor 594 anti-CD31 antibody (BioLegend) or Alexa Fluor 568 isolectin IB4 (Life Technologies) for blood vessel visualization, Alexa Fluor 647 anti-CD68 (AbD Serotec) for monocyte/macrophage visualization, and Alexa Fluor 488 anti-CD206 (AbD Serotec) or Alexa Fluor 647 anti-CD206 (Biolegend). Tissues were mounted in 50/50 glycerol/phosphate buffered saline and imaged through the entire thickness of the muscle (~200 microns) on a Zeiss LSM 710 NLO confocal microscope or a Nikon confocal microscope.

For monocyte/macrophage quantification, 3-4 different fields of view (FOVs) per muscle containing a collateral arteriole with monocytes/macrophages evident were located manually. Full-thickness z-stack (2μm step size) volume renders of these FOVs were generated using a 20X oil immersion objective. 20X confocal z-stack volume renders were used for cell association quantification. A threshold at which only the brightest $CX3CR1^{GFP/+}$ cells ($CX3CR1^{hi}$) were visible was applied to all images. Vessel-associated CD206+ and $CX3CR1^{hi}$ cells were defined as cells falling within the 2-dimensional area of the vessel in question and within 50μm of the vessel border. ImageJ (NIH) imaging software was used to quantify vessel length and density. Arterioles were distinguished from venules by degree of lectin binding, vessel size, and morphology. Cell counts and green channel thresholding to designate $CX3CR1^{hi}$ cells were performed in Adobe Photoshop (Adobe Systems Incorporated).

3.3.7 Statistical analysis

Data are presented as mean ± standard error of the mean (S.E.M.). All statistical analysis was performed in GraphPad Prism software. Comparisons of two groups were made using a two-tailed unpaired t-test, with Welch's correction if standard deviations were not equal. For studies with two independent variables, two-way ANOVA with Sidak's test for multiple comparisons was performed. Unless otherwise noted, $p<0.05$ was considered statistically significant.

3.4 Results

3.4.1 Injured skin recruits Ly6C^{lo} monocytes that give rise to CD206+ wound macrophages.

Circulating monocyte subsets were labeled *in vivo* prior to dorsal skinfold window chamber (DWC) surgery to facilitate cell tracking of each monocyte population as they entered inflamed dorsal tissue surrounding PLGA polymer implants. Non-classical Ly6C^{lo} monocyte labeling was performed by intravenous administration of fluorescent latex beads[93, 94] (Figure 5). Within two hours of intravascular administration, latex beads are phagocytosed and equally distribute within Ly6C^{lo} and Ly6C^{hi} blood monocyte populations. However, by 24 hours after injection, latex beads primarily label Ly6C^{lo} monocytes due to physiological conversion of labeled Ly6C^{hi} monocytes and this labeling is sustained for up to 1 week[93]. Utilizing this strategy, blood Ly6C^{lo} monocytes were selectively labeled compared to classical Ly6C^{hi} monocytes after DWC (83.4 ± 9.7% Ly6C^{lo} monocytes vs. 14.5 ± 9.3% Ly6C^{int} monocytes and 0.0 ± 0.0% Ly6C^{hi} monocytes, day 1 post-injury) and the label was retained at similar proportions for the duration of the study (Figure 5).

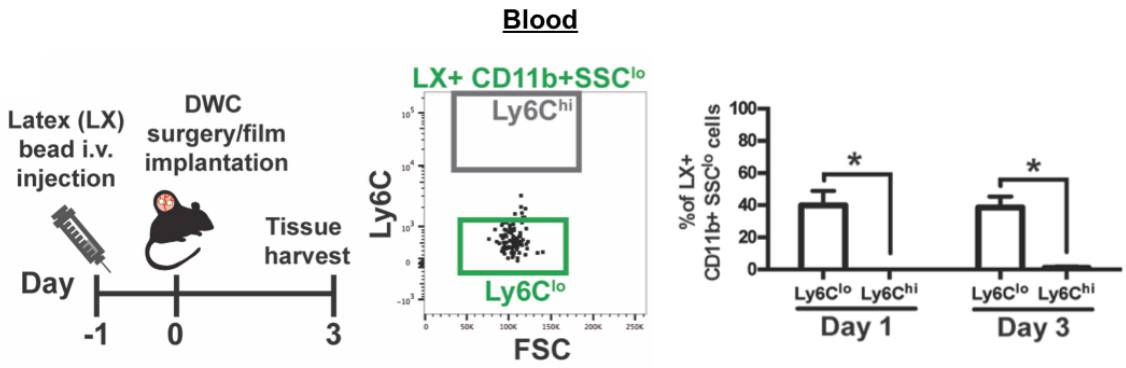

Figure 5. Intravascular administration of latex beads selectively labels circulating Ly6C^{lo} monocytes, which persists for 3 days. Data presented as mean ± S.E.M. Statistical analyses performed using two-tailed t-tests. *$p<0.05$, n=4-11 animals per group.

Analysis of digested explanted dorsal skin tissue showed labeled cells originating as Ly6C^{lo} monocytes primarily remained Ly6C^{lo} within tissue. The lower frequency of Ly6C^{hi} monocytes carrying the label in the tissue (9.6 ± 2.6% of LX+CD11b+SSC^{lo} cells) compared to the frequency of labeled Ly6C^{lo} cells (44.3 ± 8.2% of LX+CD11b+SSC^{lo} cells) indicates that circulating Ly6C^{lo} monocytes do not become Ly6C^{hi} post-extravasation (Figure 6A). Approximately half of labeled cells expressed F4/80, indicating that around half of recruited Ly6C^{lo} monocytes convert into macrophages or are phagocytosed by macrophages by 3 days post-injury (Figure 6B). LX+ labeled cells were more likely to be immunophenotyped as CD206+ macrophages (91.0±3.4% of LX+F4/80+CD11b+ cells) than CD206- macrophages (Figure 6C). These data suggest that blood-derived Ly6C^{lo} monocytes preferentially give rise to CD206+ wound macrophages in inflamed tissue surrounding material implants.

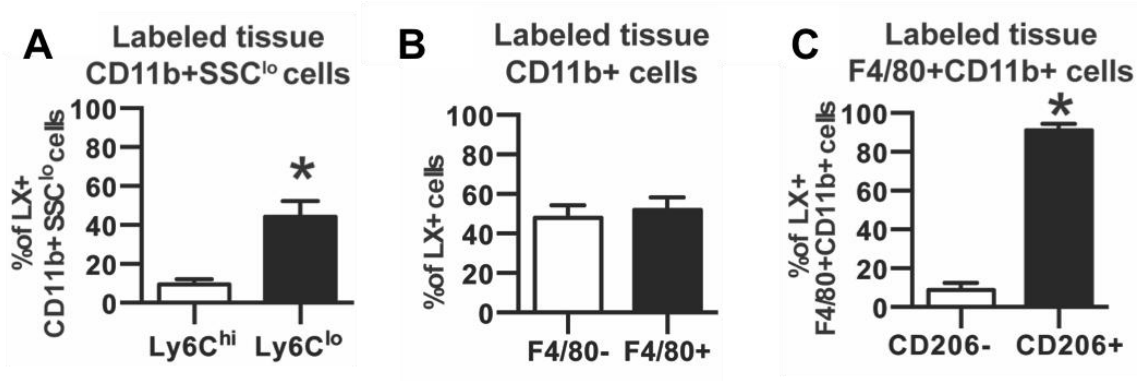

Figure 6. Fate of circulation derived Ly6C^{lo} monocytes in injured skin tissue. (A) Frequency of either Ly6C^{hi} or Ly6C^{lo} monocytes carrying fluorescent latex bead label collected from digested dorsal tissue at day 3 post injury. (B) Frequency of bead-labeled F4/80+ or F4/80- cells in animals with labeled blood Ly6C^{lo} monocytes. (C) Frequency of bead-labeled CD206+ cells out of total F4/80+CD11b+ cells. Data presented as mean ± S.E.M. Statistical analyses performed using two-tailed t-tests. *$p<0.05$, n=4-11 animals per group.

We then tracked circulating Ly6C^{hi} blood monocytes to explore whether these cells adopted similar fates during inflammation. Ly6C^{hi} monocytes were labeled by sequential administration of clodronate-loaded liposomes 2 days prior to injury followed by latex beads 16 hours later (Figure 7), as previously described[93, 94]. Clodronate liposomes administered intravascularly transiently deplete all blood monocytes, resulting in accumulation of latex beads in bone marrow cells that reappear in circulating Ly6C^{hi} monocytes 2 days later[93]. Pre-administration of clodronate liposomes before latex bead injection preferentially labeled Ly6C^{hi} monocytes (70.8 ± 13.3% Ly6C^{hi} monocytes vs. 26.9 ± 12.9% Ly6C^{int} monocytes and 2.7 ± 0.9% Ly6C^{lo} monocytes, day 1 post-surgery) for the duration of the study (Figure 7).

A relatively low frequency of labeled Ly6C^{hi} monocytes was detected in digested tissue (Figure 8A) confirming previous reports[29, 56, 88] that recruited Ly6C^{hi} monocytes do not persist as Ly6C^{hi} monocytes post-extravasation. Ly6C^{hi} monocytes likely rapidly

convert *in situ* into Ly6C^{lo} monocytes, as a significantly greater frequency of labeled Ly6C^{lo} monocytes than Ly6C^{hi} monocytes were detected (Figure 8A).

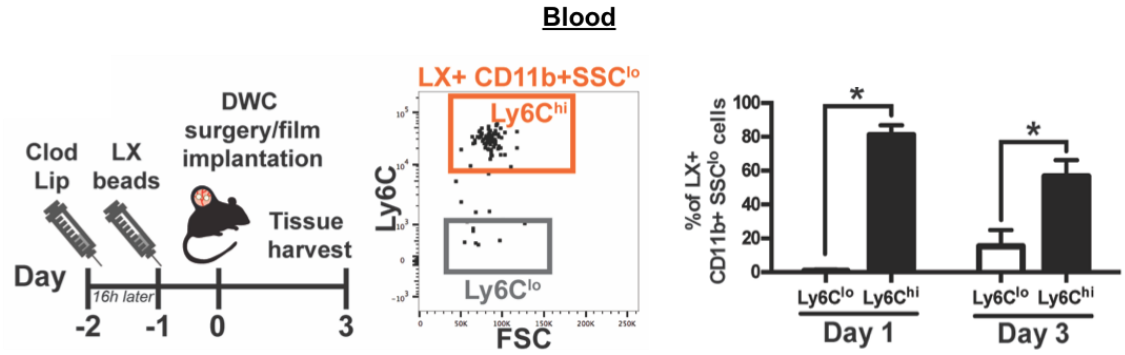

Figure 7. Depletion of monocytes via intravascular administration of clodronate liposomes followed by subsequent administration of latex beads selectively labels circulating Ly6C^{hi} monocytes, which persists for 3 days. Data presented as mean ± S.E.M. Statistical analyses performed using two-tailed t-tests. *p<0.05, n=4-11 animals per group.

The frequency of F4/80+ cells within the latex bead-positive (LX+) population was not different between Ly6C^{hi} monocyte and Ly6C^{lo} monocyte labeling (47.5± 17.3% vs. 48.0 ± 6.2% of LX+ cells), suggesting that both monocyte populations are equally capable of acquiring a macrophage phenotype after extravasation (Figure 8B) Labeled Ly6C^{hi} monocytes showed no preference for acquiring CD206 expression within 3 days of injury (Figure 8C), indicating that although blood-derived Ly6C^{hi} monocytes can contribute to CD206+ macrophages, they do so at a lower frequency than Ly6C^{lo} monocytes after clodronate liposome administration.

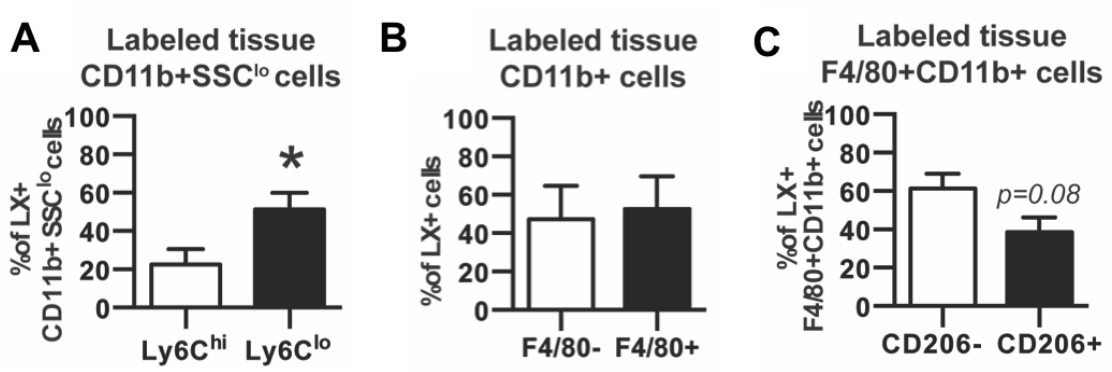

Figure 8. Fate of circulation-derived Ly6C^{hi} monocytes within injured skin tissue. (A) Frequency of either Ly6C^{hi} or Ly6C^{lo} monocytes carrying fluorescent latex bead label collected from digested dorsal tissue at day 3 post injury. (B) Frequency of bead-labeled F4/80+ or F4/80- cells in animals with labeled blood Ly6C^{hi} monocytes. (C) Frequency of bead-labeled CD206+ cells out of total F4/80+CD11b+ cells. Data presented as mean ± S.E.M. Statistical analyses performed using two-tailed t-tests. *$p<0.05$, n=4-11 animals per group.

3.4.2 Reduction of circulating Ly6C^{lo} monocytes impairs CD206+ macrophage generation.

Intravascular administration of clodronate liposomes transiently depletes all circulating monocytes; however, because blood Ly6C^{lo} monocytes are primarily derived from the conversion of Ly6C^{hi} monocytes, there is a delay in the repopulation of circulating Ly6C^{lo} monocytes[17, 22]. We employed this tool to examine how decreasing the quantity of circulating non-classical monocytes impacts the generation of CD206+ macrophages during wound healing. As expected, a deficit in blood Ly6C^{lo} monocytes, but not Ly6C^{hi} monocytes, was observed 5 days after clodronate administration (Figure 9A). No differences in either monocyte subtype (Figure 9B), total F4/80+ macrophages (Figure 9C), or CD206- macrophages (Figure 9D) were observed in digested tissue 3 days post-injury; however, a lower frequency of CD206+ macrophages was observed (Figure 9E). These

findings suggest that circulating Ly6C^{lo} monocytes are likely major contributors to the population of CD206+ wound macrophages.

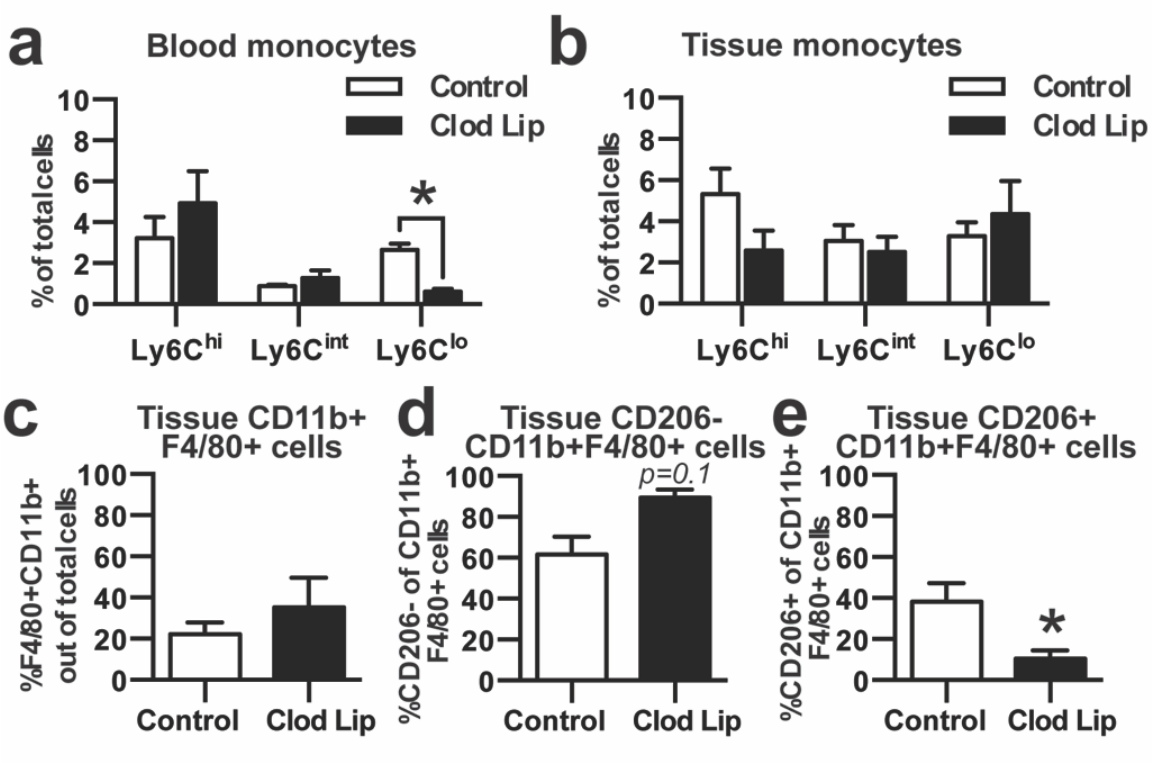

Figure 9. Loss of Ly6C^{lo} monocytes impairs generation of CD206+ alternatively activated macrophages. (A) Clodronate liposome (Clod Lip) administration two days before DWC surgery reduced the frequency in blood of Ly6C^{lo} monocytes, but not Ly6C^{hi} or Ly6C^{int} monocytes. (B) Frequency of Ly6C^{lo}, Ly6C^{int}, Ly6C^{hi} monocytes after Clod Lip administration in digested dorsal tissue 3 days post-injury. (C) Total CD11b+F4/80+ macrophages, (D) CD206- macrophages, and (E) CD206+ alternatively activated macrophages 3 days post-injury. Data presented as mean ± S.E.M. Statistical analyses were performed using two-tailed t-tests *p<0.05, n=4-8 animals per group.

.4.3 Adoptively transferred Ly6C^{lo} monocytes preferentially differentiate into CD301b+CD206+ macrophages.

To complement *in vivo* bead-based labeling strategies and further investigate the role that blood monocytes play in macrophage generation during inflammation, we adoptively transferred sorted CD45.1+ Ly6C^{hi}CD43^{lo} or Ly6C^{lo}CD43^{hi} monocytes into

CD45.2 mice at the time of DWC surgery (Figure 11A, B). While Ly6C^{lo}CD43^{hi} are a slightly more restricted population of Ly6C^{lo} monocytes, these two populations primarily overlap and the same is true for Ly6C^{hi}CD43^{lo} monocytes (Figure 10).

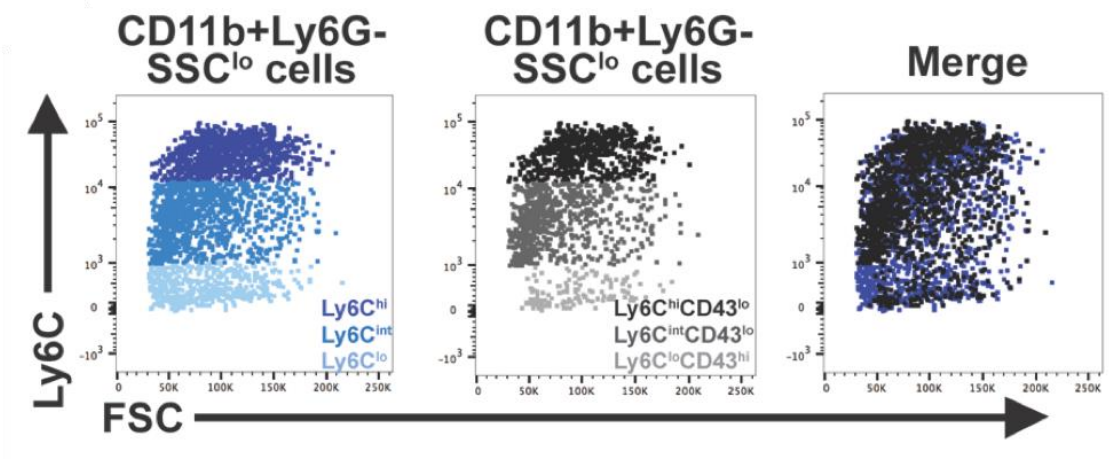

Figure 10. Immunophenotype comparison of monocyte subsets. Ly6C^{hi} and Ly6C^{lo} monocyte populations overlap with Ly6C^{hi}/CD43^{lo} and Ly6C^{lo}/CD43^{hi} monocyte populations, respectively.

At 3 days post-injury, we assayed donor cells for expression of monocyte and macrophage markers (Figure 11C). A very low frequency of CD45.1+CD45.2- cells were detected in digested dorsal tissue (Figure 11D) indicating that few donor cells are present 3 days post-injury. We detected a modest, but insignificant increase in the number of total donor cells (normalized to tissue mass) originating as Ly6C^{lo}CD43^{hi} relative to those adoptively transferred as Ly6C^{hi}CD43^{lo} (Figure 11E). CD301b marks a population of macrophages that appear in the midphase of skin wound healing and are required for effective cutaneous repair[95]. Following adoptive transfer of Ly6C^{hi} monocytes, we found that 80.7±10.4% of donor-derived CD206+F4/80+ macrophages were CD301b+. Similarly, following adoptive transfer of Ly6C^{lo} monocytes, we found that 84.2± 6.4% of donor-derived CD206+F4/80+ macrophages were CD301b+. A greater frequency of

donor-derived wound healing CD301b+CD206+F4/80+ macrophages was detected in animals receiving adoptively transferred Ly6C^{lo}CD43^{hi} monocytes compared to those that received Ly6C^{hi}CD43^{lo} monocytes (Figure 11F). While F4/80 is present on all macrophages, co-expression of CD64 and MerTK exclusively distinguishes macrophages from monocytes[96]. These two populations significantly overlap, as 25.3 ± 2.1% of total F4/80+CD11b+ cells are also CD64+MerTK+, but nearly all CD64+MerTK+ cells are F4/80+ (Figure 12A) and 88.9±1.2% of CD206+F4/80+ cells are also CD64+MerTK+. Similarly, we detected a greater frequency of donor-derived CD301b+CD206+CD64+MerTK+ macrophages in animals receiving adoptively transferred Ly6C^{lo}CD43^{hi} monocytes, supporting the conversion of these monocytes into pro-regenerative macrophages (Figure 12D). No changes in the frequency of CD301b-CD206+F4/80+ (Figure 11G), CD301b-CD206+CD64+MerTK+ (Figure 12E), or total number of macrophages (Figure 12 B, C) were detected between the two grafts. These results further support the hypothesis that circulating non-classical monocytes differentiate into wound repair macrophages.

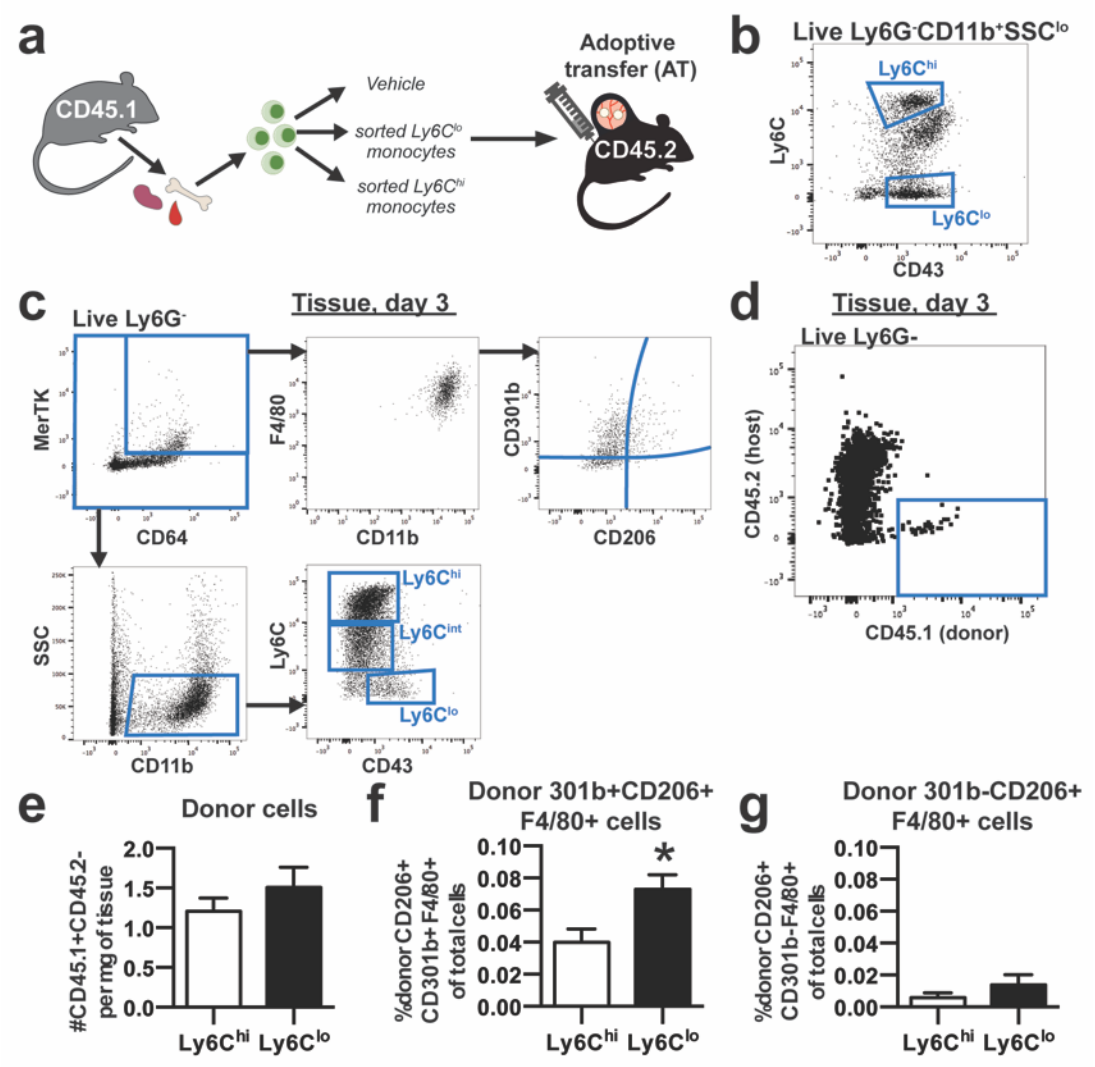

Figure 11. Adoptively transferred non-classical Ly6C^{lo} monocytes differentiate into CD206+ macrophages within inflamed peri-implant tissue. (A) CD45.1+ Ly6C^{hi} or Ly6C^{lo} monocytes sorted from pooled bone marrow, blood, and spleen were adoptively transferred by i.v. injection to CD45.2+ mice at the time of DWC surgery. (B) Monocytes were sorted based on CD11b+SSC^{lo}Ly6G-Zombie- expression and Ly6C^{hi}CD43^{lo} expression or Ly6C^{lo}CD43^{hi} expression. (C) Macrophage subpopulations in dorsal tissue at 3 days post injury were immunophenotyped as MerTK+CD64+ or F4/80+CD11b+ and characterized for CD301b and CD206 surface expression. Monocyte subpopulations in dorsal tissue were immunophenotyped as CD11b+SSC^{lo} and characterized for Ly6C and CD43 surface expression. (D) Donor-derived cells were identified in dorsal tissue 3 days post-injury as CD45.1+CD45.2-. (E) Total donor cells per milligram of tissue in mice receiving Ly6C^{hi} or Ly6C^{lo} monocytes. (F) Frequency of donor-derived CD301b+CD206+ macrophages (CD11b+F4/80+) in mice receiving adoptive transfer Ly6C^{lo} monocytes compared to mice receiving Ly6C^{hi} monocytes. (G) Frequency of donor-derived CD301b-CD206+ macrophages (CD11b+F4/80+). Data presented as mean

± S.E.M. Statistical analyses were performed using two-tailed t-tests *p<0.05, n=5-6 animals per group.

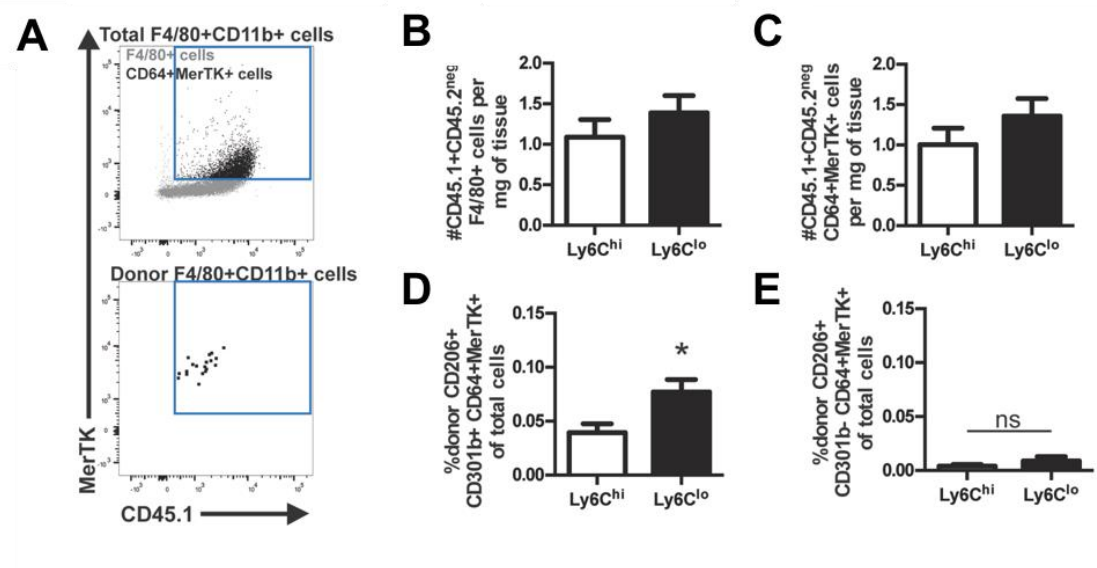

Figure 12. CD64+MerTK+ macrophage population overlaps with F4/80+ macrophage populations. (A) CD64+MerTK+is a more discriminating macrophage population within F4/80+CD11b+ cells. 25.3 ± 2.1% of all F4/80+CD11b+ cells are CD64+MerTK+; however, nearly all donor-derived F4/80+ cells are CD64+MerTK+ (90.0 ± 3.8%). (B) No differences in the number of donor-derived F4/80+ or (C) CD64+MerTK+ macrophages per milligram of tissue were detected in mice receiving adoptive transfer Ly6C^{lo} monocytes compared to mice receiving Ly6C^{hi} monocytes. (D) A higher frequency of donor-derived CD301b+CD206+ macrophages (CD64+MerTK+) were detected in mice receiving adoptive transfer Ly6C^{lo} monocytes compared to mice receiving Ly6C^{hi} monocytes. (E) No differences in the frequency of donor-derived CD301b-CD206+ macrophages (CD64+MerTK+) were detected in mice receiving adoptive transfer Ly6C^{lo} monocytes compared to mice receiving Ly6C^{hi} monocytes. Data presented as mean ± S.E.M. Statistical analyses were performed using two-tailed t-tests *p<0.05, n=5-6 animals per group.

3.4.4 On-site delivery of FTY720 promotes accumulation of CD206+ macrophages.

We have previously demonstrated that localized delivery of the small molecule FTY720 from PLGA thin films enhances the recruitment of Ly6C^{lo} monocytes to inflamed

peri-implant tissue and supports arteriogenesis [34, 97]. We explored the fate of specific blood monocyte populations in response to localized immune modulation by selectively labeling Ly6C^{lo} and Ly6C^{hi} monocytes followed by implantation of FTY720-loaded PLGA films in the DWC.

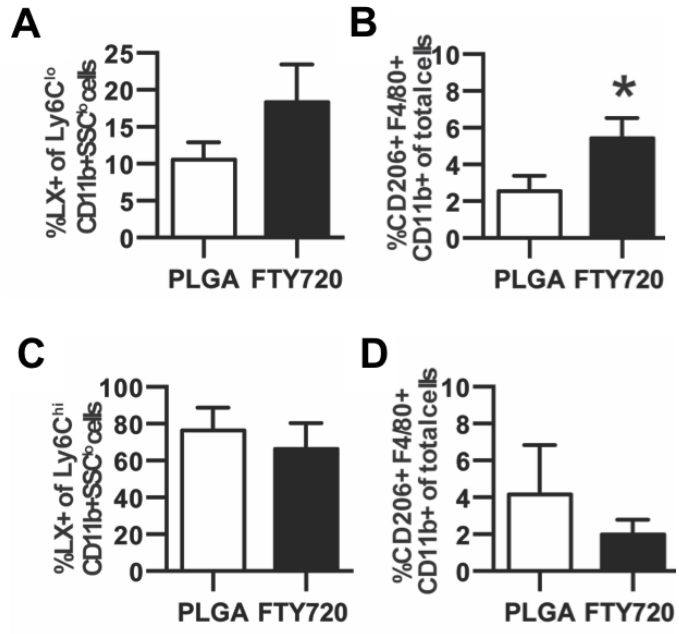

Figure 13. On-site delivery of FTY720 recruits blood-derived non-classical monocytes and increases the frequency of alternatively activated macrophages. PLGA films loaded with FTY720 were implanted immediately after DWC surgery. (A) Proportion of latex bead-positive (LX+) Ly6C^{lo} monocytes that were derived from blood in tissue 3 days post-injury following labeling of Ly6C^{lo} monocytes. (B) Overall frequency of CD206+ macrophages in the presence of FTY720. (C) Proportion of LX+ Ly6C^{hi} monocytes that were derived from blood following labeling of Ly6C^{hi} monocytes with Clod Lip. (D) Overall frequency of CD206+ macrophages in the presence of FTY720 after Clod Lip administration. Data presented as mean ± S.E.M. Statistical analyses were performed using two-tailed t-tests. *$p<0.05$, n=4-10 animals per group.

Though statistically insignificant, a trend of increased frequency of blood-derived Ly6C^{lo} monocytes was observed with on-site delivery of FTY720 compared to blank implant (Figure 13A). FTY720 increased the frequency of CD206+ macrophages within injured tissue 3 days post-surgery (Figure 13B). Selective labeling of Ly6C^{hi} monocytes

demonstrates that FTY720 does not increase the frequency of circulation-derived Ly6C^{hi} monocytes in tissue when Ly6C^{lo} blood monocytes are reduced with clodronate liposomes (Figure 13C). We observed no changes in the frequency of total CD206+F4/80+CD11b+ cells (Figure 13D), suggesting that FTY720 is unable to increase the number of alternatively activated macrophages after reduction of circulating Ly6C^{lo} monocytes.

To investigate the molecular mechanisms of FTY720-mediated recruitment, we probed non-classical monocytes for expression of the sphingosine-1-phosphate receptor 3 (S1PR3), at which FTY720 exhibits agonist activity. We have previously demonstrated that FTY720 requires S1PR3 expression on hematopoietic cells in order to promote arteriogenic remodeling[34]. In addition to Ly6C, CX3CR1 (the fractalkine receptor) can be used to distinguish classical and non-classical blood monocytes[98]. While CXC3CR1 is difficult to detect using antibody-based methods, CX3CR1$^{GFP/+}$ transgenic mice enable real-time assessment of monocyte subset identity. CX3CR1^{hi} monocytes primarily overlap with the Ly6C^{lo} monocyte population, and conversely, CX3CR1^{lo} monocytes are primarily Ly6C^{hi} (Figure 14A). S1PR3 surface expression is selectively higher on CX3CR1^{hi} blood monocytes (Figure 14B, C), which indicates that elevated S1PR3 expression is a signature of non-classical monocytes and is consistent with our previous studies that demonstrated higher S1PR3 mRNA and total protein in Ly6C^{lo} monocytes[34]. Taken together, FTY720 likely increases the tissue content of CD206+ macrophages by recruiting circulating S1PR3^{hi} non-classical monocytes from circulation.

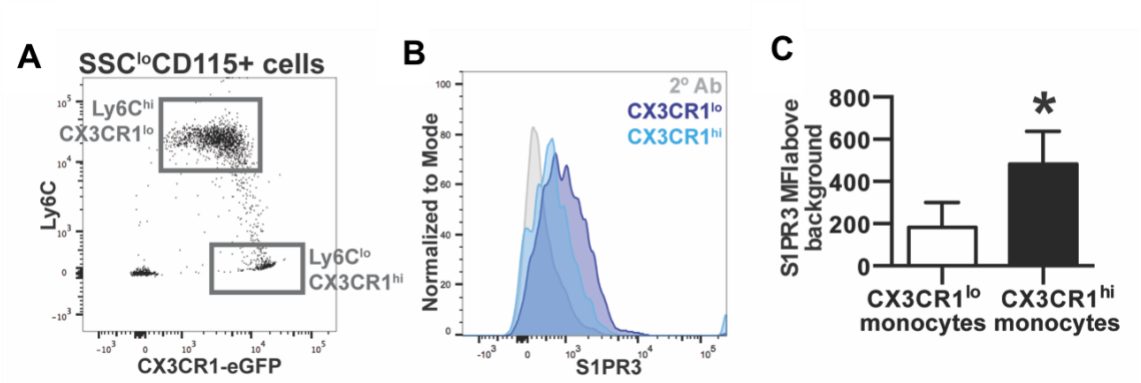

Figure 14. Sphingosine-1-phosphate receptor 3 (S1PR3) expression is upregulated on non-classical monocytes. (A) Ly6C expression in CX3CR1^{hi} monocytes and CX3CR1^{lo} monocytes obtained from the blood of CX3CR1$^{GFP/+}$ mice identify Ly6C^{lo} monocytes and Ly6C^{hi} monocytes, respectively. (B, C) Surface S1PR3 expression in blood CX3CR1^{hi} cells and CX3CR1^{lo} cells. To control for background staining, CX3CR1$^{GFP/+}$ cells were stained with secondary antibody (2º Ab) only, which is shown in the gray histogram. Data presented as mean ± S.E.M. Statistical analyses were performed using two-tailed t-tests. *$p<0.05$, n=4 animals per group.

3.4.5 FTY720 recruits non-classical monocytes that promote vascular network expansion after arteriole ligation.

The recruitment kinetics, fate, and function of myeloid cells during inflammation is heavily dependent on the specific type of tissue injury [30, 33]. Consequently, we sought to determine whether application of FTY720-loaded materials to ischemic muscle injury produces similar patterns of immunomodulation. Feeder arteriolar vessels within the murine spinotrapezius muscle were ligated in CX3CR1$^{GFP/+}$ mice and unloaded or FTY720-loaded PLGA films were implanted over the muscle immediately after injury. We observed a decrease in the overall area of CX3CR1^{hi} cells in FTY720-treated animals 3 days post-injury (Figures 15 A, B). Conversely, we observed more CD206+ cells (Figure 15C) and the area ratio of CD206+ cells to CX3CR1^{hi} cells was higher in FTY720-treated animals (Figure 15D).

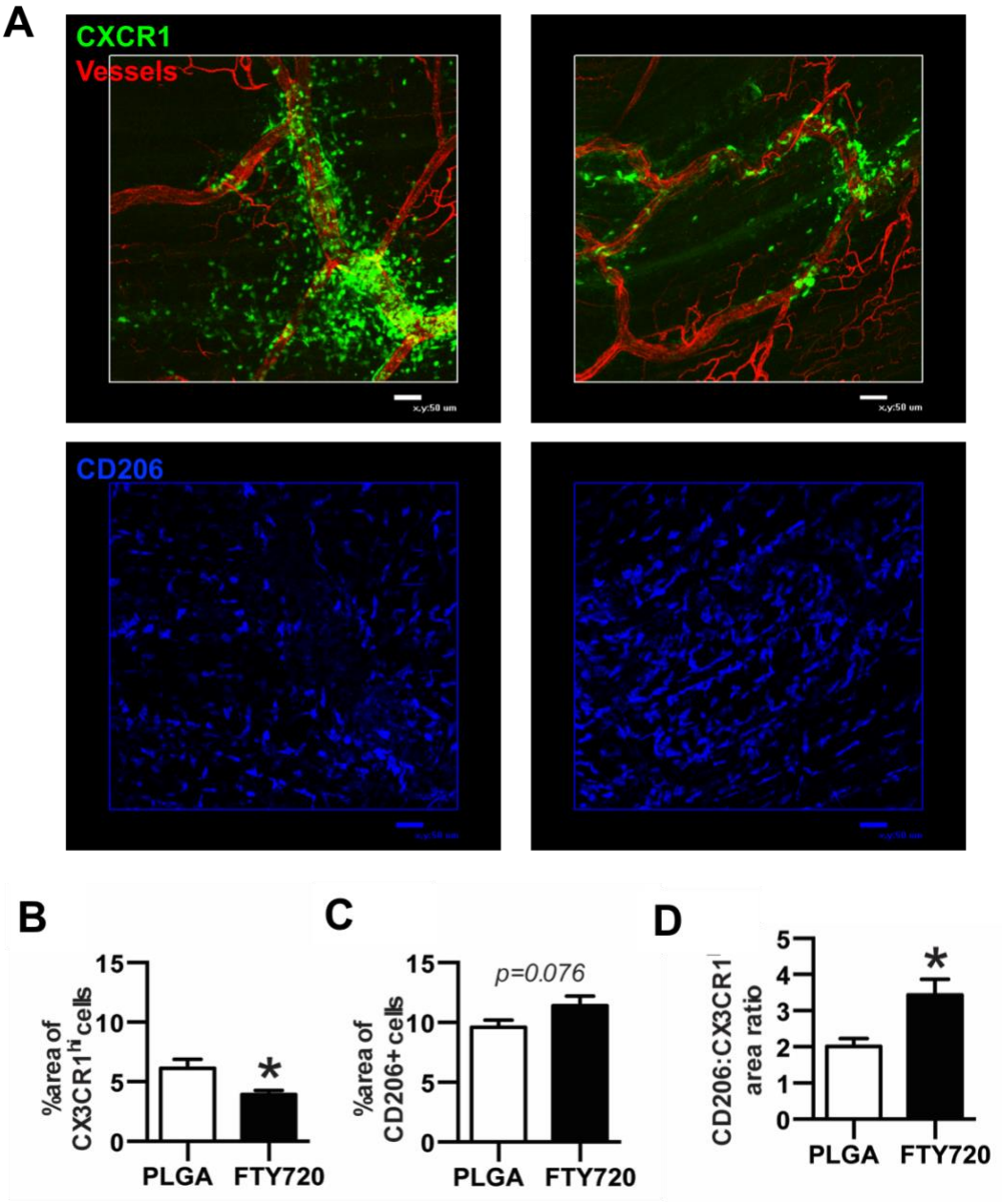

Figure 15. FTY720 increases CD206+ macrophages after arteriole ligation in the spinotrapezius muscle. (A) Immunofluorescence of muscle tissue 3 days after ligation of spinotrapezius muscle arterioles in CX3CR1$^{GFP/+}$ mice shows accumulation of CX3CR1^{hi} monocytes (top) and CD206+ macrophages (blue, bottom) to lectin-stained vasculature 3 days post-ligation. (B) % area of CX3CR1^{hi} cells and (C) CD206+ cells in muscle tissue treated with unloaded PLGA or FTY720-loaded PLGA 3 days post-ligation. (D) Area ratio of CD206+ to CX3CR1^{hi} cells. Data presented as mean ± S.E.M. Statistical analyses performed using two-tailed t-tests. *$p<0.05$, n=25-27 FOVs from 5 animals per group. Scale bars, 50µm.

Previous work has demonstrated that monocytes differentiate into alternatively activated macrophages in vascular niches[70]. We investigated the localization of CX3CR1^{hi} and CD206+ cells with respect to lectin-perfused vasculature. Fewer CX3CR1^{hi} cells (Figure 16A), but more CD206+ cells (Figure 16B) were found within 50µm of blood vessels in FTY720-treated animals, which is consistent with perivascular conversion of non-classical monocytes into alternatively activated macrophages. Additionally, FTY720-treated animals had a greater vessel density and total length of arterioles 3 days after ligation (Figure 16 D-E).

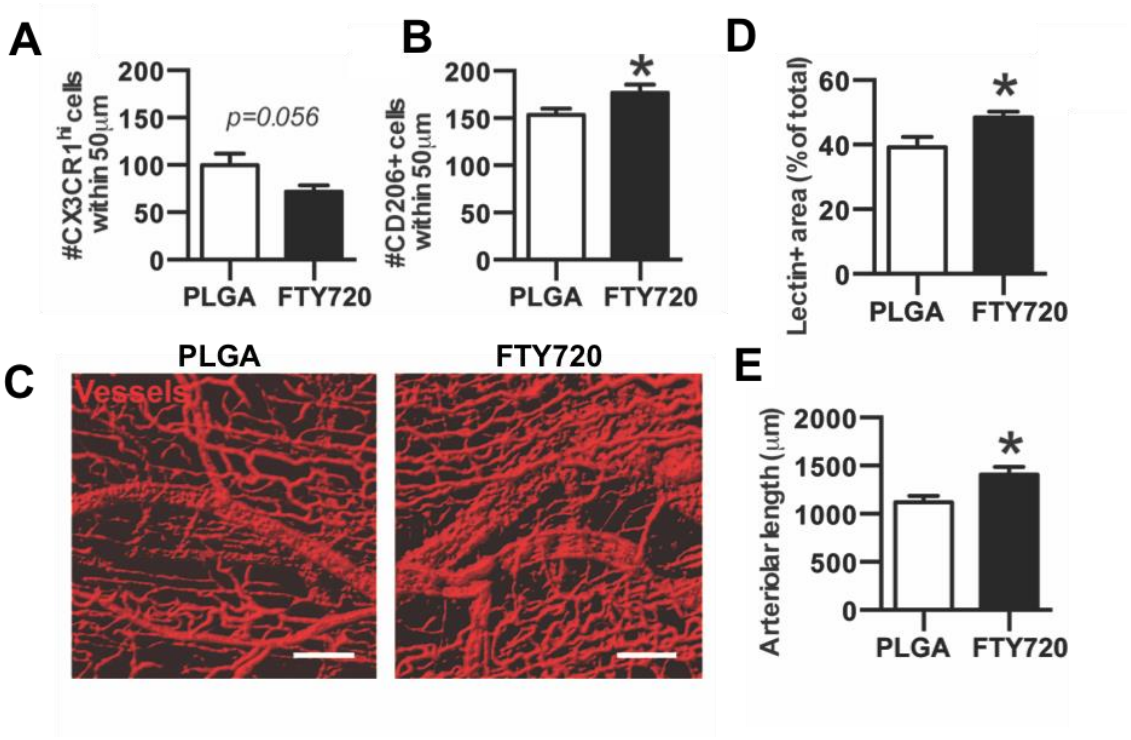

Figure 16. FTY720 promotes vascular network expansion after arteriole ligation in spinotrapezius muscle. (A) Number of CX3CR1^{hi} cells and (B) CD206+ cells within 50µm of blood vessels. (C, D) Total density of lectin+ blood vessels and (E) the length of arterioles in the spinotrapezius muscle treated with FTY720 3 days post-ligation. Data presented as mean ± S.E.M. Statistical analyses performed using two-tailed t-tests. *$p<0.05$, n=25-27 FOVs from 5 animals per group. Scale bars, 100µm.

3.5 Discussion

Monocytes are blood-borne mononuclear phagocytes that support tissue homeostasis and exit the vasculature at increased rates to differentiate into macrophages during inflammation. The precise relationship of circulating classical and non-classical monocyte subsets to defined macrophage populations remains unknown. We have shown that after skin wounding and biomaterial implantation, circulating non-classical S1PR3^{hi} monocytes extravasate into inflamed tissue and serve as biased progenitors of CD206+CD301b+ wound healing macrophages. Previous work has demonstrated that classical monocytes directly convert to non-classical monocytes and macrophages within inflamed tissue[29, 89]. Therefore, these studies elucidate a complementary role for non-classical monocytes and argue that these cells primarily differentiate into alternatively activated macrophages. Biomaterial-mediated strategies that increase recruitment of non-classical monocytes through S1PR signaling are a promising strategy to increase accumulation of alternatively activated, wound healing macrophages (Figure 7).

Intravascular non-classical Ly6C^{lo} monocytes orchestrate the disposal of necrotic endothelial cells after activation with TLR7-targeted danger signals during inflammation[12, 99], whereas extravascular Ly6C^{lo} monocytes can promote angiogenesis and matrix remodeling via secretion of VEGF and matrix metalloproteinases[33]. The unique protein signature of non-classical monocytes, characterized by higher VEGF, TGFβ, and IL-10, and lower TNFα and IL-1β expression compared to classical monocytes has resulted in the suggestion that these cells may constitute a class of "anti-inflammatory" monocytes[29, 33]. Previous studies have indicated that Ly6C^{lo} monocytes in inflamed tissues such as skeletal muscle and focal hepatic injury are derived from cells recruited as

Ly6C^{hi} monocytes from the blood and are converted *in situ* to Ly6C^{lo} monocytes to promote wound healing and tissue repair[29, 89]. Other reports suggest that Ly6C^{lo} monocytes are directly and robustly recruited from the blood, leading to extravascular accumulation during inflammation[12, 33, 35]. While we observed that blood-derived Ly6C^{hi} monocytes enter inflamed tissue, reduce Ly6C expression (Figure 6A), and differentiate into macrophages (Figure 6 B,C), our studies indicate that Ly6C^{lo} monocytes are also directly recruited from circulation to injured tissues and able to give rise to macrophages (Figure 6). Previous studies have indicated that adoptively transferred Ly6C^{lo}MHCII^{-} monocytes do not infiltrate the skin[13], but this may be a result of differences in the grafted cell population (Ly6C^{lo}MHCII^{-} monocytes vs. Ly6C^{lo}CD43^{hi} monocytes in our studies) or inflammatory stimuli (LPS injection vs. excisional skin injury). Though we observed a decrease in Ly6C^{lo} blood monocytes after clodronate liposome administration, we did not detect a difference in the frequency of Ly6C^{lo} monocytes within injured skin. Many studies have shown that Ly6C^{hi} monocytes can convert to Ly6C^{lo} monocytes in the blood or tissue[22, 29, 31]. Similarly, our data may reflect that, in the absence of Ly6C^{lo} monocytes, circulation-derived Ly6C^{hi} monocytes compensate and increase their rate of conversion into Ly6C^{lo} monocytes in inflamed tissue.

An important finding of our work is that circulating Ly6C^{lo} monocytes preferentially contribute to the CD206+ wound macrophage pool within skin injury compared to Ly6C^{hi} monocytes. Analysis of peri-implant tissue for recruited latex bead-labeled Ly6C^{lo} monocytes shows that this subset is predisposed to acquire a CD206+ alternatively activated M2-like[100] macrophage phenotype (Figure 6C). Administration of clodronate liposomes enables selective labeling of Ly6C^{hi} monocytes, while

simultaneously reducing the frequency of Ly6C^{lo} monocytes for 2-7 days after administration[22, 93]. Clodronate liposome-treated animals displayed no change in the frequency of overall macrophages within the skin injury after 3 days, but exhibited a decrease in the proportion of CD206+ macrophages (Figure 8C). Because tissue monocyte composition was unaffected by clodronate liposomes, these results may reflect a delay in generation of CD206+ macrophages. We cannot exclude the possibility that transient monocyte depletion alters myeloid cell responses and recruitment during inflammation, as monocyte subsets are known to communicate with each other[17].

Latex bead-based labeling strategies are useful because they overcome many of the limitations of adoptive transfer, including *ex vivo* cell manipulation, pooling of donor cells, and low sensitivity due to poor cell recovery[101]. Importantly, there is no evidence that these labeling techniques alter monocyte recruitment or systemic inflammation[101]. However, our interpretation of these studies relies on retention of latex beads within the cell that was originally labeled and no transfer to other cells. Therefore, cell tracking is best performed by use of complimentary tracking methods, including adoptive transfer, selective labeling techniques, and transgenic or knockout mice. We adoptively transferred $5.55x10^5$ CD45.1+ Ly6C^{hi} or Ly6C^{lo} monocytes by intravascular injection into CD45.2 mice at the time of DWC surgery. We did not detect differences in the total number of CD45.1+ donor-derived cells per milligram of dorsal tissue between the two monocytes grafts, and further probed for markers of macrophage differentiation and polarization within donor cells. CD301b+CD206+ macrophages drive midstage skin regeneration by promoting fibroblast repopulation, cellular proliferation, and re-epithelialization[95]. In our adoptive transfer studies, a higher frequency of donor Ly6C^{lo} monocytes acquired a

CD301b+CD206+ macrophage phenotype compared to donor Ly6C^{hi} monocytes (Figure 11F), indicating that circulation-derived Ly6C^{lo} monocytes may be intrinsically predisposed to convert to dermal wound healing macrophages. Conversely, there was no difference in the frequency of donor-derived CD301b-CD206+ or number of total macrophages between mice receiving Ly6C^{hi} or Ly6C^{lo} monocytes (Figure 11G, Figure 12). These data, along with the observation that FTY720 administration increases CD206+ macrophages within injured skin (Figure 13), further supports the hypothesis that non-classical monocytes undergo local conversion into alternatively activated macrophages.

While macrophages are key mediators of the host response to implanted materials that govern the integration of implants into host tissue[102, 103], the role that their monocytic precursors play in regulating implant outcome has been largely unexplored. In our studies, around 45% of monocytes surrounding PLGA implants were Ly6C$^{lo/int}$. In previous work[67], we demonstrated that around 40% of monocytes around heparin-containing PEG hydrogels were Ly6C$^{lo/int}$. While lymphocyte, granulocyte, and macrophage accumulation are impacted by the type of material implanted[104], future studies are needed to determine how different classes of materials impact infiltration of monocyte and macrophage subsets. Interestingly, we observed model-specific differences in the kinetics of monocyte recruitment during FTY720 delivery. While FTY720 increases the frequency of Ly6C^{lo} monocytes 3 days after skin wounding[34] (Figure 13A), we observed a decrease in CX3CR1^{hi} monocytes 3 days after arteriole ligation in the spinotrapezius muscle (Figure 15B). The progression of inflammation may be expedited during ischemia because of the need to rapidly restore blood supply and oxygen transport. FTY720 increases the frequency of F4/80+CD206+ macrophages both in wounded skin

(Figure 13B) and CD68+CD206+ macrophages in ischemic muscle (Figure 15C). Previously, we have detected more M2-like macrophages within mandibular bone defects 3 weeks after implantation of FTY720-loaded polymer nanofibers[61]. Taken together, these findings suggest that FTY720 delivery from different biomaterials can enhance pro-regenerative myeloid cell recruitment, but the kinetics may vary depending on the type of injury.

We found that ischemic muscles treated with FTY720 have increased numbers of perivascular CD206+ cells located (Figure 16B), which coincided with increased arteriolar length and total vessel density (Figure 16C-E). FTY720 likely acts on both immune cells and the endothelium, as loss of S1PR3 in hematopoietic or parenchymal cells impairs FTY720-induced arteriogenic remodeling[34]. Delivery of FTY720 similarly induced both increased accumulation and perivascular localization of alternatively activated macrophages after volumetric muscle loss, which was accompanied by enhanced re-vascularization and muscle healing[105]. Consequently, both the phenotype of monocytes and macrophages, as well as their spatial distribution is likely an important feature when assessing their function.

3.6 Conclusions

Taken together, our studies shed light on the functions of non-classical monocytes during inflammation and wound healing. Monocytes and macrophages are increasingly appreciated for their roles in regulating tissue homeostasis and coordinating repair after damage. Acute modulation of the inflammatory response has been shown to regulate repair of tissue at longer time scales, including bone[61] and skeletal muscle[29]. An

understanding of the origin of monocyte and macrophage populations during wound healing and the cues governing their *in situ* fate is critical to harnessing endogenous mechanisms of repair. The work in this chapter establishes non-classical monocytes as biased progenitors of alternatively activated wound healing macrophages. We will leverage this knowledge in the next two chapters to develop next-generation immunoregenerative biomaterials capable of finely tuning the inflammatory response within volumetric skeletal muscle injury.

4. SELECTIVE RECRUITMENT OF NON-CLASSICAL MONOCYTES PROMOTES SKELETAL MUSCLE REPAIR [3]

4.1 Abstract

Regeneration of traumatic defects in skeletal muscle requires the synchronized behavior of multiple cells that participate in repair. The inflammatory cascade that is rapidly initiated after injury serves as a powerful node at which to guide the progression of healing and influence tissue repair. Here, we examine the role that myeloid cells play in the healing of traumatic skeletal muscle injury, and leverage their pro-regenerative functions using local delivery of the immunomodulatory small molecule FTY720. We demonstrate that increasing the frequency of non-classical monocytes in inflamed muscle coincides with increased numbers of CD206+ alternatively activated macrophages. Animals treated with immunomodulatory materials had greater defect closure and more vascularization in the acute phases of injury. In the later stages of repair, during which parenchymal tissue growth occurs, we observed improved regeneration of muscle fibers and decreased fibrotic tissue following localization of pro-regenerative inflammation. These results highlight non-classical monocytes as a novel therapeutic target to improve the regenerative outcome after traumatic skeletal muscle injury.

[3] Portions of this chapter adapted from: San Emeterio CL, Olingy CE, Chu Y, Botchwey EA. Selective recruitment of non-classical monocytes promotes skeletal muscle repair. Biomaterials. 2017;117:32-43. License No. 4143750636563

4.2 Introduction

Recovery of traumatic skeletal muscle injury relies on precise regulation of the inflammatory cascade that is initiated immediately after injury. While muscle progenitor cells called satellite cells directly differentiate into muscle fibers to regenerate injured skeletal muscle [5], their success is dependent on supportive cues from innate immune cells, such as monocytes and macrophages, that are acutely recruited to damaged tissue and remain until repair is complete [29, 37, 41]. Monocytes and macrophages are phagocytes that are highly sensitive to inputs from their microenvironment and can synthesize this information to direct healing processes [59, 89]. *In vivo*, monocyte subsets appear sequentially after injury, with classical, inflammatory monocytes accumulating in the muscle after the onset of injury and peaking at around one day post-injury [29]. Non-classical, anti-inflammatory monocytes numbers steadily rise thereafter, and return to baseline once regeneration is complete [29]. Monocyte recruitment following the onset of injury is crucial for repair, as multiple studies have shown that depletion of circulating monocytes before toxin-induced muscle injury results in incompletely healed, fibrotic muscle [29, 37, 41].

Following extravasation from blood, recruited monocytes may transiently remain monocytes [56] or differentiate into macrophages that persist through the resolution of inflammation [29, 42, 88]_ENREF_6. Macrophages designated as classical inflammatory "M1" macrophages predominate early after injury, while alternatively-activated "M2" macrophages (AAMs) orchestrate the later phases of tissue repair. Inflammatory macrophages respond to tissue damage signals and upregulate genes associated with alarmins and acute inflammatory-phase proteins [106]. Later during the inflammatory

response, AAMs are a potent source of insulin-like growth factor (IGF-1) required for muscle regeneration [48] and highly express genes encoding extracellular matrix (ECM) and ECM remodeling proteins [106]. Though some resting tissues such as the lung, liver, and brain have macrophage populations that are seeded embryonically [15, 17], skeletal muscle possesses very few macrophages during homeostasis [29]. Upon inflammatory insult, circulating classical monocytes are recruited to muscle injury and substantially contribute to the wound macrophage pool [29]. However, whether non-classical monocytes are directly recruited to volumetric skeletal muscle injury or play a role in repair remains unknown.

Knowledge of how different myeloid populations affect tissue micro-compartments within injured muscle is especially important in a volumetric defect context in which all tissue architecture must be regenerated *de novo*. Deposition of new ECM provides scaffolding for nascent vasculature [107], and AAMs have been shown to control collagen fibril formation in regenerating skin [53] and promote ECM deposition by fibroblasts [54]. However, the unchecked activity of AAM in chronic muscle inflammation can perpetuate fibrosis [55], which impairs restoration of native mechanical properties [108]. Muscle tissue must also be revascularized in order to provide necessary oxygen, nutrients, and metabolic waste removal. AAMs promote angiogenesis [63, 65] and arteriogenesis [109], distinct processes that regulate post-injury vascular remodeling. Additionally, failure to reinnervate skeletal muscle after injury results in muscle fiber atrophy [110] that significantly impairs motor function. Increasing AAMs in peripheral nerve transections by hydrogel-based delivery of IL-4 enhances both Schwann cell infiltration and axonal growth [111]. Consequently, biomaterial-based strategies that increase the number of AAMs

within volumetric muscle loss are a promising approach to enhance endogenous programs of muscle repair.

Sphingosine-1-phosphate (S1P) is a pleiotropic bioactive signaling lipid that is produced endogenously by red blood cells, platelets, and endothelial cells [112]. S1P activates signaling through five known G protein-coupled receptors, S1PR1-5, which are differentially expressed in almost every cell type. We have previously demonstrated that non-classical anti-inflammatory Ly6C^{lo} monocytes express relatively high levels of S1PR3, which they leverage to exert pro-regenerative effects *in vivo* [113]. Local delivery of FTY720, a small molecule agonist of S1P1 and S1PR3-5, selectively recruits non-classical Ly6C^{lo} monocytes upon local delivery to inflamed skin injuries and promotes arteriogenic microvascular growth in an S1PR3-dependent manner. Release of FTY720 from polymer nanofibers to mandibular bone defects increases the frequency of AAMs, promotes re-vascularization, and facilitates boney ingrowth [61]. Thus, S1PR3 has emerged as a therapeutic target that can orchestrate the inflammatory response and subsequent healing of musculoskeletal injuries.

In this work, we explore the role of specific monocyte and macrophage populations after volumetric muscle loss. Using a novel model of volumetric muscle injury within the murine spinotrapezius muscle, we demonstrate that biomaterial-based delivery of FTY720 increases anti-inflammatory Ly6C^{lo} monocytes and amplifies the number of CD206+ AAMs. The localization of pro-regenerative inflammation in the injured skeletal muscle increases the kinetics of wound healing, leading to earlier vascularization and collagen deposition. Additionally, we observed improved regrowth of muscle fibers at later time points and less fibrotic collagen architecture within regenerated tissue. These results

indicate that immunomodulatory biomaterials that target specific monocyte populations can coordinate favorable healing outcomes within volumetric skeletal muscle injuries.

4.3 Materials and Methods

4.3.1 Film fabrication

Films were fabricated as previously described [113]. Briefly, 350 mg PLGA (50:50 DLG 5E – Evonik Industries) was added to 2 ml dichloromethane in a glass scintillation vial and vortexed on high-speed for 30 minutes. For drug loaded films, 1.75 mg of FTY720 (Cayman Chemical) was added at a 1:200 drug:polymer weight ratio, and polymer solution was vortexed until completely incorporated. The polymer solutions were then poured into Teflon-coated petri dishes and dried at -20°C for 7 days. Films were lyophilized overnight before implantation to remove any traces of solvent.

4.3.2 Spinotrapezius volumetric muscle loss model

All animal procedures were conducted according to protocols approved by the Georgia Institute of Technology Institutional Animal Care and Use Committee. Male C57BL/6J (The Jackson Laboratory) or B6.129P-Cx3cr1tm1Litt/J mice ($CX3CR1^{GFP/+}$) (The Jackson Laboratory) of age 8-12 weeks old were used for all animal studies. A 1mm full thickness defect in the spinotrapezius muscle was created as follows. The dorsum of the mouse was shaved and hair removal cream applied to completely remove hair. Skin was sterilized with three washes of 70% ethanol and chlorhexidine. A longitudinal 1 inch incision (cranial to caudal) was made just after the bony prominence of the shoulder blade. The overlying fascia was dissected away and the spinotrapezius muscle identified. Using

flat-tipped tweezers, the edge of the spinotrapezius was lifted up. The muscle was reflected and positioned against a sterile piece of wood. A 1mm biopsy punch was made through the muscle, using the wooden piece as support. The muscle was replaced and 1.5 mm implant placed over the punch defect. The incision was closed with mouse wound clips.

4.3.3 RAW264.7 macrophage and C2C12 myoblast culture and immunohistochemistry

RAW264.7 macrophages (ATCC) were maintained in growth media (DMEM supplemented with 10% fetal bovine serum (FBS), 1% sodium pyruvate, 1% L-glutamine, 1% penicillin/streptomycin) according to manufacturer protocols. To generate RAW 264.7 macrophage conditioned media (CM), RAW 264.7 macrophages were treated 18 hours with polarization cytokines. For M(IFN-γ, LPS) polarization, cells were treated with 1μg/ml LPS (Sigma) and 20 ng/ml IFN-γ (Peprotech). For M(IL-4) polarization, cells were treated with 10 ng/ml IL-4 (Peprotech). Polarization media was removed after treatment, cells were washed with phosphate-buffered saline (PBS), fresh RAW264.7 media was replaced into the wells. Cells were allowed to condition media for an additional 24 hours.

C2C12 cells (ATCC) were maintained in growth media (DMEM supplemented with 10% FBS, 1% sodium pyruvate, 1% L-glutamine, 1% penicillin/streptomycin) according to manufacturer protocols. To investigate the effects of polarized macrophage soluble factors on C2C12 myogenic differentiation, C2C12 cells were cultured on fibronectin-coated glass coverslips in 50% C2C12 differentiation media (DMEM supplemented with 2% horse serum, 1% sodium pyruvate, 1% L-glutamine, 1% penicillin/streptomycin), and 50% RAW 264.7 CM for 5 days, with daily media change. At the 5 day timepoint, cells were fixed in

4% paraformaldehyde (PFA), permeabilized with 0.1% Triton-X, and blocked using 5% goat serum for 1 hour. Cells were stained with myosin heavy chain antibody (MF-20, DSHB) overnight at 4°C in humidity chamber. Cells were washed, then stained with Dylight 488-conjugated anti-chicken antibody for 1 hour at room temperature. Cells were washed, counterstained with DAPI, then overturned onto glass slides with Vectashield mounting media (Vector Labs). Cells were imaged on a Zeiss LSM 700 confocal microscope. A total of 12 field of views (640.2μm x 640.2μm) were used for histomorphometric analysis of myosin heavy chain-positive cells.

4.3.4 Labeling of blood Ly6C^{lo} monocytes in CX3CR1$^{GFP/+}$ mice

In order to visualize cells within injured muscle originating as circulating Ly6C^{lo} monocytes, CX3CR1^{GFP}/+ mice were administered Fluoresbrite® Polychromatic Red latex beads (0.5μm, Polysciences) intravenously 1 day prior to surgery via jugular vein injection. Prior to injection, latex beads were diluted 1:25 in sterile saline as previously described [101]. Labeling was confirmed by retro-orbital blood draw immediately prior to surgery (1 day after bead administration) and subsequent flow cytometry analysis.

4.3.5 Flow cytometry

To collect blood (days 0, 3 and 7) and tissue for flow cytometry analysis (days 1, 3, and 7), mice were euthanized via CO_2 asphyxiation. Blood was then collected via cardiac puncture. Red blood cells were lysed in ammonium chloride (1 part blood, 9 parts ammonium chloride) prior to immunostaining for flow cytometry. For characterization of myeloid cell composition in spinotrapezius muscles without an implant, a 6mm biopsy punch of muscle tissue centered on the defect was taken. For studies with an implant (unloaded or FTY720-

loaded), the entire spinotrapezius muscle was collected. Spinotrapezius muscles were harvested and digested in collagenase I (Sigma) for 45 minutes at 37°C. The digested muscles were filtered through a cell strainer to obtain a single cell suspension. The standard recovery of cells from a 6mm biopsy of the spinotrapezius muscle is 5501±1965 cells/mg tissue (measured in similar, but unrelated studies). Single-cell suspensions from were stained for flow cytometry analysis in 3% FBS according to standard procedures and analyzed on a FACS AriaIIIu flow cytometer (BD Biosciences). The following antibodies were used for cell phenotyping: BV510-conjugated anti-CD11b (BioLegend), PerCP eFluor-710-conjugated anti-CD115 (eBioscience), APC-Cy7 conjugated anti-CD11b (BioLegend), BV421-conjugated anti-CD11c (BioLegend), APC conjugated anti-Ly6C (BioLegend), PE-Cy7 conjugated anti-GR-1 (BioLegend), BV711-conjugated anti-CD64 (BioLegend), PE-conjugated anti-MerTK (R&D Systems), APC-Cy7-conjugated anti-Ly6G (BioLegend), PE-Cy7-conjugated anti-CD206 (BioLegend).

4.3.6 Whole mount immunohistochemistry of muscle tissue

Mice were euthanized 3 or 7 days after surgery via CO_2 asphyxiation. For lectin-based labeling of the vasculature in CX3CR1$^{GFP/+}$ mice, Alexa Fluor 568 isolectin IB4 (1mg/mL, Life Technologies) was diluted (50µL of isolectin, 150µL saline) and administered by jugular vein injection 15 minutes prior to euthanasia. Post-euthanasia, mouse vasculature was perfused with warm saline followed by 4% PFA until tissues were fixed. The entire spinotrapezius muscle was explanted and permeabilized overnight with 0.2% saponin, then blocked overnight in 10% mouse serum. For immunofluorescence, tissues were incubated at 4˚C overnight in a solution containing 0.1% saponin, 5% mouse serum, 0.5% bovine serum albumin, and the following conjugated fluorescent antibodies: PE anti-CD31

antibody (1:100 dilution, eBioscience), Alexa Fluor 488 anti-CD206 (1:200 dilution, ABD Serotec), and Alexa Fluor 647 anti-CD68 (1:200 dilution, ABD Serotec). For desmin immunostaining, identical tissue processing procedures were followed and muscles were incubated overnight with Alexa Fluor 488 anti-desmin (1:200 dilution, Abcam) alone or in combination with PE anti-CD31 and Alexa Fluor 647 anti-CD206 (1:200 dilution, BioLegend). Following immunostaining, tissues were washed 4 times for 30 minutes each, and then mounted in 50/50 glycerol/PBS.

4.3.7 Imaging and quantification of whole mount immunohistochemistry

Tissues were imaged on a Zeiss LSM 710 NLO confocal with acquisition parameters kept identical across all animals. For collagen imaging, a two-photon chameleon laser (tuned to λ=810nm) and collection range of 380-420nm was utilized with acquisition parameters kept identical across animals. Z-stacks were collected from the beginning to end of collagen signal visible across the entire x-y plane analyzed. Max intensity projections were generated from 3D confocal images for 2D analysis in Zen software (Zeiss). Quantification of vascularization and collagen deposition was performed in ImageJ software (NIH). An elliptical region of interest (1.370mm high by 1.778mm wide) was centered over each defect and the image was thresholded to display only areas of positive fluorescence signal. The number of pixels positive for the fluorescence channel of interest was normalized to the total area of the region of interest. In Figures 1 and 6, defect area was determined by tracing the edges of desmin-positive immunostaining to outline the desmin-negative area. The defect area was identified as the area that was desmin-negative. In Figure 5, the percentage of cell infiltration was determined by tracing the border between lectin- or CD31-positive regions and the avascular zone. The area of this region was measured. A

secondary trace between the cellular (CX3CR1+ or CD206+) region and acellular zone was made. The area of this region was measured and subtracted from first measurement to measure the region of cell infiltration into the defect. This value was normalized to the first measurement. In Figure 6, "void area" was measured by tracing the edges of collagen-positive signal and identifying void area as the area that is collagen-negative. 2D fiber diameter was determined by measuring the widest portion of each regenerated muscle fiber (determined based on the morphology of desmin-positive regions) within the defect region from the day 7 2D maximum intensity projections.

For 3D analysis in Imaris (Bitplane), 1 crop per animal of 332x332μm was taken from the area adjacent to the defect to show immune cell distribution in the close surrounding tissue. Crops were chosen based on matching anatomical vessel morphology from both $CX3CR1^{GFP/+}$ images and the subsequently stained CD206, CD68, and CD31 images. Simultaneous visualization of CX3CR1-GFP cells with immunohistochemical markers is not possible due to leakage of GFP from the cells following permeabilization. Therefore, imaging of CX3CR1-GFP spinotrapezius muscles occurred immediately after perfusion fixation and further immunostaining was performed as described in the previous methods section. Cells co-expressing CD68 and CD206 were identified in Imaris using the surface tool. CD68+ surfaces were identified by smoothing with a 1.5μm grain size and an automatic threshold on absolute intensity. Touching objects were split using a seed points diameter of 13.8μm. Cells that co-expressed two markers were identified by applying an additional filter to select surfaces with a high fluorescence intensity in the CD206 channel (above 17.7 mean intensity). Vessels were identified in Imaris by drawing a surface on the CD31 fluorescent channel with a 1.66μm grain size, manually-selected threshold value

(determined based on each image), and manually-selected volume filter to remove small debris. To calculate the distance between CD68+CD206+ cells and the nearest blood vessel, a distance transformation was applied to CD31+ vessel surfaces and the median position of each CD68+CD206+ cell within this plane was recorded.

4.3.8 Statistical analysis

Data are presented as mean ± standard error of the mean (S.E.M.), unless otherwise noted. All statistical analysis was performed in GraphPad Prism software. For pairwise comparisons, unpaired t-test (according to experimental design) with Welch's correction if variance was significantly different was used. For grouped analyses, two-way ANOVA with Sidak's post-test was used for multiple comparisons. Unless otherwise noted, $p<0.05$ was considered statistically significant.

4.4 Results

4.4.1 Full-thickness defect in the murine spinotrapezius muscle results in dynamic myeloid cell kinetics both locally and systemically.

In order to better model clinical muscle loss induced by trauma or surgery, we developed a novel model of volumetric muscle loss (VML) in the murine spinotrapezius (Figure 1A). The spinotrapezius muscle is a stabilizing muscle in the mouse dorsum that is extremely thin (60-200μm) [114, 115], enabling the use of three-dimensional (3D) confocal microscopy to examine tissue microstructures. A 1mm circular defect in the spinotrapezius muscle heals over the course of 7 days, as observed by desmin immunostaining of muscle fibers (Figure 17).

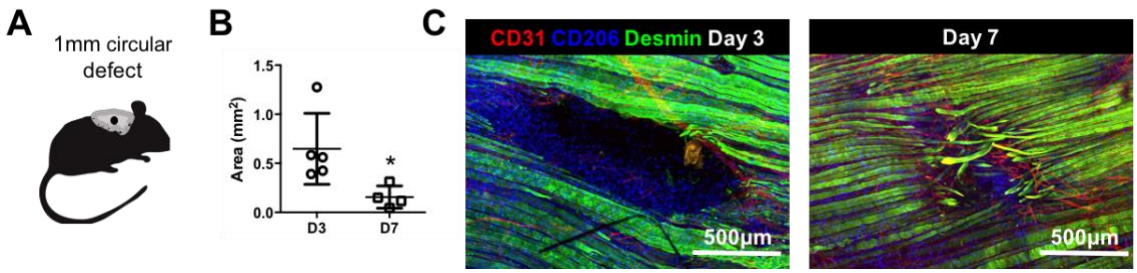

Figure 17. Volumetric muscle loss in the murine spinotrazpeius. (A, B) A 1 mm circular volumetric defect made in the spinotrapezius of wildtype mice heals over 7 days, as quantified by (C) desmin immunostaining. Data presented as mean ± S.E.M. Statistical analyses were performed using two-tailed t-tests. *$p < 0.05$, $n = 4–5$ animals per group.

Consequently, removal of a 1mm diameter muscle defect is not critical-sized, but enables investigations into the mechanisms, rate, and quality of muscle repair. We examined healing at the defect edge, specifically focusing on granulation tissue formation and myofiber ingrowth.

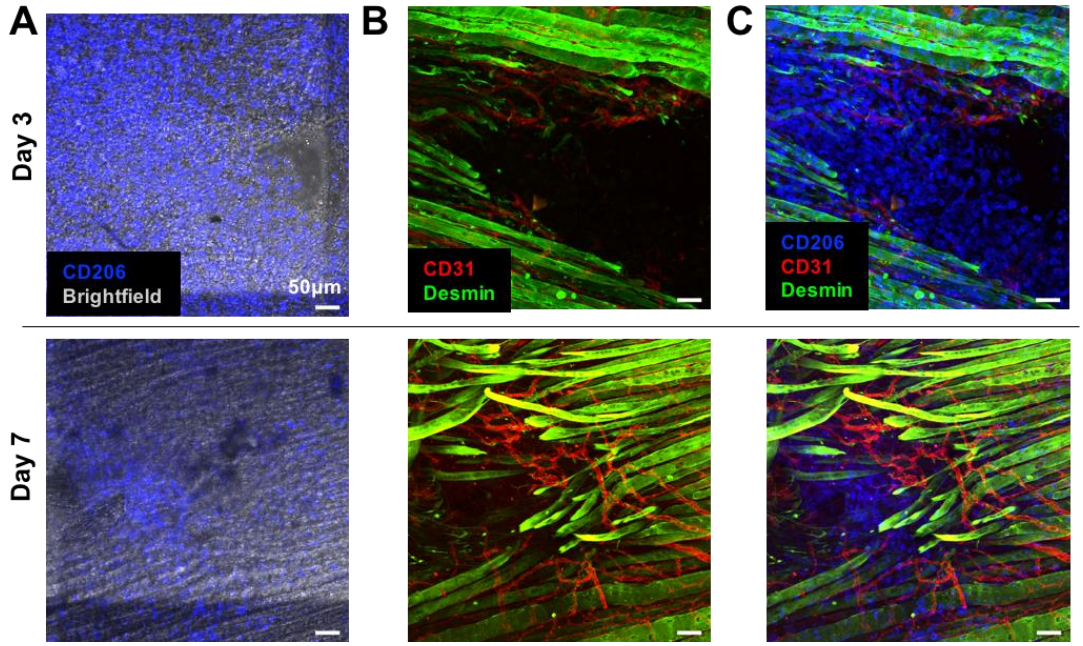

Figure 18. VML in the murine spinotrapezius enables study of cellular interactions during muscle healing. A) High-powered 3D images show granulation tissue under brightfield microscopy at days 3 and 7 post-injury, coinciding with accumulation of

immunostained CD206+ cells. (B) Revascularization (shown by CD31 immunostaining) occurs along the defect edge. (C) Merged 3D images show the distribution of CD206+ cells among muscle fibers and revascularized muscle tissue.

Granulation tissue was defined as tissue lacking desmin+ mature muscle fibers, but including CD31+ and CD206+ immunostaining, as the proliferative phase of the wound healing response involves angiogenesis and the presence of fibroblasts and macrophages, the latter of which can express CD206 and play an active role in repair [52, 59, 116]. High power images of the defect edge reveals granulation tissue containing CD206+ cells, indicating the presence of AAMs (Figure 18A). CD31 immunostaining reveals vessel regrowth within the granulation tissue, with CD206+ cells interacting closely with nascent vasculature. This revascularization appears to occur before the regrowth of desmin+ muscle fibers at day 7 (Figure 18B, C).

We then investigated the kinetics of myeloid cell trafficking in response to spinotrapezius VML injury. The phenotypic complexity of myeloid cells during inflammation necessitates understanding baseline healing conditions in order to design therapies that leverage their behavior. Blood neutrophils were transiently elevated roughly 5 fold from baseline 3 days after VML injury (11.9±2.7% at day 3 vs. 2.1±0.8% at day 0, mean±SD as a percentage of all cells), and subsequently decreased (Figure 19A). Blood classical Ly6C^{hi} monocytes slowly increased over 7 days (1.0±0.3% at day 0 compared to 3.8±1.6% at day 7), while blood non-classical Ly6C^{lo} monocytes increased more rapidly from baseline by 3 days (2.6±0.8% at day 0 to 8.5±1.6%) and plateaued at 7 days post-injury (Figure 19B). Within injured spinotrapezius muscle tissue, neutrophils peaked at 3 days post-injury (0.7±0.2% of all cells) and quickly decreased to baseline levels by 7 days

post-injury (0.1±0.3%) (Figure 19C). Ly6C^{hi} monocytes decreased from days 1 (0.7±1.2%) to 7 (0.3±0.5%), while Ly6C^{lo} monocytes peaked at day 3 (1.5±0.9%) post-injury and were retained at a similar frequency at day 7 (Figure 19D). MerTK and CD64 exclusively identify macrophages (MerTK+CD64+) [117], which steadily increase from day 1 (0.5±0.6%) to day 7 (3.0±1.0%) (Figure 19E). CD206+ macrophages also similarly increase over time (0.4±0.6% at day 1 to 2.8±1.0% at day 7) (Figure 19F). Other cells involved in wound healing may express CD206, including fibrocytes [118] and immature dendritic cells [119], but further immunophentoyping of these cells is necessary to identify other CD206+ populations within injured skeletal muscle. Taken together, our kinetic data suggest that neutrophils and Ly6C^{hi} monocytes accumulate in the acute inflammatory phase of VML injury, while macrophages, particularly CD206+ AAMs, predominate in the later phases of muscle injury and healing.

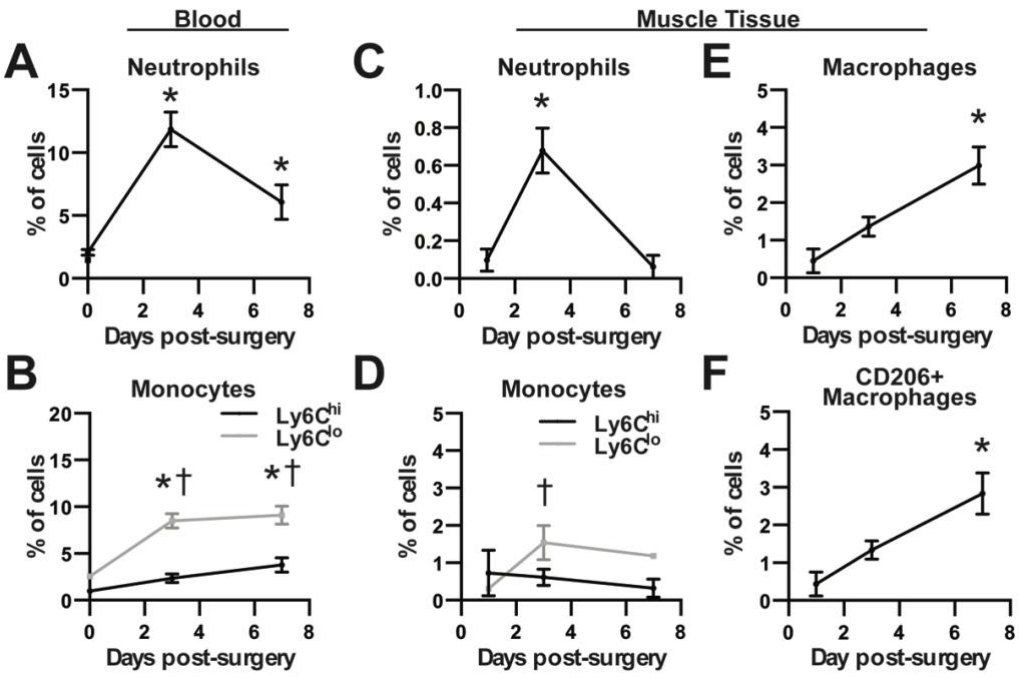

Figure 19. Spinotrapezius volumetric muscle loss results in dynamic myeloid cell kinetics at both the systemic and tissue levels. (A) Following volumetric muscle injury in wildtype mice, blood neutrophils peak at day 3 post-injury and return to baseline levels by day 7 (blood neutrophils gated on CD11b+SSC^{hi}Ly6G^{hi}). (B) Blood Ly6C^{hi} monocytes increase over 7 days, while blood Ly6C^{lo} monocytes gradually increase and plateau over days 3–7 (blood monocytes gated on CD11b+ SSC^{lo}CD115+). (C) Neutrophils in injured muscle tissue peak at day 3 and decrease by day 7 post-injury (tissue neutrophils gated on CD11b+SSC^{hi}Ly6G^{hi}MerTK-CD64-CD11c-). (D) Ly6C^{hi} monocytes in injured muscle tissue decrease from day 1 to day 7 post-injury, while Ly6C^{lo} monocytes increase from day 1–3 and decrease by day 7 (tissue monocytes gated on CD11b+SSC^{lo}MerTK-CD64-CD11c-). (E) MerTK+CD64+ macrophages increase from day 1–7 post-injury. (F) CD206+ macrophages increase from day 1–7 post-injury. Data presented as mean ± S.E.M. Statistical analyses were performed using one-way ANOVA. $^{\dagger}p < 0.05$ compared to Day 0 for Ly6C^{lo} monocytes or $*p < 0.05$ compared to Day 0 for all other cell types, n = 4–12 animals per group.

4.4.2 Non-classical blood monocytes are directly recruited to volumetric muscle injury.

Intravascular administration of latex (LX) beads can be used to track the recruitment and fate of circulating monocytes [90, 101]. We administered LX beads one

day prior to injury in heterozygous CX3CR1$^{GFP/+}$ mice, which constitutively express green fluorescence protein (GFP) under the CX3CR1 promoter (Figure 21A).

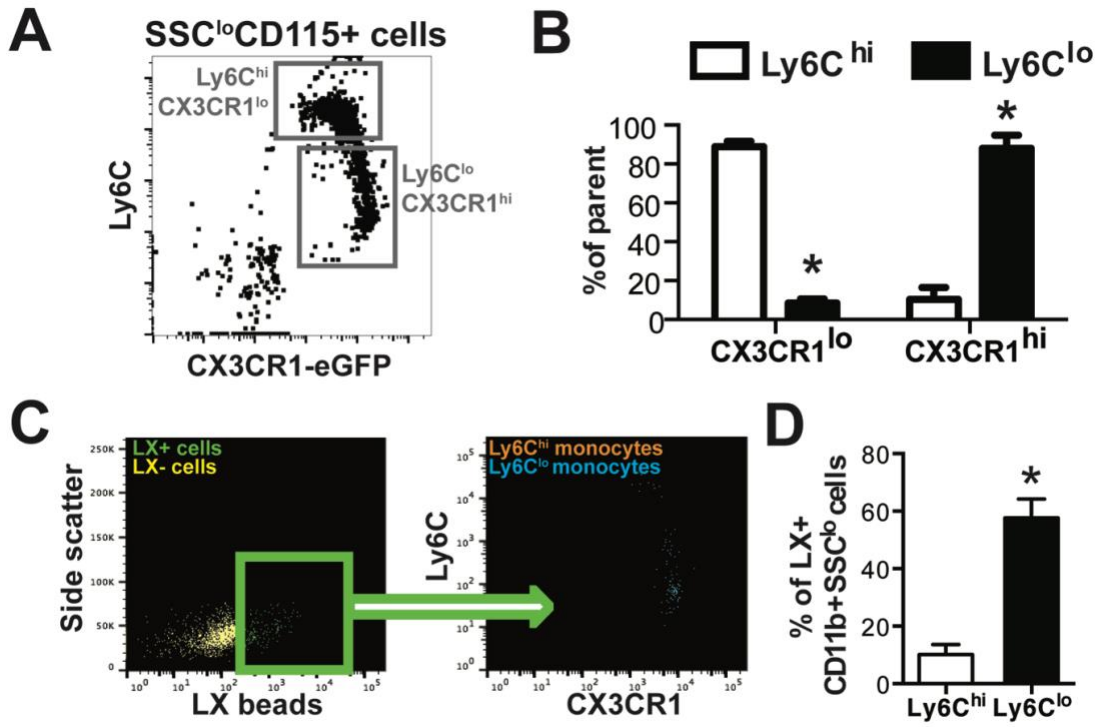

Figure 20. CX3CR1$^{GFP/+}$ transgenic mice were injected i.v. with rhodamine-labeled LX beads 1 day prior to blood draw. (A, B) Ly6C^{hi} monocytes are predominately CX3CR1^{lo}, and Ly6C^{lo} monocytes are predominately CX3CR1^{hi}. (C) LX+ cells are Ly6C^{lo}, CXCR1^{hi} (D) LX beads preferentially label Ly6C^{lo}monocytes. Data presented as mean ± S.E.M. Statistical analyses were conducted using two-tailed t-tests. *p<0.05, n=3 animals per group.

Circulating Ly6C^{lo}CX3CR1^{hi} monocytes are selectively labeled with LX beads 1 day after injection (Figure 20). During surgery, a 1.5mm poly(lactic-co-glycolic acid) (PLGA) film was placed over the defect (Figure 19B) to model biomaterial implantation within VML. Accumulation of LX+ cells in injured skeletal muscle tissue was monitored with confocal microscopy. Both CX3CR1^{lo} and CX3CR1^{hi} monocytes were present in spinotrapezius muscle tissue 3 days post-injury (Figure 21C). Interestingly, a high frequency of LX+ cells

were also seen in the muscle tissue, indicating that labeled Ly6C^{lo} monocytes were directly recruited from circulation to the injured tissue (Figure 21C). This phenomenon stands in contrast to studies conducted using a toxin-induced muscle injury model in which no LX bead-labeled Ly6C^{lo} monocytes were recruited from blood [29].

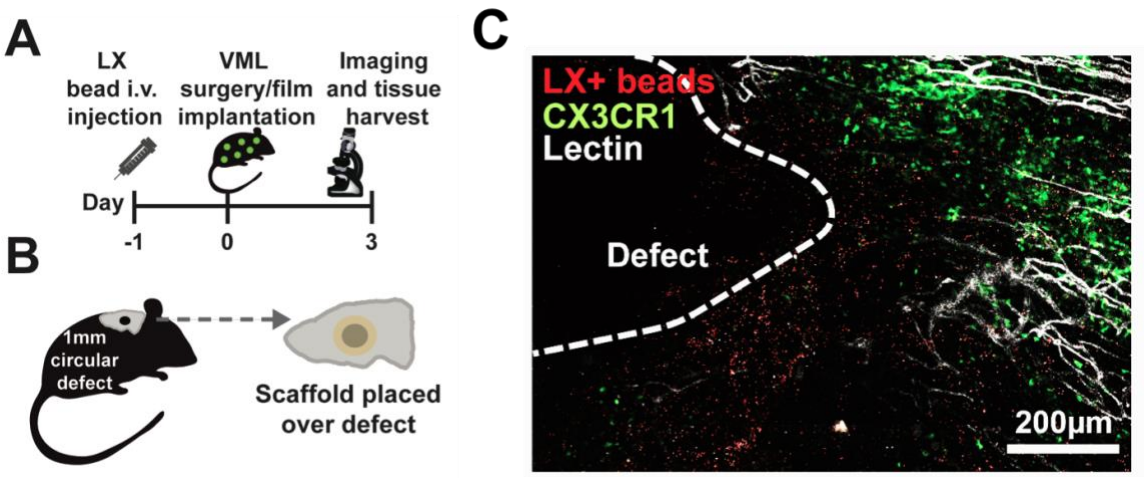

Figure 21. Circulating latex bead-labeled non-classical monocytes are directly recruited to injured spinotrapezius muscle. (A) Ly6C^{lo}monocytes were selectively labeled by intravenous (i.v.) injection of latex (LX) beads 1 day prior to VML surgery in CX3CR1$^{GFP/+}$ mice. (B) PLGA thin films were acutely implanted over spinotrapezius VML defects. (C) Both CX3CR1^{hi} and CX3CR1^{lo} cells, as well as LX+ cells, are recruited to the defect 3 days post-injury.

High-power 3D images of immunostained peri-defect muscle tissue at 3 days post-injury show LX+ cells spatially co-localizing with CD68+CD206+ cells, an immunophenotype indicative of pro-regenerative AAMs (Figure 22). These results suggest direct conversion of blood-derived Ly6C^{lo} monocytes into CD206+ macrophages within muscle tissue and provide a novel therapeutic target for regulating the accumulation of pro-regenerative macrophages in inflamed tissue.

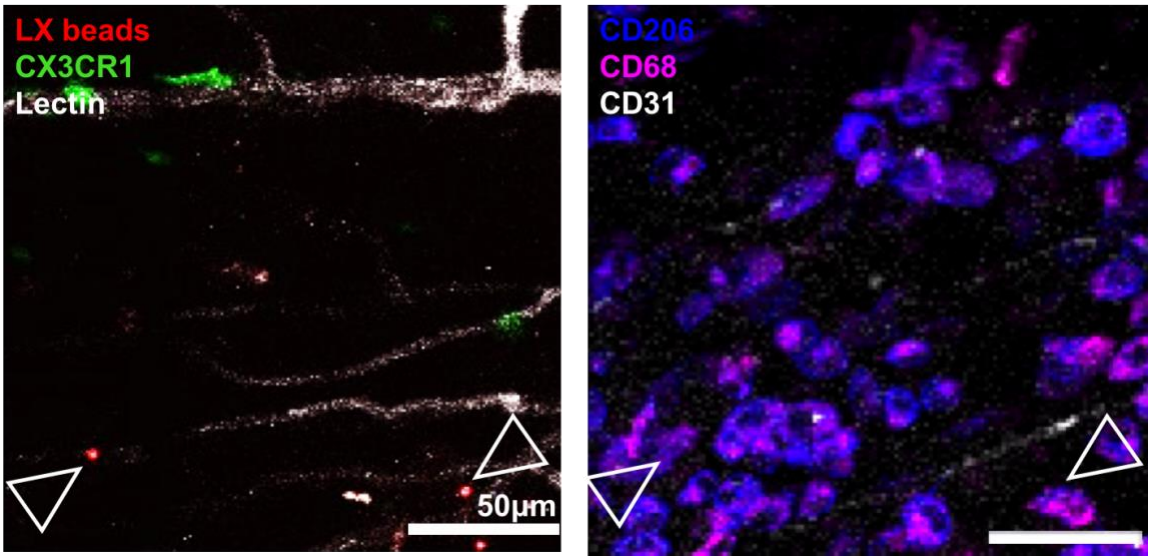

Figure 22. Whole-mount immunofluorescence images of injured spinotrapezius muscle receiving blank polymer implant 3 days post-injury. LX beads co-localize spatially with immunostained CD68+CD206+ macrophages 3 days post-injury.

4.4.3 M(IL-4) macrophage conditioned media promotes myogenic differentiation of C2C12 myoblasts.

To more closely probe effects of macrophage phenotype on myogenesis, we conducted an *in vitro* differentiation assay using C2C12 myoblasts treated for 5 days with conditioned media from polarized RAW264.7 macrophages stimulated with either LPS and IFN-γ (M(LPS, IFN-γ)), or IL-4 (M(IL-4)). C2C12 cells treated with M(LPS, IFN-γ) macrophage conditioned media exhibited no differentiation over the course of 5 days (Figure 23, Table 1). Conversely, C2C12 cells treated with M(IL-4) macrophage conditioned media exhibited high myogenic differentiation, with the presence of several multinucleated myotubes in the culture. These results indicate that secreted factors from M(IL-4) AAM-like macrophages support myogenesis, and provides further motivation for

developing therapeutic strategies that increase this phenotype of macrophage within injured muscle.

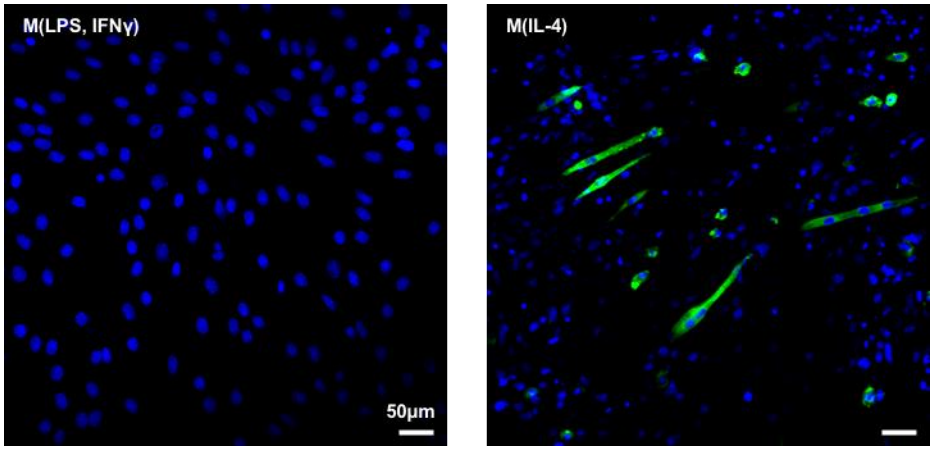

Figure 23. Assessment of myogenic differentiation of C2C12 cells in response to polarized macrophage conditioned media. Conditioned media from alternatively-activated macrophages stimulated with IL-4 (M(IL-4)) promotes differentiation of C2C12 cells *in vitro* compared to conditioned media from inflammatory macrophages stimulated with LPS and IFN-γ (M(LPS, IFN-γ)).

Table 1. Number of Myosin Heavy Chain positive cells in response to macrophage conditioned media treatment.

Conditioned Media Type	MHC+ cells/FOV
M(LPS, IFN-γ)	0 ± 0
M(IL-4)	21.92 ± 1.333

4.4.4 Local delivery of FTY720 from polymeric biomaterials increases Ly6C^{lo}, CX3CR1^{hi} monocytes and CD206+ macrophages in injured muscle tissue.

Previous work in our lab demonstrated that local administration of FTY720 to skin injury increases the frequency of CD206+ macrophages that were derived from blood Ly6C^{lo} monocytes [113]. We sought to determine whether this strategy could be leveraged in VML injury to enhance accumulation of CD206+ macrophages within damaged muscle tissue. Implantation of an FTY720-loaded PLGA thin film over the muscle defect increased the frequency of Ly6C^{lo}, but not Ly6C^{hi}, monocytes compared to PLGA only or no implant controls, as determined by flow cytometry (Figure 24A).

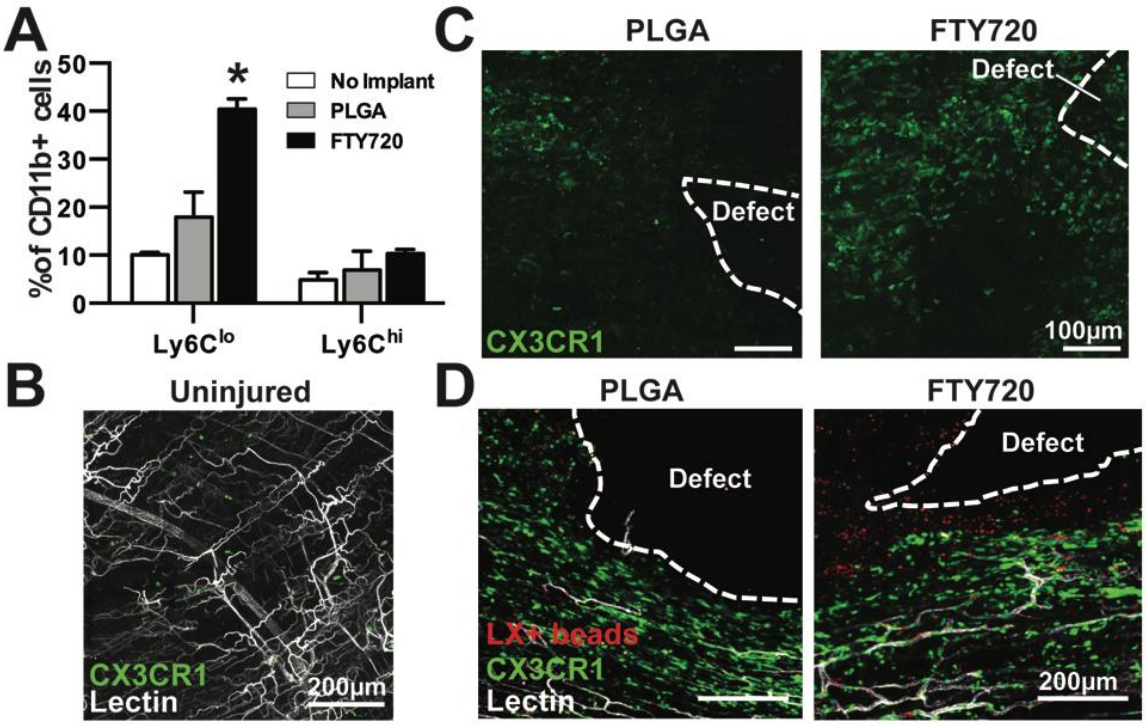

Figure 24. On-site delivery of FTY720 increases Ly6C^{lo}, CX3CR1^{hi} monocytes in injured muscle. (A) Delivery of FTY720 from PLGA thin films to VML injury in wildtype mice increases the frequency of Ly6C^{lo} monocytes, but not Ly6C^{hi} monocytes 3 days post-injury compared to unloaded PLGA and no implant controls (tissue monocytes gated on CD11b+SSC^{lo}). (B) Few CX3CR1-GFP+ cells are seen in uninjured,

contralateral spinotrapezius muscle in CX3CR1$^{GFP/+}$ mice. (C) More CX3CR1^{hi} cells are recruited to peri-defect tissue at day 3 in CX3CR1$^{GFP/+}$ mice treated with FTY720. (D) LX+ cells cluster around defect in FTY720-treated CX3CR1$^{GFP/+}$ mice at day 3 post-injury. Data presented as mean ± S.E.M. Statistical analyses were performed using two-way ANOVA. *$p < 0.05$ compared to Ly6C^{lo} monocytes in PLGA and no implant controls, n = 3–4 animals per group.

After induction of VML injury in CX3CR1$^{GFP/+}$ mice, very few CX3CR1-GFP+ cells were detected in the uninjured contralateral spinotrapezius muscle (Figure 24B). Qualitative analysis of whole mount tissues shows that on-site delivery of FTY720 increased accumulation of CX3CR1^{hi} cells in the peri-defect muscle tissue (Figure 24C), which is consistent with the flow cytometry data that shows increased Ly6C^{lo} monocyte frequency following FTY720 treatment, and analysis of blood monocytes shows inverse correlation of surface CX3CR1 and Ly6C expression (Figure 20). Ly6C^{lo} blood monocytes were labeled in CX3CR1$^{GFP/+}$ mice with LX beads 1 day prior to VML surgery to track the fate of Ly6C^{lo} monocytes during FTY720-mediated immunomodulation. Inspection of whole mount confocal images reveals more LX+ beads in the muscle tissue of FTY720-treated animals and that these LX+ beads were positioned closely around the defect (Figure 24D).

To measure cellular infiltration into the defect, we measured the relative size of the avascular region with high myeloid cellularity (both CX3CR1+ and CD68+CD206+ cells). FTY720-treated animals had a larger percentage of the defect filled with CX3CR1+ cells (Figure 25A, B). We observed a similar, but insignificant, trend following quantification of the proportion of the defect filled with CD68+ and CD206+ cells (Figure 25C, D). Interestingly, we noticed cellular regions that were sparse in CX3CR1+ cells but contained numerous CD68+ CD206+ cells.

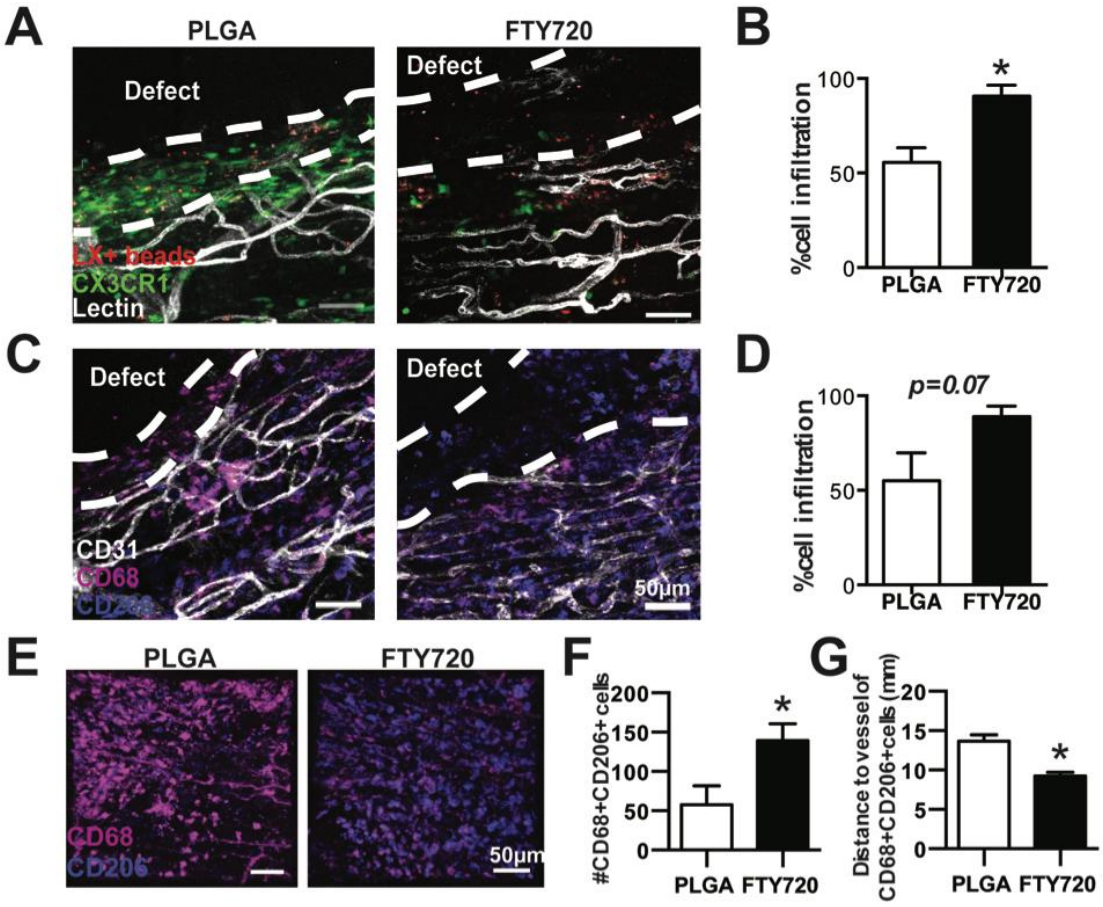

Figure 25. FTY720 increases the frequency of CD68+CD206+ cells in injured muscle of CX3CR1$^{GFP/+}$ mice. (A) FTY720-treated mice have a greater proportion of the defect region filled with infiltrating cells at 3 days post-injury, including LX+ and CX3CR1+ cells. (B) Quantification of cellular infiltration in CX3CR1/LX bead/lectin-labeled muscles shows a higher percentage of cellular infiltration in defects treated with FTY720. (C) FTY720-treated mice have a greater proportion of the defect region filled with CD68+CD206+ cells compared to PLGA controls 3 days post-injury. (D) Quantification of cellular infiltration in CD68/CD206/CD31 immunostained muscles shows a higher percentage of cellular infiltration in defects treated with FTY720. (E, F) Mice receiving FTY720 have increased density of CD68+CD206+ cells 3 days post-injury. (G) CD68+CD206+ cells are significantly closer to CD31+ blood vessels in the presence of FTY720 3 days post-injury. Data presented as mean ± S.E.M. Statistical analyses were performed using two-tailed t-tests. *$p < 0.05$, n = 3–4 animals per group.

Since we observed conversion of Ly6C^{lo} monocytes into CD206+ macrophages (Figure 22), we investigated whether FTY720 also increases the frequency of CD206+

macrophages in injured muscle. Animals treated with FTY720 had more CD68+CD206+ macrophages in peri-defect tissue 3 days post-injury (Figure 25E, F). Close interactions of macrophages and endothelial cells have been associated with enhanced vascular remodeling and arteriogenesis [68, 113]. Quantification of the distance between CD68+CD206+ macrophages and the nearest CD31+ blood vessel within damaged spinotrapezius muscles revealed that AAMs homed closer to vasculature with FTY720 treatment (Figure 25C, G).

4.4.5 Ly6C^{lo} monocytes / CD206+ macrophages promote skeletal muscle healing after traumatic injury.

To investigate whether FTY720-induced perivascular accumulation of CD206+ macrophages was associated with repair of injured skeletal muscle, we assessed wound healing parameters. By 3 days post-injury, local delivery of FTY720 was able to induce increased revascularization of the defect region (Figure 26A, B), as quantified by CD31 immunostaining. Interestingly, the amount of revascularization in FTY720-treated animals was similar to animals with no implant (Figure 26B), indicating that PLGA may impair revascularization. Increased collagen deposition within the defect area, as measured by imaging the second harmonic generation (SHG) signal, was observed in FTY720-treated animals (Figure 26C, D) coinciding with a significantly decreased non-collagenous void area. Regrowth of mature desmin+ muscle fibers was more prominent in muscles treated with FTY720 and these animals demonstrated a trend of reduced defect area at 3 days post-injury (Figure 26E, F). Defects left untreated (no implant) had a lower average defect area than PLGA-treated mice and a lower average defect area than FTY720-treated mice (Figure 26F), indicating that PLGA may impair defect closure.

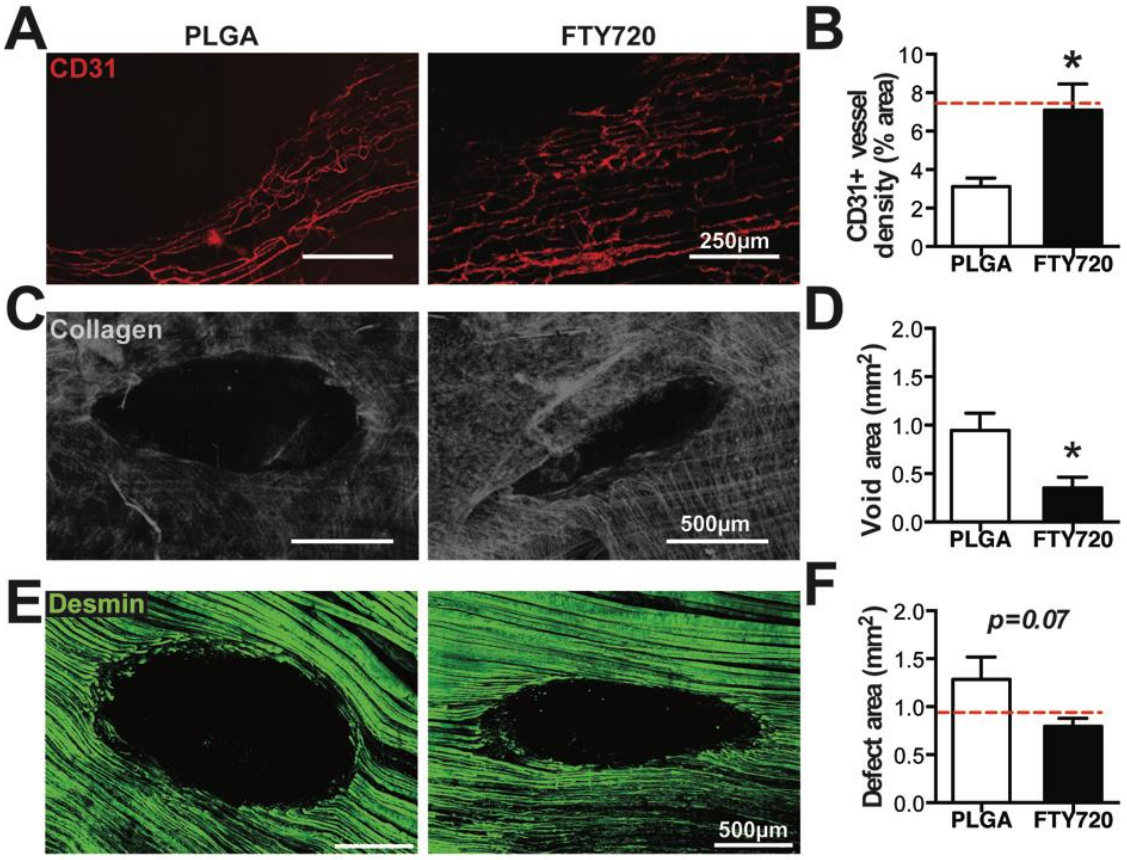

Figure 26. On-site delivery of FTY720 promotes muscle healing 3 days post-injury in CX3CR1$^{GFP/+}$ mice. (A) FTY720-treated mice have increased vascularization in the defect region, as detected by CD31 immunostaining and (B) quantification of CD31+ vessel density. (C) FTY720-treated mice have more collagen deposition within the defect region, as visualized by two-photon microscopy and (D) quantification of the non-collagenous void area. (E) Mice treated with FTY720 have a smaller defect area as measured by desmin immunostaining and (F) quantification of desmin-negative area (dotted red line indicates the mean value of wildtype mice undergoing VML and treated with no implant). Data presented as mean ± S.E.M. Statistical analyses were performed using two-tailed t-tests. *$p < 0.05$, n = 3–4 animals per group.

At day 7 post-injury, injured muscles were imaged with two-photon confocal microscopy for immunostained desmin and SHG collagen signal. We rendered the 3D images in Imaris^{TM} to generate quantitative volumes of desmin and collagen signal. FTY720-treated animals displayed a lower volume ratio of collagen to desmin compared to PLGA animals (Figure 27A, B), indicating less interstitial fibrosis. Furthermore, control

animals displayed highly aligned collagen fibrils compared to uninjured muscle, which is indicative of fibrotic scarring [120]. Regenerated fiber diameter was significantly higher in animals treated with FTY720 compared to PLGA only (Figure 27C, D), and comparable to that observed qualitatively in uninjured spinotrapezius muscle. Taken together, these findings demonstrate that immunomodulatory biomaterial strategies that tune myeloid cell infiltration can improve skeletal muscle repair.

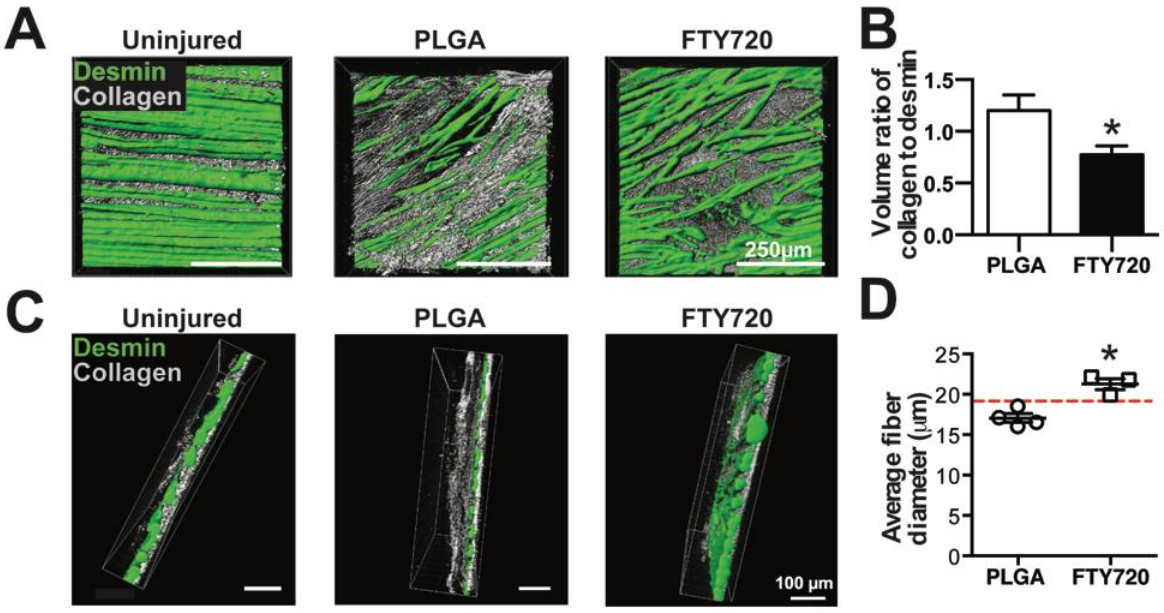

Figure 27. Local immunomodulation with FTY720 improves muscle repair 7 days post-injury in wildtype mice. (A) FTY720-treated mice have larger and more desmin+ muscle fibers (detected by immunostaining) that more closely recapitulates the structure of an uninjured contralateral control, as well as less dense and aligned collagen (detected by two-photon microscopy) compared to PLGA controls. (B) FTY720-treated mice have a reduced volume ratio of collagen to desmin. (C–D) FTY720-treated mice have regenerated muscle fibers with a larger diameter (dotted red line indicates the mean value of wildtype mice undergoing VML and treated with no implant). Data presented as mean ± S.E.M. Statistical analyses were performed using two-tailed t-tests. *$p < 0.05$, n = 3–4 animals per group.

4.5 Discussion

In the present work, we have demonstrated that blood-derived non-classical monocytes infiltrate skeletal muscle after volumetric injury and convert into perivascular CD68+CD206+ macrophages. Biomaterial-based strategies that increase recruitment of non-classical monocytes concomitantly increase perivascular accumulation of AAMs, which correlates with the initiation of repair programs such as injury site re-vascularization, collagen deposition, and regeneration of damaged skeletal muscle. We demonstrate that accelerating the progression of muscle healing by targeting pro-regenerative monocytes and macrophage populations improves muscle regeneration while minimizing fibrotic scarring.

Volumetric muscle injury appears to elicit an inflammatory cascade similar to that observed in toxin-induced injury with peak accumulation of $Ly6C^{hi}$ monocytes at 1 day post-muscle injury and continued increase in $Ly6C^{lo}$ monocytes following toxin insult [35]. Within the spinotrapezius VML model, $Ly6C^{hi}$ inflammatory monocytes are present at 1 day post-injury and decrease over time, whereas $Ly6C^{lo}$ anti-inflammatory monocytes peak at 3 days post-injury. Both monocyte subsets may exert pro-regenerative effects through production of key enzymatic and soluble cues such as inducible nitric oxide synthase (iNOS) by $Ly6C^{hi}$ monocytes [121, 122], and vascular endothelial growth factor (VEGF) [33] and IGF-1 [123] by $Ly6C^{lo}$ monocytes. Once extravasated, however, monocytes mostly differentiate into macrophages that continue to support repair [124]. *In vitro*, monocyte/macrophage subpopulations exert differential effects on myogenic precursors through their secreted factors [42]. Conditioned media from inflammatory macrophages promotes myogenic precursor cell proliferation and motility, whereas the soluble factors

from anti-inflammatory macrophages promote myogenic differentiation and myotube formation [29, 42]. Monocytes and macrophages may also direct their own behavior and fate through paracrine and autocrine signaling. Monocytes and macrophages produce tumor necrosis factor-alpha (TNF-α) and IL-1β which leads to self-amplification of inflammatory responses [125], and their phagocytosis of cellular debris results in downregulation of inflammatory cytokine expression [126]. Thus, controlling the accumulation of specific monocyte and macrophage populations *in vivo* represents an important step in better understanding their role in the intricate wound healing process.

Several studies have documented the recruitment of $Ly6C^{hi}$ inflammatory monocytes to injury where they convert *in situ* to $Ly6C^{lo}$ monocytes and become the primary contributor to wound macrophages [29-32]. Conversely, accounts of direct recruitment of $Ly6C^{lo}$ monocytes have been reported in myocardial infarction [33] and excisional skin injury [113]. Recruitment of non-classical $Ly6C^{lo}$ monocytes may therefore be dependent on the type of injury and tissue of origin. We have built upon this knowledge by demonstrating for the first time that endogenous $Ly6C^{lo}$ monocytes are directly recruited to VML (Figure 21C), suggesting that $Ly6C^{lo}$ monocytes may play an indispensable role in the healing of traumatic injuries that require the *de novo* growth of tissue. Use of LX bead-based labeling of $Ly6C^{lo}$ monocytes in the $CX3CR1^{GFP/+}$ mouse enables tracking of GFP+LX+ monocytes in tissue, and also LX+ cells that may have lost GFP expression due to differentiation into macrophages [101]. LX+ cells appear in spinotrapezius muscle following VML (Figure 21C, Figure 24D), indicating direct recruitment of $Ly6C^{lo}$ monocytes from circulation. Important to the interpretation of trafficking studies, previous work has indicated that intravenous LX bead administration does not alter the kinetics of

Ly6C^{hi} and Ly6C^{lo} monocyte recruitment [101]. Additionally, LX bead administration does not induce changes in monocyte gene expression or systemically elevate plasma inflammatory mediators such as TNF-α, IFN-γ, or IL-6 [101]. In CX3CR1$^{GFP/+}$ mice, blood monocyte composition is the same compared to wildtype mice [127, 128] and CX3CR1 is not required for transendothelial migration of monocytes in a model of acute peritonitis [129], thus simplifying interpretation of data collected in CX3CR1$^{GFP/+}$ mice.

VML defect healing follows similar phases to that of wound healing in injured skin[52]. 3D confocal microscopy of explanted spinotrapezius muscles at 3 days post-injury shows granulation tissue and nascent vasculature within the defect next to truncated muscle fibers (Figure 18 A, B). This region of granulation tissue appeared to co-localize with CD206+ cells. The distribution of CD206+ cells is consistent with studies that indicate AAMs directly promote collagen production in fibroblasts [54] and support vascularization of Matrigel subcutaneous implants [63]. In the resolving phases of inflammation, muscle macrophages upregulate genes for ECM construction and remodeling [106], and depletion of these macrophages severely impairs muscle regeneration [29]. These findings motivated us to investigate whether preferentially increasing AAMs within injured skeletal muscle would enhance healing of volumetric muscle defects.

Biomaterial-based therapies such as ECM-derived scaffolds and macrophage-polarizing hydrogels [111] can increase the ratio of anti-inflammatory to inflammatory macrophages [130, 131] and improve regenerative outcome, but the origin of the AAMs (whether resident or circulation-derived) remains unknown. Recent intriguing insights into the functional differences between resident AAMs and those derived from circulating monocytes have highlighted the importance of considering AAM origin when designing

pro-regenerative biomaterials. Monocyte-derived AAMs have a unique gene expression profile compared to tissue resident AAMs, upregulating genes important during inflammation such as *Socs2, IL-31ra, Ccl17, Ch25h, Jag2,* and *Ccl22* [132]. Monocyte-derived AAMs also specifically drive the differentiation of CD4+ T cells to Foxp3+ regulatory T cells in a retinoic acid dependent manner [132]. Foxp3+ regulatory T cells are crucial to the healing of damaged skeletal muscle [81], and increasing their recruitment via IL-33 delivery to injured skeletal muscle in aged mice improves regeneration [82]. Therefore, circulating monocytes likely possess an intrinsic capacity for promoting wound repair and should be strongly considered in the design of biomaterials that seek to leverage pro-regenerative inflammation. Previously, we have used local delivery of the small molecule FTY720 as a means to localize circulating pro-regenerative monocytes to sites of bone and skin injury to coordinate microvascular expansion and bone healing. In this work, we utilized on-site delivery of the small molecule FTY720 to explore the contributions of circulating non-classical monocytes within VML injury. The effects of FTY720 are pleiotropic, as all cells express some combination of S1P receptors [133]. When administered systemically, FTY720 induces lymphopenia and bradycardia [133]; however, systemic effects are avoided during the local delivery strategies that we have extensively investigated in previous work [61, 113, 134] and the current study.

FTY720 delivery from a polymer PLGA thin film was able to significantly increase the frequency of $Ly6C^{lo}$ monocytes within injured muscle (Figure 24A). Adoptively-transferred non-classical monocytes differentiate into CD206+ macrophages in injured skin [113]. Therefore, we investigated whether increasing non-classical monocyte frequency would also result in increased numbers of CD206+ macrophages. Analysis of

CD68+CD206+ macrophages in peri-defect tissue revealed increased numbers of this population in FTY720-treated animals (Figure 25F). Monocytes and macrophages are known to position themselves strategically by remodeling blood vessels [57, 68, 113], where the crosstalk between vasculature and immune cells can provide instructional cues for AAM differentiation [70]. During chronic arterial occlusion, CD163+ AAMs are clustered in the perivascular space at sites of collateral growth in remodeling vasculature [135]. Here, spatial analysis reveals that CD68+CD206+ cells are positioned significantly closer to vessels with FTY720 treatment (Figure 25G). This increased perivascular positioning of AAMs coincides with increased density of vasculature in the muscle defect area (Figure 26 A, B) compared to PLGA control animals. AAMs also support healing of damaged skeletal muscle by providing a source of regenerative growth factors such as IGF-1 [48] and promoting satellite cell differentiation into mature myotubes [29, 42]. AAMs control collagen deposition from fibroblasts in an IL-4rα-dependent manner [53], a process that is vital to wound healing within the skin. Assessment of the defect area via SHG imaging of collagen showed that FTY720 results in increased collagen content and a smaller defect area 3 days post-injury (Figure 26 C-F). By 7 days post-injury, regenerated fiber diameter was significantly higher in FTY720 animals and the collagen architecture more closely mimicked that of native uninjured muscle (Figure 27 C, D).

Though we have focused primarily on FTY720's effects on the behavior of monocytes and macrophages, agonism of S1PR1 and S1PR3 on other cell types present within the injury may have contributed to the accelerated healing we observed in muscle regeneration. S1PR1 and S1PR3 are differentially expressed during toxin-induced muscle injury, indicating that specific S1P receptors differentially regulate phases of healing [136].

S1PR3 in muscle tissue is highly expressed during the acute inflammatory phase post-injury, and S1PR3 may positively regulate the growth of regenerating fibers [136]. Conversely, S1PR1 expression increases during regeneration and S1PR1 agonism produced a net decrease in regenerated fiber cross-sectional area [136]. Genetic knockout of S1PR3 promotes satellite cell proliferation and attenuates muscle degeneration in the mdx mouse model that simulates Duchenne muscular dystrophy [137]. Our work demonstrates that the signaling induced by FTY720 likely affects multiple cell types during muscle repair, given that we observed changes in myeloid cells, blood vessels, and myofibers. Because the current work is unable to distinguish between direct and paracrine effects induced by FTY720, additional studies employing loss-of-function models are needed to understand the precise interplay between different compartments during skeletal muscle repair.

A major clinical concern with large volumetric muscle injuries is the debilitating fibrosis that often occurs in place of satisfactory healing [108, 138]. Fibrotic muscle not only lacks the contractility of healthy muscle, but also exhibits decreased elasticity, rendering the tissue more susceptible to re-injury [139]. While granulation tissue formation and its subsequent remodeling into mature ECM is crucial for the restoration of functional tissue in the volumetric void, a fibrotic response often progresses faster than a myogenic response [140]. Macrophages have the capacity to sense the injury microenvironment and instruct fibroblasts to either continue producing matrix or undergo apoptosis [55]. Increasing the frequency of AAMs may provide an endogenous command center capable of controlling and alleviating hyper-fibrotic responses within volumetric muscle defects. We utilized 3D analysis of the SHG collagen signal along with fluorescently-labeled

desmin to determine extent of fibrosis between fibers 7 days post-injury. Strikingly, areas of regrown fibers within FTY720-treated animals displayed a lower ratio of collagen to desmin volume (Figure 27B), indicating either faster healing in place of fibrosis, or attenuation of hyper-fibrotic responses in the defect to allow for increased parenchymal muscle fiber ingrowth. These observations are particularly promising for the treatment of larger, critically sized volumetric defects where prolonged fibrotic response after injury results in impaired progenitor and stromal cell migration and subsequently, decreased angiogenesis, reinnervation, and skeletal muscle regrowth [141, 142]. Future studies should explore how acute modulation of inflammatory cell recruitment impacts long-term reconstruction of critical sized traumatic muscle injury.

4.6 Conclusions

Taken together, our data strongly suggest that greater accumulation of CD68+CD206+ cells achieved through increased recruitment of non-classical $Ly6C^{lo}$ monocytes promotes early volumetric muscle wound closure and improves healing outcome within regenerated muscle. These findings indicate that localizing endogenous pro-regenerative inflammation with material-based FTY720 delivery is a promising strategy to promote healing of traumatic musculoskeletal injuries. We use the knowledge gained from these studies to design a nanofiber scaffold releasing FTY720. We will evaluate the immune cell response and muscle healing in response to FTY720 nanofibers in a non-healing volumetric defect within the murine spinotrapezius.

5. LOCALIZING PRO-REGENERATIVE INFLAMMATION VIA NANOSCALE FIBER SCAFFOLDS IMPROVES VOLUMETRIC MUSCLE DEFECT HEALING

5.1 Abstract

The current gold-standard of therapy for volumetric muscle loss involves the autologous transfer of tissue which exhibits limited success and donor site morbidity. Strategies for treating volumetric muscle injuries will require the delivery of cues that initiating and promoting endogenous repair programs. We demonstrate that nanofiber-based delivery of FTY720, a novel recruitment cue acting through the S1P signaling axis, acutely decreases CD4+ and CD8+ T-lymphocytes within a non-healing model of volumetric skeletal muscle injury. Animals treated with immunomodulatory materials exhibited increased numbers of pro-regenerative non-classical monocytes, and alternatively-activated CD206+ macrophages. Muscle stem cells, or satellite cells, were also increased in response to local immunomodulation. Assessment of regenerating muscle defects revealed that biomaterial-based delivery of FTY720 improves regenerated fiber alignment with the pre-injury fiber axis. These findings elucidate a possible connection between lymphoid and myeloid immune cell subset distribution after muscle injury, and demonstrate that FTY720 nanofibers are able to positively impact aspects of regeneration in a non-healing muscle volumetric defect.

5.2 Introduction

Though skeletal muscle possesses robust potential for healing after injury, large volumetric wounds that occur during combat, accidents or surgical resection often do not heal completely, resulting in fibrotic scarring and limited range of motion[140]. Current standard of care involves the autologous transfer of tissue but exhibits limited success and complications at both the donor and injury site[143]. Moreover, extensive soft tissue injury and concomitant damage to collateral blood vessels results in inadequate vascularization and can result in chronic muscle strength deficits.

Monocytes and macrophages have become increasingly recognized as key regulators of microenvironmental cues within injured skeletal muscle[29, 42]. Tightly coordinated signals from monocyte/macrophages subpopulations govern the endogenous muscle stem (satellite) cell niche and dictate either regenerative or fibrotic healing outcomes. Monocytes within circulation exist as two subsets, distinguished by characteristic surface marker profiles. The classical, inflammatory monocyte is $Ly6C^{hi}CX3CR1^{lo}$ whereas non-classical, anti-inflammatory monocytes are $Ly6C^{lo}CX3CR1^{hi}$[98]. $Ly6C^{hi}$ monocytes are rapidly recruited to injury, where they can convert in situ into $Ly6C^{lo}$ monocytes and become the primary contributors to alternatively-activated macrophages[29]. Most notably during muscle injury recovery, monocyte-derived cells release mitogenic growth factors that protect muscle progenitor cells from apoptosis, and stimulate myogenic processes[49]. Monocytes and macrophages are highly plastic immune cells that display a range of phenotypes *in vivo* broadly classified as inflammatory ("M1"), or anti-inflammatory ("M2"), and are able to change their phenotype in response to cues that come from other myeloid and/or lymphoid cells within the injury microenvironment. T-lymphocytes have been shown to accumulate in injured

muscle[81, 83]. In particular, regulatory T-lymphocytes (Treg) cells are crucial to muscle regeneration and are though to govern the critical phenotypic switch in the injury niche from an inflammatory environment to an anti-inflammatory, pro-regenerative environment[81]. However, functions of lymphocyte subsets in the repair of volumetric muscle defects remains unknown. To address this question, we seek to develop biomaterial delivery systems that modulate adaptive and innate immune cell accumulation kinetics towards the goal of enhancing volumetric muscle healing outcomes.

In the present studies, we expand our knowledge of the possible interplay between lymphoid and myeloid cell subset distribution in a non-recovering model of volumetric muscle injury. Using nanofiber scaffold-based delivery of the immunomodulatory signal FTY720, we demonstrate how decreasing acute CD8+ lymphocyte accumulation within injured skeletal muscle may positively influence the accumulation of pro-regenerative subsets of monocytes and macrophages. This increase in non-classical and alternatively-activated macrophages coincides with amplified satellite cell numbers in peri-defect muscle tissue. We observed increased deposition of collagen with FTY720 treatment in the non-healing muscle defect, and revealed increased alignment of regenerated muscle fibers to the pre-injury fiber axis. These results indicate that modulation of lymphoid and myeloid cell subpopulations can positively impact the organization of regenerated muscle tissue after traumatic injury.

5.3 Materials and Methods

5.3.1 Nanofiber scaffold fabrication

Electrospun nanofiber scaffolds were fabricated as previously described[61]. Polycaprolactone (PCL, Sigma) and PLGA were combined in a 1:1 weight/weight ratio at 18% polymer concentration for blank fibers and 20% polymer concentration for FTY720-loaded fibers. Polymers were dissolved in a 1:3 volume ratio solution of methanol to chloroform and vortexed for 2+ hours prior to spinning. For FTY720 loaded fibers, drug was added to the polymer solution at a 1:200 drug:polymer weight ratio. 2 mL of either polymer solution was loaded into a 3 mL syringe with diameter of 10mm. Electrospinning was performed at an applied voltage of 19 kV, and flow rate of 1 mL/hr for both blank and FTY720 fibers. Working distance was set at 10 cm for blank fibers and 12 cm for FTY720 fibers. After 2 mL of polymer was spun, fibers were wrapped in low-binding plastic folders and stored at -20°C.

5.3.2 Drug release from nanofiber scaffolds

3mm circular biopsy punches were used to punch out 3mm discs from electrospun nanofiber sheets. Discs were placed in 100μL of simulated body fluid containing 4% fatty acid-free bovine serum albumin. Releasate was collected at the defined timepoints and replaced with fresh release medium.

5.3.3 Mass Spectrometry quantification of FTY720 release samples

FTY720 was extracted from release samples using a long chain base spingolipid extraction protocol. 100μL of release media was placed in glass culture tubes with screw caps (tubes: Kimble-Chase 73750-13100, caps: Kimble-Chase 73802-13415) and 50μL of phosphate buffered saline was added to bring total sample volume to 150μL. 1.5mL of 2:1

methanol to dichloromethane (by volume) extraction solvent was added to each tube. 50 picomoles of C17 sphingosine was added to each tube to serve as an internal standard. Tubes were capped, sonicated for 1 min, vortexed briefly, and incubated overnight at 48°C. The following day, tubes were allowed to cool to room temperature. 150μL of 1N KOH was added to each tube, sonicated for 1 min, vortexed briefly, and tubes were incubated at 37°C for two hours. Samples were allowed to cool to room temperature, and 8μL of glacial acetic acid was added to each tube before being sonicated for 1 min, and vortexed briefly. Each sample was checked to ensure a neutral (7.0) pH. Samples were centrifuged at 3000rpm and supernatant collected in separate open top glass tubes. 0.5mL of extraction solvent was added to each original sample tube, and samples were sonicated for 1 min and vortexed briefly before being centrifuged again at 3000rpm. The second supernatant was collected and added to first supernatant. Extraction solvent was evaporated off overnight by speed vac. The next day, 300μL of mass spectrometry analysis solvent was added to each tube before being sonicated for 2 mins. Samples were transferred to microcentrifuge tubes and centrifuged at 18,000 xg for 10 minutes. 200μL of each supernatant was transferred to mass spectrometry sample vials. Samples were analyzed on a Micromass Quattro LC mass spectrometer.

5.3.4 Scanning Electron Microscopy

Nanofiber scaffolds were sputter coated with gold for 30 seconds at 20 mA (~7nm of gold deposited) and imaged on a Hitachi SU8010 Scanning Electron Microscope.

5.3.5 Spinotrapezius Volumetric Muscle Loss Surgery and Nanofiber Scaffold Implantation

All animal procedures were conducted according to protocols approved by the Georgia Institute of Technology Institutional Animal Care and Use Committee. Unless otherwise noted, male C57BL/6J (The Jackson Laboratory) of age 8-12 weeks old were used for all animal studies. A 2mm full thickness defect in the spinotrapezius muscle was created as follows. The dorsum of the mouse was shaved and hair removal cream applied to completely remove hair. Skin was sterilized with three washes of 70% ethanol and chlorhexidine. A longitudinal 1 inch incision (cranial to caudal) was made just after the bony prominence of the shoulder blade. The overlying fascia was dissected away and the spinotrapezius muscle identified. Using flat-tipped tweezers, the edge of the spinotrapezius was lifted up. The muscle was reflected and positioned against a sterile piece of wood. A 2mm biopsy punch was made through the muscle, using the wooden piece as support. The muscle was replaced and 3 mm nanofiber scaffold disc implant placed over the punch defect. The nanofiber scaffold disc was sutured at the top to the spinotrapezius muscle with a 10-0 suture. The incision was closed with mouse wound clips. For FTY720 superfusion, a 3mm blank nanofiber scaffold was sutured over the defect, and 0.3mg/kg of FTY720 was superfused on top of the scaffold/muscle, before the incision was closed with wound clips.

5.3.6 Flow cytometry

To collect blood and tissue for flow cytometry analysis, mice were euthanized via CO_2 asphyxiation. Blood was then collected via cardiac puncture. Red blood cells were lysed in ammonium chloride (1 part blood, 9 parts ammonium chloride) prior to immunostaining for flow cytometry. For analysis of cell composition in spinotrapezius muscles, a 6mm biopsy punch of muscle tissue centered on the defect was taken and weighed. For analysis of lymphocyte populations, spinotrapezius muscles were harvested

and digested in 1mg/ml collagenase I (Sigma) for 45 minutes at 37°C. For analysis of satellite cell populations, injured spinotrapezius muscle punches were harvested and digested with 5,500U/ml collagenase II and 2.5U/ml Dispase II for 1.5 hours in a shaking 37°C water bath.The digested muscles were filtered through a cell strainer to obtain a single cell suspension. Single-cell suspensions from were stained for live cells using either Zombie Green or Zombie NIR (Biolegend) dyes in cell-culture grade PBS per manufacturer instructions. Cells were then stained with cell phenotyping antibodies in a 1:1 volume ratio of 3% FBS and Brilliant Stain Buffer (BD Biosciences) according to standard procedures and analyzed on a FACS AriaIIIu flow cytometer (BD Biosciences). The following antibodies were used for cell phenotyping: BV605-conjugated CD4 (Biolegend), BV785-conjugated CD8 (Biolegend), PE-Cy7-conjugated CD3ε (Biolegend), PE-conjugated anti-CD115 (BioLegend), PerCP-Cy5.5-conjugated anti-CD115 (BioLegend), PE-conjugated anti-CD25, FITC-conjugated anti-FoxP3 (eBioscience), BV510-conjugated anti-CD11b (BioLegend), BV421-conjugated anti-CD11b (BioLegend), BV510-conjugated APC (BioLegend), APC conjugated anti-Ly6C (BioLegend), BV711-conjugated anti-CD64 (BioLegend), PE-conjugated anti-MerTK (Biolegend), APC-Cy7-conjugated anti-Ly6G (BioLegend), PE-Cy7 conjugated anti-CD206 (BioLegend) FITC-conjugated anti-CD206 (BioLegend), APC-conjugated Lineage antibody cocktail (BD Pharmigen), PE-Cy5 conjugated anti-CD29 (BioLegend), PerCP-Cy5.5-conjugated anti-CXCR4 (BioLegend), 30μL of Accucheck Counting Beads (Invitrogen) were added per sample for absolute quantification of cell populations.

5.3.7 Whole mount immunofluorescence of spinotrapezius tissues

Mice were euthanized 14 days after surgery via CO_2 asphyxiation. Post-euthanasia, mouse vasculature was perfused with warm saline followed by 4% PFA until tissues were fixed. The entire spinotrapezius muscle was explanted and permeabilized overnight with 0.2% saponin, then blocked overnight in 10% mouse serum. For immunofluorescence, tissues were incubated at 4˚C overnight in a solution containing 0.1% saponin, 5% mouse serum, 0.5% bovine serum albumin, and the following conjugated fluorescent antibodies: Alexa Fluor 488 or Alexa Fluor 650 anti-desmin (1:200 dilution, Abcam), Alexa Fluor 594 anti-CD31 (1:100 diltuion), Alexa Fluor 650 anti-CD68 (1:200 dilution), Alexa Fluor 488 anti-GFP tag (1:200 dilution), rhodamine alpha-bungarotoxin (1:200 dilution). Following immunostaining, tissues were washed 4 times for 30 minutes each in 0.2% saponin for the first two washes, 0.1% saponin for the third wash, and PBS for the final wash, and then mounted in 50/50 glycerol/PBS.

5.3.8 Imaging and Quantification of Whole-Mount Immunofluoresence

3-dimensional, tiled scans of whole-mount spinotrapezius muscles was performed on a Zeiss LSM 710 confocal microscope. Immunofluorescence imaging parameters were kept similar across all samples, with adjustments made only to keep image quality similar. Second harmonic generated signal was collected via 40x objective using a Chameleon laser to excite tissues at 790nm and signal collected over 380-420nm with acquisition parameters kept identical across animals. Quantification of 2-dimensional fiber diameter was performed as described in the previous chapter. Briefly, the widest portion of each regenerated muscle fiber (determined based on the morphology of desmin-positive regions) within the defect region was measured in ZEN from the day 14 2D maximum intensity projections. Desmin and SHG signal from 3-D z-stacks were rendered in Imaris as surfaces

to quantify volume. For desmin surfaces the following parameters were used: auto-smoothing, thresholding set to 14 units, surfaces selected by eye. For SHG surfaces, the following parameters were used: no smoothing, auto-threshold set, all surfaces selected. To quantify alignment, a parallel grid was overlaid on the 3-D maximum intensity projection of desmin, following the axis of uninjured fibers. The angle between regenerated fibers (determined based on morphology of desmin positive regions) and the parallel lines in the grid was measured in FIJI. All angles were measured to be between 0 and 90°.

5.3.9 Functional Assessment of Injured Spinotrapezius Muscles

The length of the lateral edge of the spinotrapezius muscle was measured *in situ* (L) via electronic calipers, and then explanted. The length of the lateral edge was measured again *ex vivo*. The difference in length was calculated as x and residual strain was calculated as $\varepsilon=x/L$. Muscle ends were wrapped in aluminum foil to evenly distribute tension across width of muscle and pinned close to *in situ* length on Sylgard 184 coated petri dishes, with pinned muscles submerged in skinning solution. In the case of nanofiber implant treated animals, the nanofiber implant was left attached to the muscle. Per 100mL, the skinning solution was composed of: 12.5 mL 1M propionate (7.56 mL propionic acid in 100 mL H2O. Add KOH pellets & pH to 7.0), 10 mL 200mM Imidazole pH 7.0 , 2 mL 100mM EGTA, 0.1 mL 1M $MgCl_2$, 25.4 mL autoclaved deionized water , 245 mg ATP (Sigma A7699, ATP disodium salt hydrate), and 50 mL Glycerol. pH of skinning solution was adjusted to 7.0 and stored at -20°C until use.

Relaxing and activating solutions for contractile force testing were prepared as follows. Per 250 mL, relaxing solution was composed of: 12 mL 100mM ATP, 36 mL

100mM phosphocreatine, 25 mL 200mM Imidazole pH 7.0, 17.5 mL 100mM EGTA, 20 mL 1M KCl, 40 μL 100mM $CaCl_2$, 1.4 mL 1M $MgCl_2$, and diluted to 250 with autoclaved deionized water. pH was adjusted to 7.0 with KOH and HCl. Per 250 mL, activating solution was composed of: 12 mL 100mM ATP, 36 mL 100mM phosphocreatine, 25 mL 200mM Imidazole pH 7.0, 17.5 mL 100mM EGTA, 16 mL 1M KCl, 17.5 mL 100mM $CaCl_2$, 1.3 mL 1M $MgCl_2$, and diluted to 250 with autoclaved deionized water. pH was adjusted to 7.0 with KOH and HCl. For best results, activating and relaxing solutions were prepared without the addition of ATP and PC and frozen at -20°C for storage, and ATP and PC solutions prepared fresh at the time of testing, and added to activating and relaxing solutions. Additional ATP (100mM) and $CaCl_2$ (700mM) was added to the activating solution at the time of testing each at 5% (by volume) of the original activating solution volume.

At the time of contractile force testing, muscles were unpinned and removed from skinning solution and washed for 2 minutes in relaxing solutions. The muscles were cut into 3.5 x 8mm strips with the aid of razor and sapphire blades. The muscles were mounting onto a custom built contractile force measuring setup. One end of the muscle strip was attached to an SI-KG2 force transducer (World Precision Instruments) via a spring clip (#97924, World Precision Instruments), and the other end was attached to a 1/2" (12mm) XZ dovetail translation stage (ThorLabs) via another spring clip. The force transducer was connected to an SI-BAM21-LC optical transducer amplifier (World Precision Instruments) which was connected to a USB-1608G data acquisition device (Measurement Computing Corporation). DASYlab software was used to collect force data. The setup is shown in Figure 28.

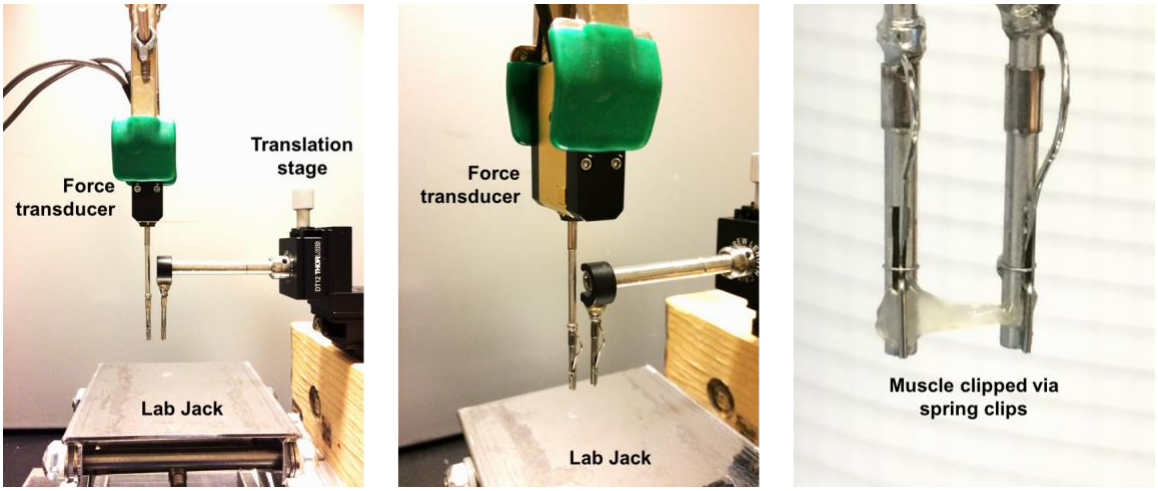

Figure 28. Contractile force testing apparatus. Muscle is mounted via spring clips and submerged in relaxing or activating bath by raising or lowering the lab jack as necessary.

The muscle strip was clipped under slack. The translation stage was moved to extend the muscle under tension until voltage change due to tension began to register. This length was measured and then L was calculated from the residual strain. The muscle was then stretched to length L via translation stage before being submerged for 2 minutes in relaxing solution, at which time data acquisition commenced. After 2 minutes, the muscles were switched into activating solution (additional ATP and $CaCl_2$ added as described in previous paragraph) and contractile force monitored until force did not change for 1 minute. The muscles were then switched back into relaxing bath and monitored for further force generation. When force decreased down to 0, the muscle was then switched back into activating solution and force generation monitored until there was no change in force detected for one minute, at which time data acquisition was terminated.

To assess creatine kinase activity within regenerated skeletal muscle, 4mm punches centered on the defect were taken from injured spinotrapezius muscle. In the case that nanofiber scaffolds were implanted, the scaffolds were collected along with the muscle.

Muscle was mechanically homogenized with Pyrex glass pestle tissue grinders in 100mM phosphate buffer and 1x HALT protease and phosphatase inhibitor. Creatine kinase activity was assessed with a creatine kinase activity kit from Sigma-Aldrich (MAK-116). Creatine kinase activity per muscle sample was normalized to total protein determined by Pierce BCA protein analysis kit (Thermo Fisher).

5.3.10 Statistical Analysis

Data are presented as mean ± standard error of the mean (S.E.M.), unless otherwise noted. All statistical analysis was performed in GraphPad Prism software. Normality was assumed for all data sets possessing a sample size too small to run the D'Agostino and Pearson test of normality. For pairwise comparisons, unpaired t-test (with Welch's correction if variances was significantly different) was used. For instances where the data failed the D'Agostino and Pearson test of normality, two-tailed Mann-Whitney test was used. For comparisons of more than two means, one-way ANOVA with Sidak's post-test was used. For grouped analyses, two-way ANOVA with Tukey's post-test was used. Unless otherwise noted, $p<0.05$ was considered statistically significant.

Power analysis was performed via G*Power software at a power set at 80%. Sample effect sizes were taken from statistically significant results from previously published data[105], when available. The flow cytometry experiments presented in this chapter represent the first studies of their kind in the spinotrapezius volumetric muscle loss model, and thus the effect sizes from observed statistically significant differences were used to compute required sample size for future studies. For flow cytometry, we computed a necessary sample size of 5 to detect differences in lymphocyte populations, and a sample

size of 18-21 was necessary to detect differences in satellite cells and myeloid cell populations. For image analysis, we computed a necessary sample size of 7 to detect statistically significant differences in collagen:desmin ratio, a sample size of 3 to detect significant differences in desmin+ fiber diameter, and a sample size of 4 to detect significant differences in regenerated muscle fiber aligment. Based on this analysis, some of our flow cytometry studies and imaging studies where the sample size is less that described above (sample sizes denoted in figure legends) are considered underpowered, and warrant the addition of more animals.

5.4 Results

5.4.1 Characterization of FTY720-loaded electrospun nanofiber scaffolds

Scanning electron micrographs of FTY720-loaded 50/50 (by weight) Poly-lactic co-glycolic acid (PLGA)/ Polycaprolactone (PCL) electrospun nanofibers (NF) reveal morphology similar to that of blank 50/50 PLGA/PCL electrospun nanofibers (Figure 29). The average diameter of PLGA/PCL nanofibers was 1.2 ± 0.71 μm whereas the average diameter of FTY720-NF was 0.45 ± 0.17 μm.

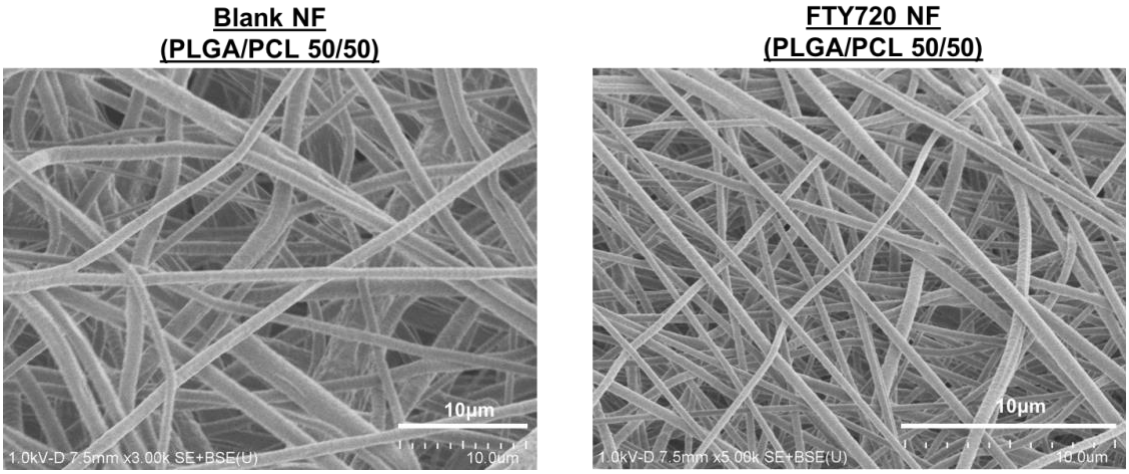

Figure 29. Scanning electron micrographs of electrospun nanofiber scaffolds. Blank and FTY720-loaded nanofiber exhibit similar morphology.

Drug release was measured from 3mm discs (Figure 30A-B) via mass spectrometry. 1.91 ± 0.27 μg of FTY720 was released over the course of 75 hours, with approximately 98 ± 0.02% of drug release occurring over the first 24 hours. After 75 hours, 96.7 ± 0.22% of incorporated drug was released from the scaffold, with 0.065 ± 0.004 μg FTY720 remaining within the scaffold.

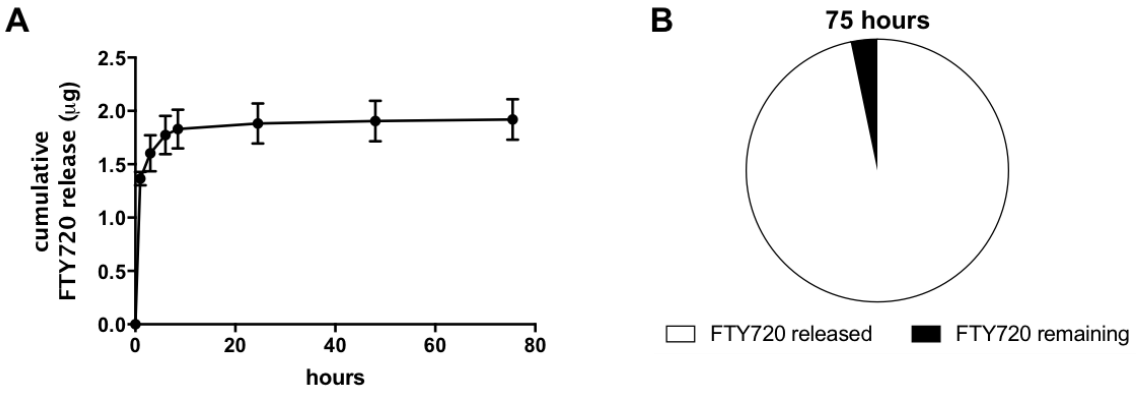

Figure 30. Drug release from 3mm diameter FTY720 nanofiber scaffolds. (A) Cumulative FTY720 drug release from 3mm diameter nanofiber discs. (B) FTY720 released versus FTY720 remaining in nanofiber scaffold after 75 hours. Data presented as mean ± S.E.M.

5.4.2 FTY720 delivery from composite nanofiber scaffolds alters systemic and local tissue lymphocyte levels at 1 day post-injury.

A 2mm full-thickness defect in the murine spinotrapezius was created and was either left untreated, or underwent implantation of 3mm blank or FTY720 loaded nanofiber scaffolds over the defect. Because systemically-administered FTY720 is known to induce lymphopenia, we sought to determine if any system-level effects were detectable with scaffold-based, local administration of drug. Analysis of blood lymphocyte populations by flow cytometry 1-day post-injury revealed that both CD3+CD4+ and CD3+CD8+ T-lymphocytes were significantly decreased in the circulation of FTY720-NF treated animals compared to no implant control (Figure 31A-C).

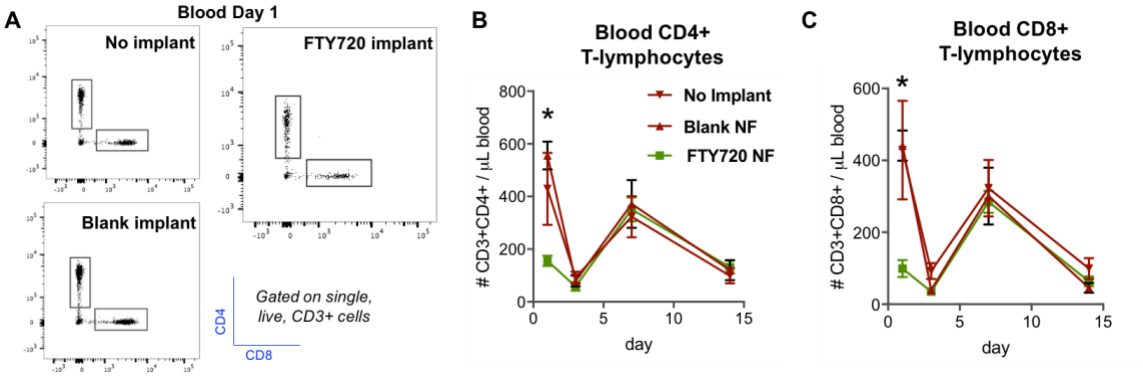

Figure 31. FTY720 nanofiber implantation within spinotrapezius volumetric muscle defect induces acute lymphopenia. A) CD4+ and CD8+ T-lymphocytes are decreased in blood 1 day after volumetric muscle defect creation and FTY720 nanofiber scaffold implantation. B-C) CD4+ and CD8+ blood counts at days 1, 3, 7, and 14 days after surgery. Data presented as mean ± S.E.M. Statistical analyses were performed by two-way ANOVA with Tukey's post-hoc test to compare means, *$p<0.05$, n=4-6 animals per group.

We hypothesized that the systemic decrease of these lymphocytes would correspond to decreases in injured muscle tissue. Indeed, we observed a decrease in

CD3+CD8+ lymphocytes within injured spinotrapezius muscles 1 day post-injury (Figure 32A, B). Since regulatory T-cells have been shown to play a crucial role in skeletal muscle repair, we also examined the frequency of Foxp3+CD25+ Tregs within the injured tissue. Interestingly, blank NF implant treatment reduced the frequency of Tregs within the CD3+CD4+ lymphocyte population compared to no implant, whereas treatment of the muscle with FTY720 NF implants raises the frequency of Tregs back to no implant levels (Figure 32C). There were no significant treatment-specific differences observed in overall CD11b+ cells, Ly6C^{hi} or Ly6C^{lo} monocyte subpopulations within the injured tissue 1 day after surgery and FTY720 nanofiber implantation (Figure 32D-F).

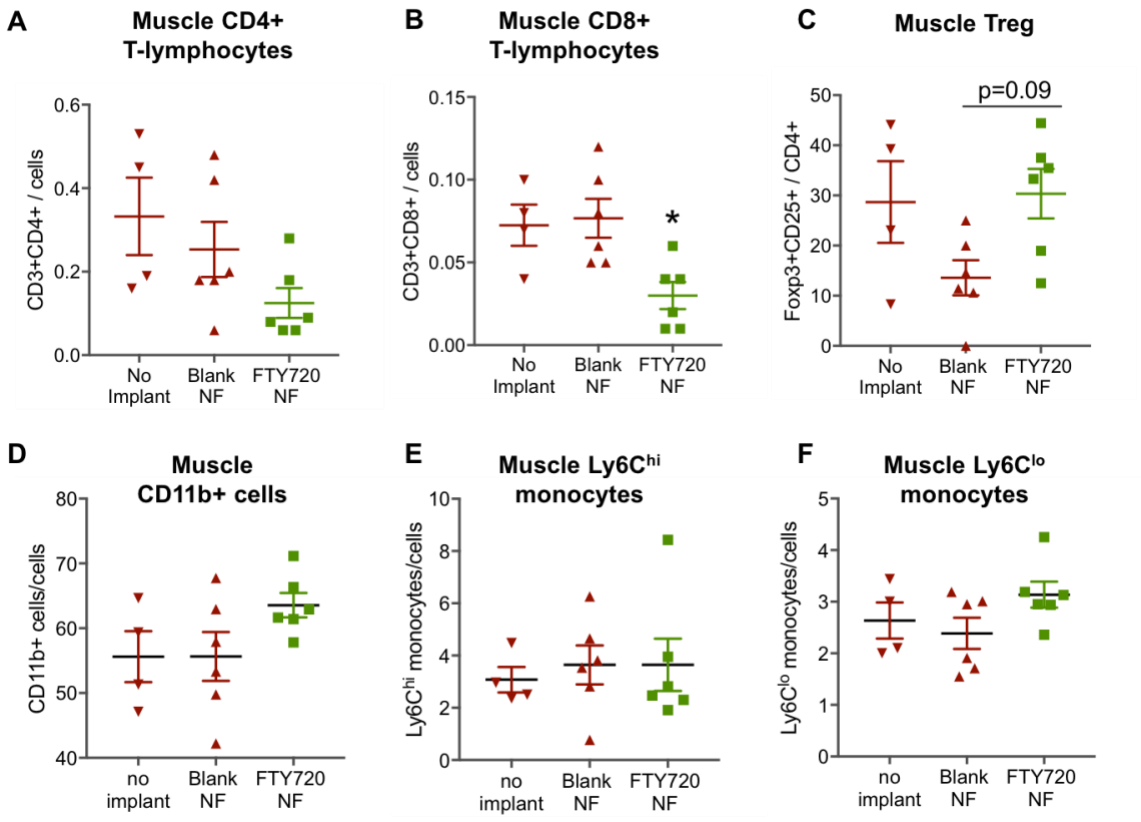

Figure 32. FTY720 nanofiber scaffolds induces changes in lymphocyte accumulation in injured spinotrapezius muscle 1 day after injury. A) No significant changes detected in muscle CD4+ lymphocytes with blank or FTY720 NF implantation. B)

Muscle C8+ lymphocytes are decreased with FTY720 NF implantation. C) No significant changes detected in muscle regulatory T-lymphocytes were detected between groups. No changes in D) CD11b+ cells, E) Ly6C^{hi}, or F) Ly6C^{lo} monocytes were detected in spinotrapezius muscle tissue 1 day after FTY720 nanofiber implantation. Data presented as mean ± S.E.M. Statistical analyses were performed within each day with one-way ANOVA with Sidak's post-hoc test to compare means, *$p<0.05$ compared to no implant, n=4-6 animals per group.

5.4.3 Enrichment of pro-regenerative myeloid cells within muscle injury coincides with increased satellite cell numbers

We have previously shown that FTY720 delivery from a polymer thin film increases the frequency of Ly6C^{lo} and CD206+ macrophages within sub-critically injured muscle at 3 days post-injury. We sought to determine if FTY720 delivery from a nanofiber scaffold to a larger, 2mm defect would elicit similar responses. Interestingly, we observed significantly higher live cellularity within FTY720-NF treated animals compared to blank NF, though the percentage of live cells out of total single cells was not significantly different between groups (Figure 33A, B). Though there was no difference in the number of classical Ly6C^{hi} monocytes per milligram of injured tissue (Figure 33C), the number of non-classical Ly6C^{lo} monocytes/mg tissue was significantly higher in animals treated with FTY720 NF treatment (Figure 33D). Because Ly6C^{lo} monocytes have been demonstrated to be biased progenitors of CD206+ alternatively-activated macrophages[36], we hypothesized that the observed increase of Ly6C^{lo} monocytes would correspond to an increase in CD206+ macrophages. Indeed, though there was no difference in the number of inflammatory Ly6C+CD206- MerTK+CD64+ macrophages between blank and FTY720 NF animals (Figure 33E), we detected a significantly higher number of Ly6C-CD206+ macrophages in FTY720 NF animals (Figure 33F).

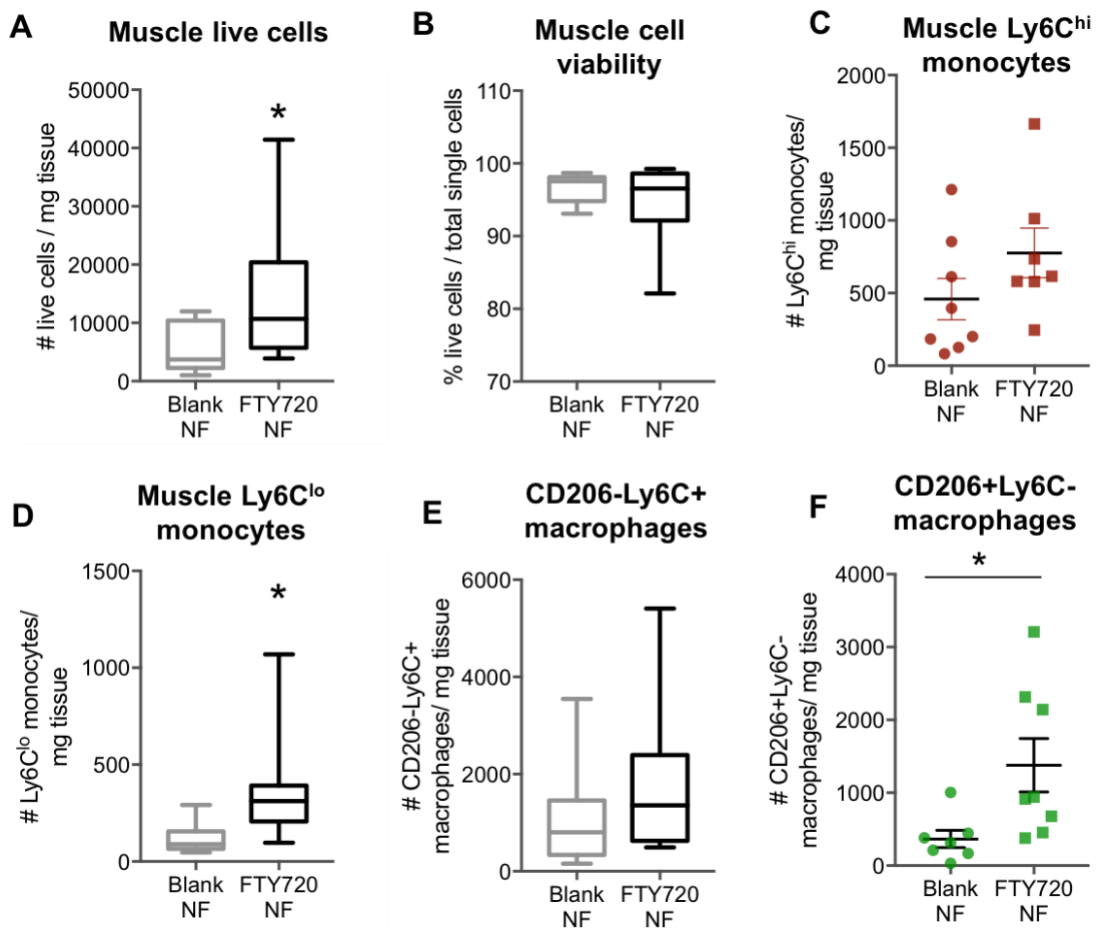

Figure 33. FTY720 nanofiber scaffolds increases pro-regenerative myeloid cell populations within injured spinotrapezius muscle 3 days post-injury. (A) FTY720 NF scaffolds induces higher live cell count but does not affect cell viability (B). C) No difference in number of Ly6C^{hi} monocytes was detected in injured spinotrapezius tissue. D) Ly6C^{lo} monocytes are increased in response to FTY720 nanofiber implantation. E) No difference in number of inflammatory CD206-Ly6C+ macrophages were detected between treatment groups. F) CD206+Ly6C- anti-inflammatory macrophages are increased in response to FTY720 nanofiber implantation. Data presented as mean ± S.E.M. Statistical analyses were performed using two-tailed t-tests with Welch's correction or two-tailed Mann-Whitney tests. *$p < 0.05$, n = 7-8 animals per group.

Since macrophages are known to affect satellite cell proliferation and differentiation, we looked at the number of cells possessing an immunophenotype indicative of satellite cells (lineage-, Beta-1 integrin+, CXCR4+) within blank and FTY720 NF treated muscle (Figure 34A). Interestingly, FTY720 NF treated animals possessed a

higher number of Lin- Beta-1 integrin+ CXCR4+ cells within injured muscle compared to blank scaffold control (Figure 34B).

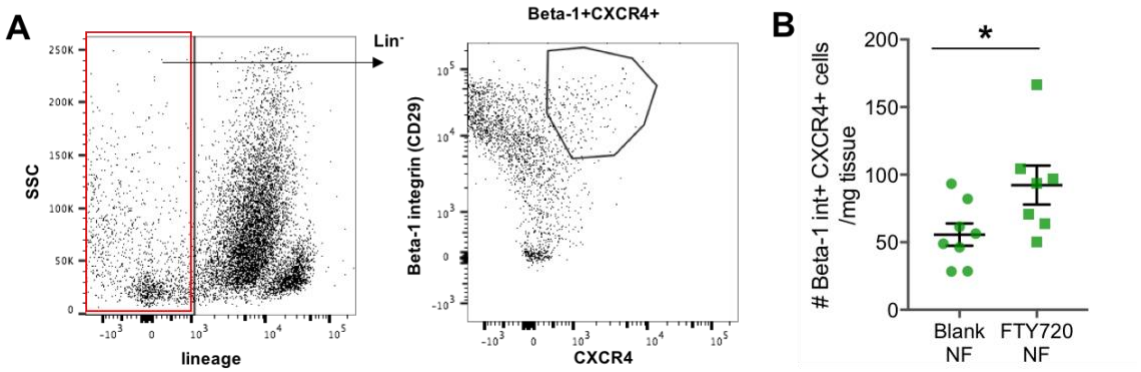

Figure 34. FTY720 nanofibers increases satellite cells in injured spinotrapezius muscle 3 days post-injury. A) Satellite cells were defined as live, lineage^{neg}, Beta-1 integrin+, CXCR4+. B) Satellite cells were increased in response to FTY720 nanofiber treatment. Data presented as mean ± S.E.M. Statistical analyses were performed using two-tailed t-test. *$p < 0.05$, n = 7-8 animals per group.

5.4.4 FTY720 nanofibers increases alignment of regenerated muscle fibers

We assessed healing parameters by confocal imaging in injured skeletal muscles at 14 days post-injury. Though not statistically significant, desmin+ regenerated muscle fiber diameter in animals treated with FTY720 nanofiber implants displayed a mean diameter value higher than that observed in blank nanofiber implants (Figure 35A), and warrants the addition of more animals to the study. Though untreated defects exhibited a fiber diameter mean comparable to FTY720 nanofiber treated animals, qualitative assessments of fiber diameter within 40x crops rendered in Imaris show improved circular fiber morphology in FTY720 treated animals compared to untreated animals (Figure 35B).

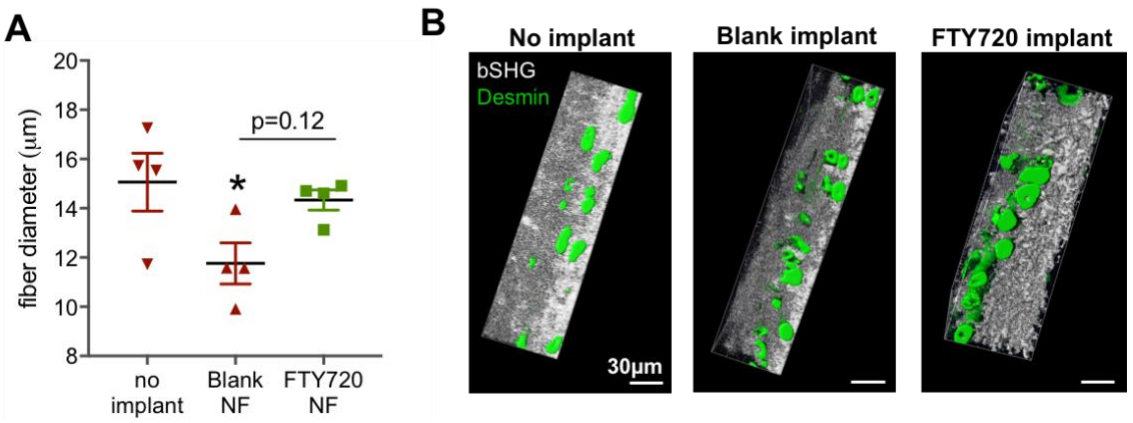

Figure 35. FTY720 nanofibers improves regenerated fiber diameter compared to blank implant control 14 days after injury. A) 2-dimensional fiber diameter measured from maximum intensity projection images reveals higher fiber diameter in FTY720 NF treated animals compared to blank NF control, but not untreated controls. B) 3-dimensional Imaris renderings of desmin and backward SHG generated signal show that the regenerated fibers in the FTY720 NF group have improved circular fiber morphology compared to untreated animals. Data presented as mean ± S.E.M. Statistical analyses were performed with one-way ANOVA with Sidak's post-hoc test to compare means, *$p<0.05$ compared to no implant, n=4 animals per group.

Macrophages are known to interact with satellite cells via contact dependent mechanisms to prevent satellite cell apoptosis[49]. However, it is unclear whether macrophages interact directly with regenerating muscle fibers. We observed close spatial interactions between CD68+ cells and regenerating desmin+ muscle fibers in all three treatment conditions (Figure 36). In addition, FTY720 nanofiber treated animals exhibited distinctly formed vasculature amongst regenerating fibers, whereas untreated and blank nanofiber treated animals did not display a fully formed vascular network (Figure 37). Qualitatively, FTY720 nanofiber treated animals possess increased CD68+ macrophage staining in the area of regenerating fibers (Figure 37).

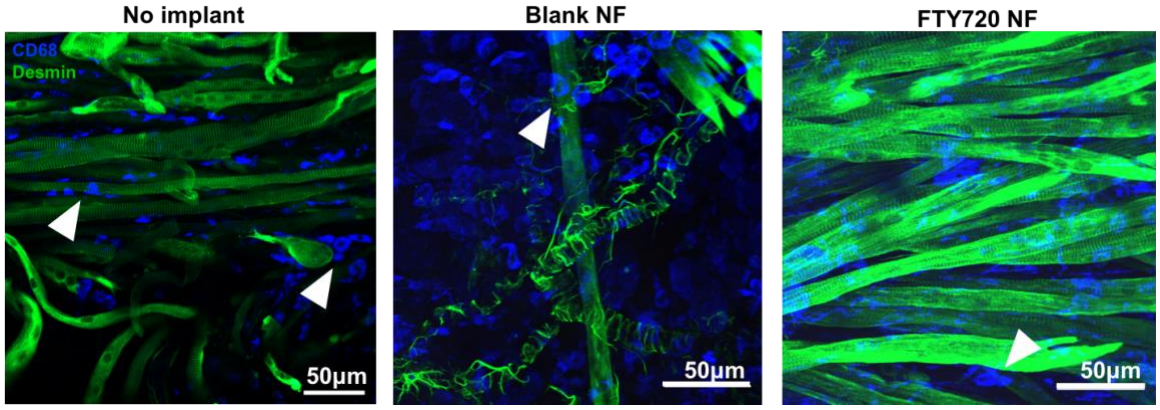

Figure 36. Immunofluorescence images of CD68+ cells (blue) and regenerating desmin+ muscle fibers (green) 14 days post-injury. CD68+ cells (blue closely interact with regenerating muscle fibers (green).

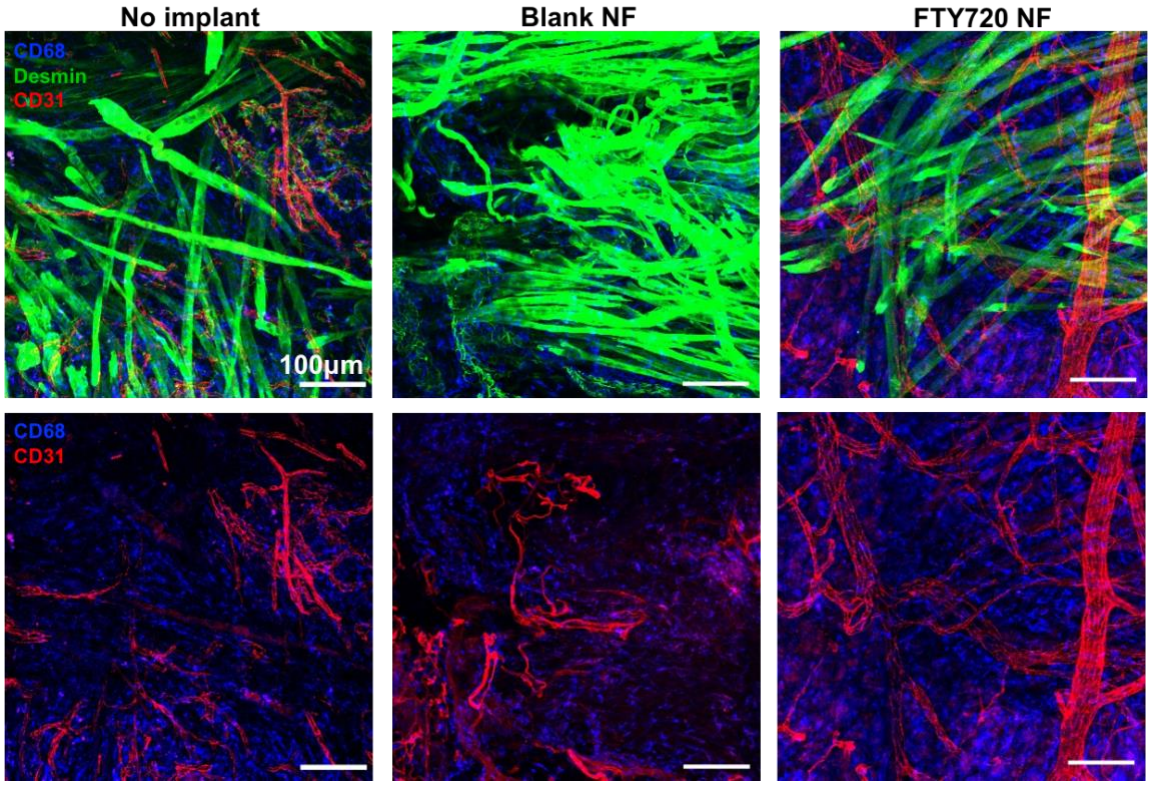

Figure 37. Immunofluorescence images of CD68+ cells (blue), blood vessels (red) and regenerating desmin+ muscle fibers (green) 14 days post-injury. FTY720 nanofiber treated animals display a distinct vascular network (red) amongst regenerated muscle fibers, and increased CD68+ cells (blue), compared to no implant, and blank implant controls.

We then examined the relationship between desmin+ muscle fibers and collagen architecture. The second harmonic generated signal generated by collagen was imaged on a 40x objective, only in the z-depth range where fluorescently labeled muscle fibers were detected. Qualitatively, we observed increased collagen deposition around regenerating fibers (identified by central nucleation) in the FTY720 NF treated animals compared to both untreated and blank NF implant controls (Figure 38, 39). The architecture of collagen superficial to the regenerating muscle fibers exhibited a crosslinked morphology, compared to the aligned collagen bundles seen immediately adjacent to regenerating muscle fibers (Figure 38) which are deeper in z-depth. Assessing the quantitative volume ratio of collagen to desmin reveals that FTY720 nanofiber scaffolds induces a higher collagen:desmin ratio compared to no implant and blank implant controls (Figure 39).

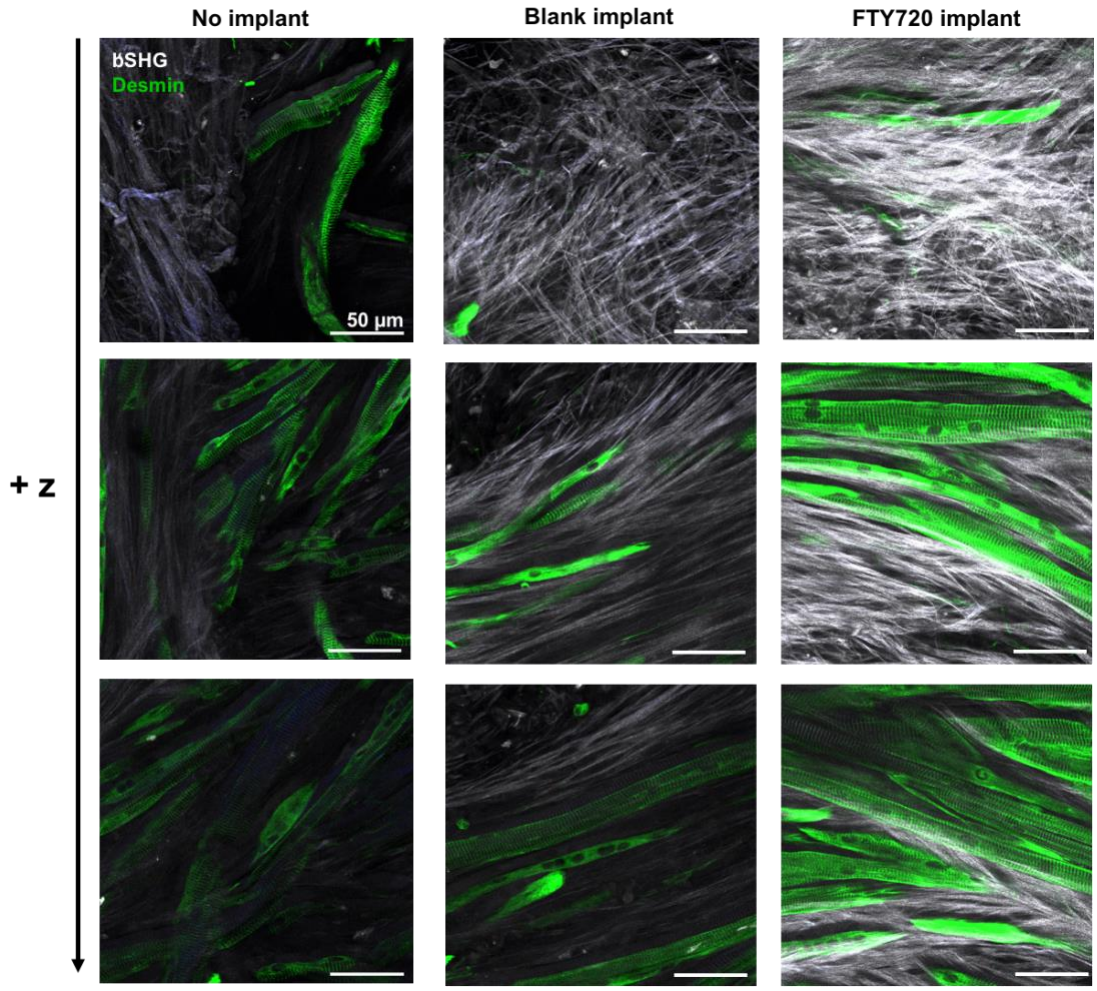

Figure 38. Fluorescence images of injured skeletal muscle 14 days post-injury. Second harmonic generated signal (white) produced by collagen reveals differences in density of collagen deposited among regenerating muscle fibers between treatment groups, as well as tissue depth.

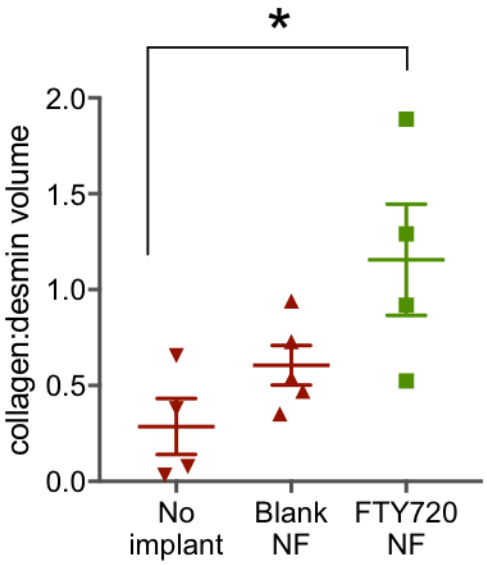

Figure 39. FTY720 nanofiber scaffolds induces higher collagen:desmin ratio compared to no implant 14 days post-injury. Data presented as mean ± S.E.M. Statistical analyses were performed with one-way ANOVA with Sidak's post-hoc test to compare means, *p<0.05 compared to no implant, n=4-5 animals per group.

Extracellular matrix can serve as structural guides for cell migration[144, 145]. We hypothesized that the increased collagen seen in FTY720 treated animals could serve as an architectural conduit along which muscle fibers could elongate in an aligned manner. Thus, we measured the angle between centrally nucleated regenerating fibers and the axis of original, uninjured muscle fibers, with a higher angle measurement (0° - 90°) between new and old fibers indicating poorer alignment. FTY720 NF treated defects exhibited significantly lower angle measurement (17.82° ± 5.4°) compared to both untreated and blank NF treated defects (50.07° ± 3.2° and 43.1° ± 8.79°, respectively), indicating improved alignment. We attributed this increased alignment to FTY720 release from the nanofiber scaffold, as FTY720 superfusion with blank nanofiber implant did not induce improved alignment of muscle fibers (Figure 40).

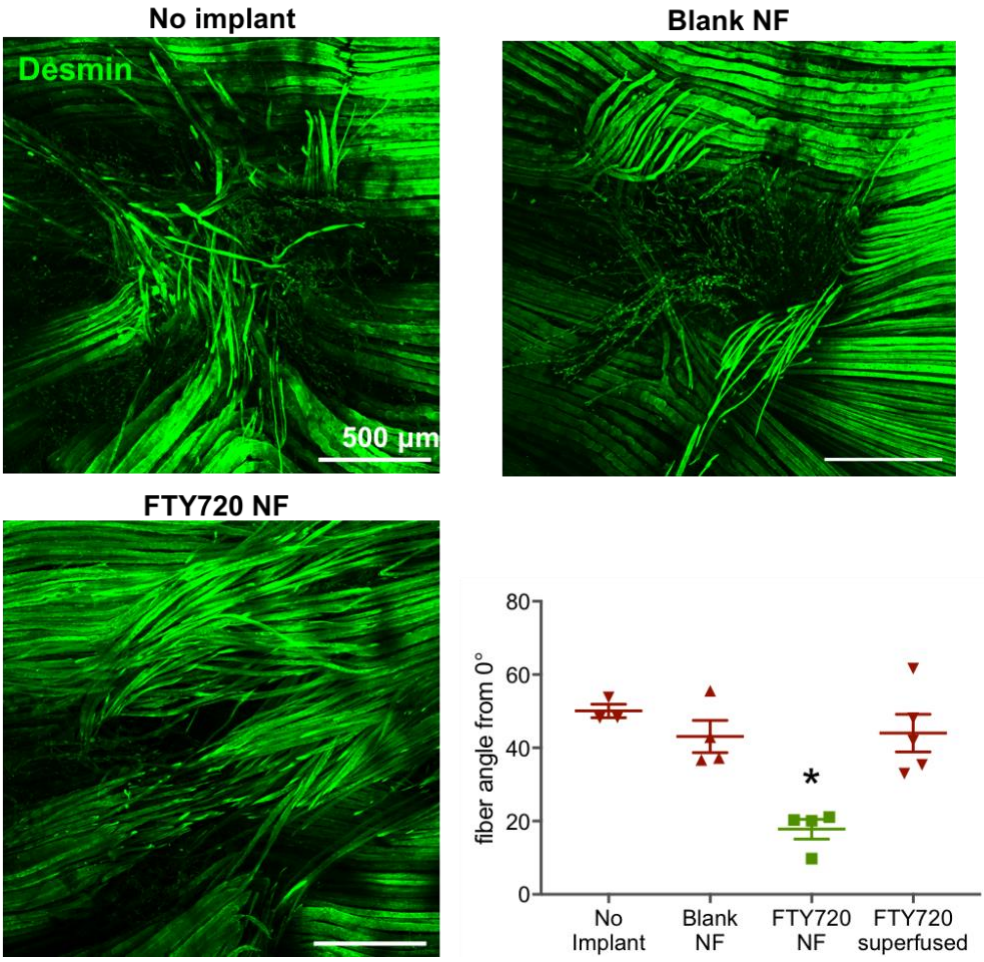

Figure 40. FTY720 nanofibers induce higher alignment of regenerated muscle fibers to original fiber axis 14 days post-injury. Data presented as mean ± S.E.M. Statistical analyses were performed with one-way ANOVA with Sidak's post-hoc test, *$p<0.05$, n=4-5 animals per group**.**

We then sought to determine if this improved alignment was attributed to the immunomodulatory effects of FTY720 or the nanofibrous architecture of the electrospun scaffold. We similarly measured the angle in 1mm defects either left untreated, or treated with blank and FTY720 loaded polymer thin films. We have shown previously that FTY720-loaded films are able to locally modulate inflammation in skeletal muscle, but do not possess nanofibrous architecture. Interestingly, animals receiving FTY720 from

polymer thin films also exhibit higher alignment (lower angle measurement) with the pre-injury fiber axis compared to untreated or blank film controls. (Figure 41).

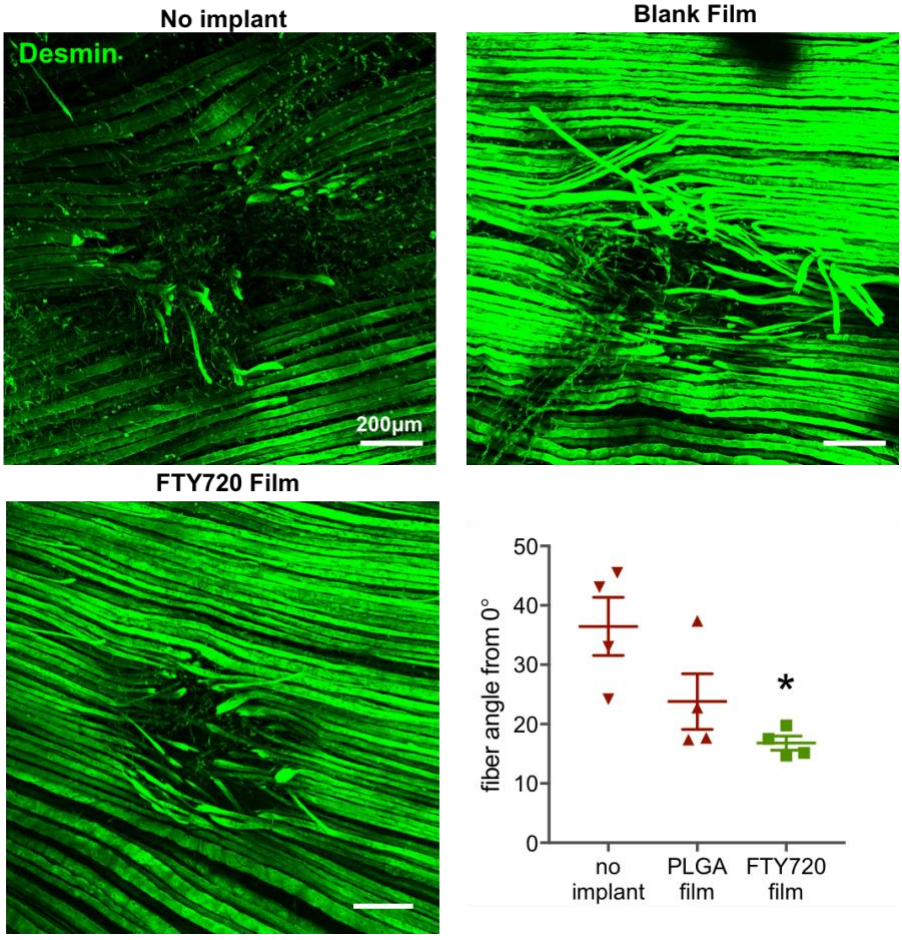

Figure 41. FTY720 film induces higher alignment of regenerated muscle fibers to original fiber axis 7 days post-injury. Data presented as mean ± S.E.M. Statistical analyses were performed with one-way ANOVA with Sidak's post-hoc test, *$p<0.05$ compared to no implant, n=4-5 animals per group.

Restoration of functional properties of skeletal muscle relies on reinnervation of regenerated fibers. FTY720 nanofibers were implanted into Thy1-YFP mice, in which motor neurons are labeled wi th YFP and able to be detected via immunofluorescence. We observed in preliminary studies thaanimals receiving FTY720 nanofibers displayed greater axonal density in regenerating muscle regions 28 days post-injury (Figure 42). Regenerated

neuromuscular junctions were detected by identifying regions of overlap of Thy1+ presynaptic junctions and acetylcholine receptor+ post-synpatic junction, and the junctions seen in FTY720 treated animals adopted similar morphology to that in healthy muscle (Figure 43). Further studies adding additional animals to each group will be necessary in order to fully elucidate FTY720-NF mediated effects on motor neuron regeneration. Desmin marks activated pericytes which stabilize nascent vasculature during muscle regeneration. Interestingly, Thy1+ axons could be observed running alongside desmin+ vascular-like structures in close spatial proximity (Figure 44).

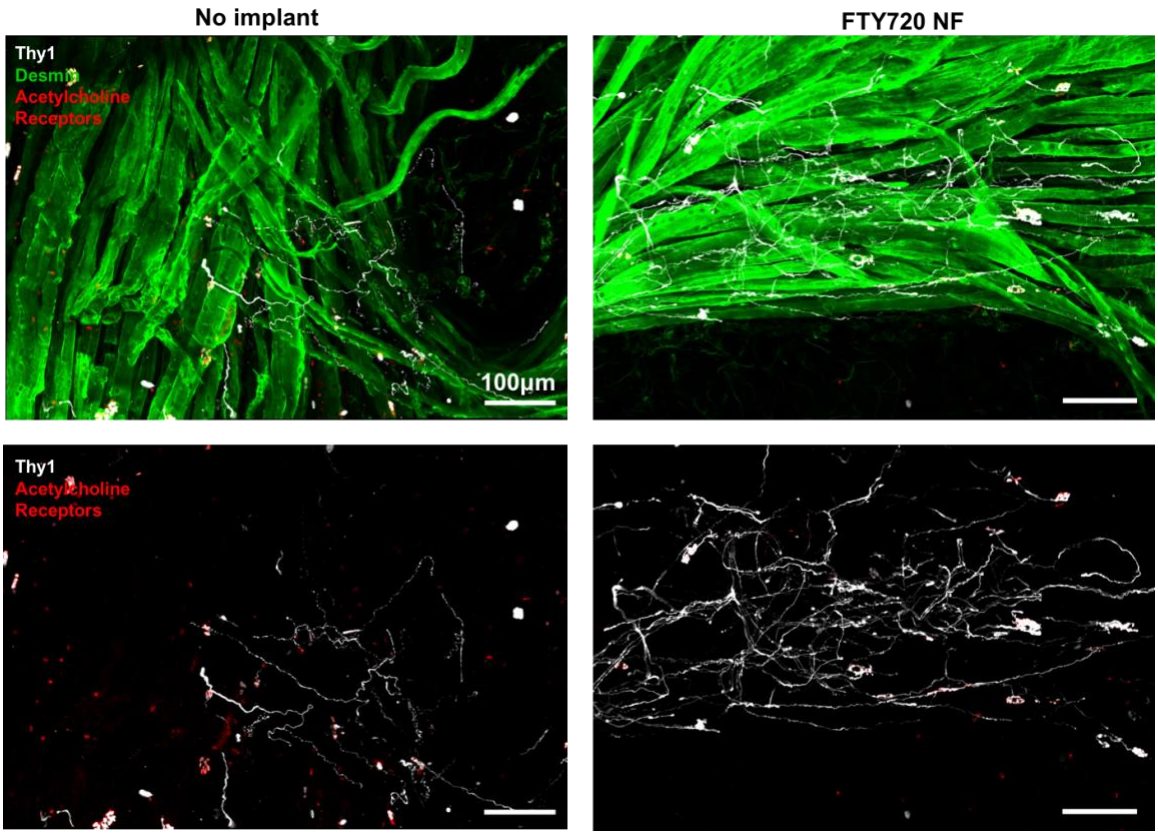

Figure 42. Immunofluorescence images of regenerating motor neurons (white), regenerating post-synpatic neuromuscular junctions (red), and regenerating desmin+ muscle fibers (green) 28 days post-injury. FTY720 nanofiber treated animals display increased motor axon regrowth in regenerating tissue area compared to no implant control.

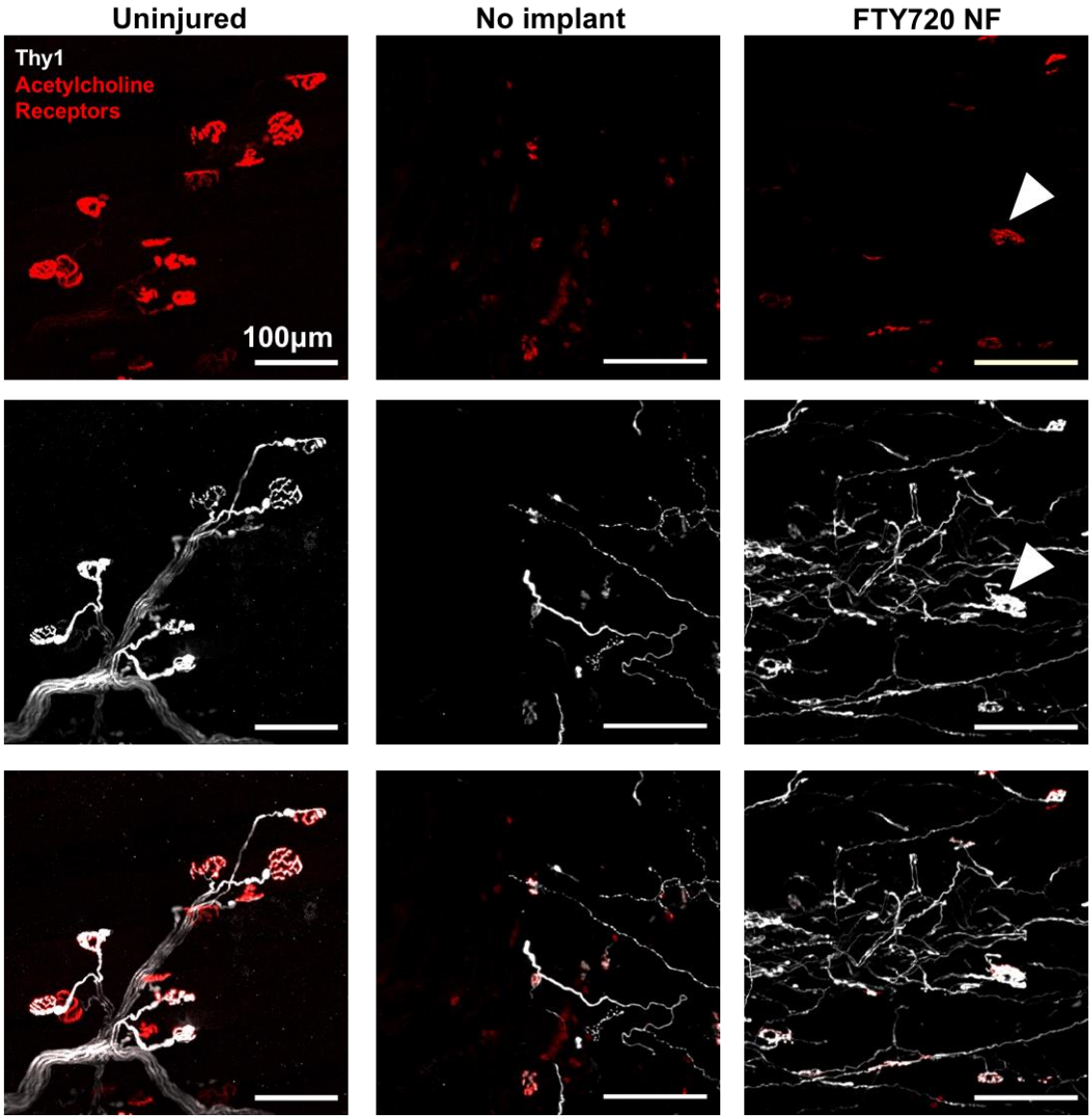

Figure 43. High powered immunofluorescence images of regenerating motor neurons (white), regenerating post-synpatic neuromuscular junctions (red) 28 days post-injury. FTY720 nanofiber treated animals exhibit regenerated pre-synapatic and post-synaptic neuromuscular junctions (white arrow) with similar morphology to that observed in uninjured muscle.

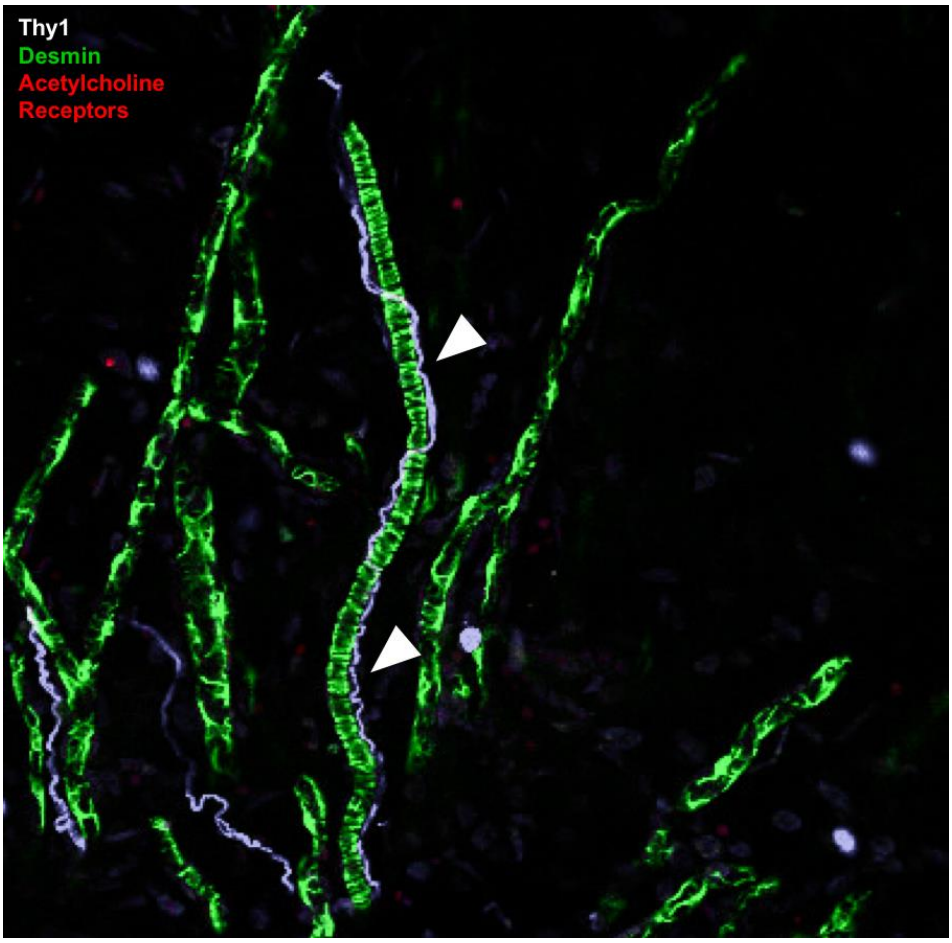

Figure 44. Immunofluorescence image of regenerating motor neurons (white), regenerating post-synpatic neuromuscular junctions (red) and pericyte covered vascular structure (green) 28 days post-injury. Regenerating motor axon (white) closely follows desmin+ pericyte vascular structure (green) (white arrows).

We then sought to determine if the improved healing metrics seen with FTY720 nanofiber treatment would manifest in functional differences. We designed and built a custom testing apparatus that would enable the measurement of contractile force generated from injured spinotrapezius muscles at 28 days post-injury. We collected three data points: the peak force generated upon the muscle's initial submersion into the high calcium, high ATP activating bath, the peak force generated upon the muscle's return into relaxing bath, and the peak force generated upon the muscle's second entry into the activating bath. While

it is unclear why the muscle continues to generate force upon return to the relaxing bath, we suspect that the muscle may experience a form of tetanus in the activating bath, and upon return to the low calcium, low ATP bath, the extra calcium and ATP within the muscle that has not diffused out may be able to then stimulate additional force generation. An example force plot is shown in Figure 43A. Though we were able to detect a statistically significant difference in force generation between healthy and injured muscles 28 days post-injury, we could not detect differences in force generation between injured treatment groups at the 3 peak forces collected (Figure 45B-D).

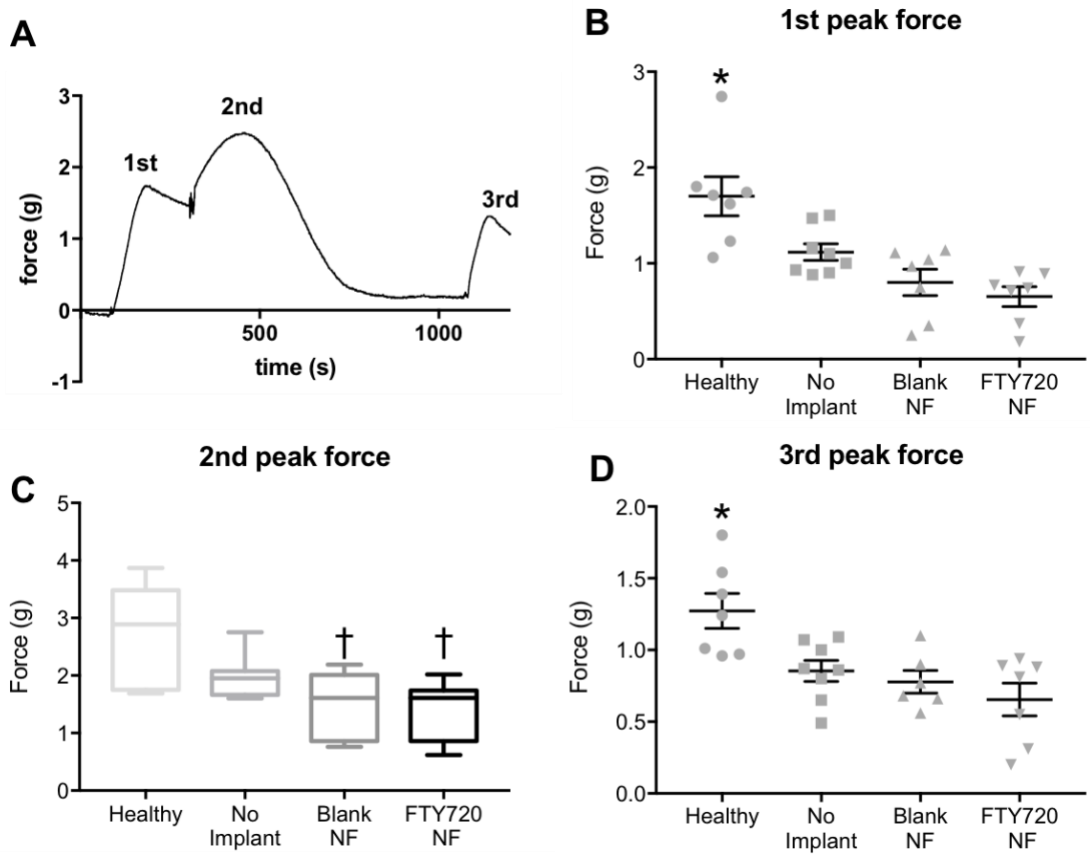

Figure 45. Contractile force measurements in healthy vs. injured spinotrazpeius muscles 28 days post-injury. A) Force vs time plot of healthy muscle. B-D) Healthy muscle generates significantly higher force than injured muscles that were left untreated, treated with blank NF, or treated with FTY720. Data presented as mean ± S.E.M.

Statistical analyses were performed with one-way ANOVA with Sidak's post-hoc test or Kruskal-Wallis with Dunn's post-hoc test, *p<0.05 compared to all other groups, †p<0.05 compared to healthy muscle, n=7-8 animals per group.

Creatine kinase activity was measured in muscle lysate samples collected 28 days post-injury, and normalized to total protein content. Muscles undergoing a 2mm defect injury that were allowed to heal without an implant displayed significantly higher CK activity than healthy muscles, or injured muscles treated with blank nanofibers or FTY720 nanofibers. There were no statistically significant differences between treatment groups in injured muscles (Figure 46.)

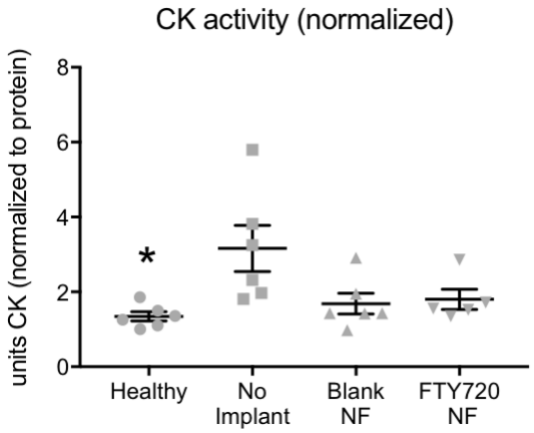

Figure 46. Creatine kinase activity in muscle lysates collected 28-days post-injury. Data presented as mean ± S.E.M. Statistical analyses were performed with one-way ANOVA with Sidak's post-hoc test, *p<0.05 compared to no implant, n=5-6 animals per group.

5.5 Discussion

Volumetric muscle defect injuries comprise 50-70% of combat injuries and are the cause of 80% of limb amputations in soldiers[143]. The therapeutic options for volumetric muscle loss are few (autologous tissue transfer, muscle flap transposition) and exhibit poor clinical prognosis due to donor site morbidity, and inadequate integration of donor tissue

into the local vascular and motor neural network. Extracellular matrix-derived scaffolds have been utilized as void filling substitutes for autografts, and promote M2 macrophage polarization in the injury vicinity, however immunogenicity of allogenic or xenogenic ECM scaffolds remains a concern [146],[147]. Scaffolds seeded with mesenchymal stem cells or myoblasts have been shown to improve volumetric defect healing and functional outcome[148], [149], but translation of cell-based therapies into the clinic remains a regulatory challenge. The employment of endogenous tissue engineering techniques, in which cues are provided *in situ* to influence the mobilization, homing, phenotype, and function of key regenerative cell populations, represents an attractive therapeutic strategy for the treatment of volumetric muscle injuries.

Our previous work utilized a 1mm diameter full-thickness defect in the murine spinotrapezius muscle to investigate the role that non-classical monocytes play within sub-critically sized volumetric muscle injury (Chapter 4). In the present studies, 2mm diameter defects were created in the murine spinotrapezius to model a volumetric muscle injury of critical size. To test whether this defect size represented a critical injury, the contractile forces generated from uninjured spinotrapezius muscles and muscles that underwent 2mm defect injury were compared. These functional measurements revealed that 28-days post-injury, injured muscles generated a significantly lower force than uninjured muscles (Figure 45), indicating that a 2mm defect is does not regain full contractile function at this longer term time point. Thus, we employed the 2mm defect model to further expand our knowledge of the roles that innate and adaptive immune cells have in the repair of a non-healing volumetric muscle injury.

Nanoscale fiber scaffolds fabricated from biocompatible polymers are an easily tunable material platform that enables the incorporation of bioactive molecules suited to the application at hand. Here, we engineered PLGA/PCL nanofiber scaffolds encapsulating FTY720, an immunomodulatory molecule known to redirect non-classical Ly6C^{lo} monocytes from peripheral circulation into injured tissues when locally applied [34]. The use of nanofiber technology enabled us to suture the implants over the spinotrapezius volumetric defect, ensuring localized drug release to the injury site. We observed that implantation of FTY720 nanofibers into 2mm volumetric muscle defects results in acute lymphopenia at day 1 (Figure 31). Within injured spinotrapezius tissue, CD4+ and CD8+ T lymphocytes were similarly decreased at day 1 with FTY720 NF treatment (Figure 30). Though the role of CD4+ and CD8+ T lymphocytes in volumetric muscle defect healing remains unclear, these cells are able to secrete cytokines that could influence the polarization of myeloid cells. CD4+ T lymphocytes produce IL-4 and IL-13[150], which may lead to anti-inflammatory M2 polarization[151], and CD8+ T lymphocytes secrete IFN-γ[152], promoting inflammatory M1 polarization[151]. Though both CD4+ and CD8+ T lymphocytes were reduced in muscle tissue with FTY720 treatment, the complex interplay between lymphoid and myeloid cells is such that even slight shifts in cytokine balance due to decreases in these lymphoid populations could result in a tissue microenvironment more favorable towards anti-inflammatory, M2 polarization.

To test whether FTY720-mediated decreases in CD4+/CD8+ T-cells influenced myeloid phenotype distribution in injured skeletal muscle, we analyzed monocyte and macrophage subsets by flow cytometry. Though there were no differences in either classical Ly6C^{hi} or non-classical Ly6C^{lo} monocyte subsets at day 1 post-injury (Figure 32),

we did observe robust increases in non-classical Ly6C^{lo} monocytes, and pro-regenerative Ly6C-CD206+ macrophages at day 3 post-injury (Figure 33). Since macrophages are known to impact satellite cell behavior, we evaluated the effect of FTY720 nanofiber treatment on satellite cell numbers. Interestingly, we detected a significantly increased number of Lin-CD29+CXCR4+ cells (an immunophenotype indicative of satellite cells) within injured spinotrapezius muscle upon treatment with FTY720 nanofiber scaffolds compared to blank scaffold control (Figure 34).

Defining functional effects of alternatively-activated M2 macrophages on satellite cells remains a challenge due to the marked heterogeneity that M2 macrophages exhibit both in *in vitro* polarization paradigms, and in *in vivo* injury niches. IL-4-polarized macrophages have been shown *in vitro* to suppress satellite cell proliferation and promote satellite cell differentiation [29], whereas macrophages polarized via IL-10 exposure promoted C2C12 myoblast proliferation but had no effects on myoblast differentiation as evaluated by myoD and myogenin protein expression[24]. An intriguing hypothesis to investigate in future work is that the decreases in CD4+ (which produce IL-4) and CD8+ T-lymphocytes (which produce IFN-γ) observed at day 1 with FTY720 nanofiber treatment may shift the injury cytokine milieu towards favoring IL-10-mediated M2 polarization. IL-10 is secreted by regulatory T-lymphocytes (Treg)[23], and we observed increased CD25+Foxp3+ Treg cells in injured muscle with FTY720 nanofiber treatment at day 1 compared to blank scaffold (Figure 33). Further studies that probe the muscle cytokine profile in response to FTY720 are necessary in order to further elucidate the connection between lymphoid and myeloid cell populations within skeletal muscle injury.

To explore whether the immunological profile and increased satellite cell numbers induced by FTY720 nanofibers at 3 days, we assessed healing parameters. FTY720 nanofiber treated animals displayed increased fiber diameter compared to control animals, and increased collagen:desmin ratio. Though we have previously attributed high collagen:desmin ratio to an increased fibrotic response, those observations were made in 1mm volumetric defects which close over 7 days (Figure 17) [105]. In this 2mm defect model, tissue must regenerate over 3-fold more area than that in the 1mm defect model. Thus, increased matrix deposition may be beneficial in this context to guide the growth of muscle fibers. Skeletal muscle fibers produce maximum force along a single axis. Consequently, it is crucial for injured fibers to regenerate in alignment with pre-existing muscle fibers. We observed a lower angle between regenerating muscle fibers and the original fiber axis in animals treated with FTY720 NF scaffolds, indicating improved alignment (Figure 40). This higher alignment may be primarily due to the effects of FTY720, and not the presence of nanoarchitecture within the scaffold, as polymer thin films released FTY720 also induced a degree of alignment comparable to that observed with FTY720 nanofiber treatment (16.73 ± 2.35° in films, versus 17.82 ± 5.6° in nanofibers) (Figure 41).The delivery of FTY720 from a biomaterial scaffold was crucial to inducing increased fiber alignment, as animals receiving superfusion of FTY720 with blank scaffold did not display increased fiber alignment (Figure 40).

The mechanism by which FTY720 mediates fiber alignment is unknown at this point. Alternatively-activated macrophages have been shown to promote extracellular matrix synthesis within fibroblasts [53] and fibroadipogenic progenitors [55]. We observed increased collagen deposition in animals treated with FTY720 nanofibers. Recently, it was

demonstrated that fibroblasts encapsulated within a collagen matrix rapidly generate tensile forces to close micro surgically induced defects [153]. It is possible that the increases in CD206+Ly6C- macrophages (mediated by FTY720 nanofibers) enhances activity of infiltrating fibroblasts that generate mechanical contractile forces over the defect void that encourage muscle cell alignment (as has been demonstrated *in vitro)*[154]. Cells present within the injury niche may also interact directly with the provisional support provided by the nanofiber scaffolds themselves[155], and indeed, stem cell proliferation and differentiation [156] and fibroblast adhesion and proliferation [157] has been shown to be dependent on nanofiber diameter. The average diameter of individual PLGA/PCL nanofibers was 1.2 ± 0.71 μm whereas the average diameter in that of FTY720-NF was 0.45 ± 0.17 μm. Though both scaffolds possess individual fiber diameter on scales at which cells can interact [155], fibroblasts have been shown to exhibit increased proliferation in response to smaller diameter fibers (250-300 nm) versus larger diameter fibers (500 nm-1 μm)[158]. FTY720-NF scaffolds displayed smaller individual fiber diameter and this topographical feature may have encouraged increased fibroblast proliferation and matrix deposition compared to blank scaffolds in which fiber diameter was higher. Future studies that more closely pair fiber diameter between blank and drug-loaded scaffolds will be necessary. In addition, we observed aligned morphology of collagen fibers alongside the regenerated muscle fibers (Figure 38) within FTY720-NF treated animal. Mechanical and architectural cues from either the scaffold itself or from cells interacting with the scaffold may contribute to the increased alignment of regenerated muscle fibers observed in FTY720 treated animals. However, inspection of FT720 treated defects at later time points

will be crucial to ensure that the increased matrix seen with treatment is remodeled sufficiently so that persistent fibrosis does not occur.

Though we observed improved healing metrics within volumetric muscle defects treated with FTY720 nanofibers, whether the regenerated muscle can undergo contractions and generate force cannot be determined from imaging. Thus, we designed a testing apparatus that enables the measurement of contractile forces generated by spinotrapezius muscles. Using this apparatus, we were able to detect a statistically significant difference in force generation between healthy and injured muscles 28-days post-injury. It is possible that this difference is due to atrophy of the muscle either from denervation [159], or from muscle underuse/disuse [160] following injury. The proportion of resected muscle out of the total muscle strip was 11%, and thus a theoretical decrease of 11% of muscle force generation in a completely unhealed defect may be expected. The mean initial force generation of healthy muscle spinotrapezius strips was 1.7±0.5 grams of force. An 11% theoretical decrease in force generation would be 1.5 grams, however, all injured groups exhibited a mean initial force generation less than 1.5g (untreated: 1.1±0.2 g, blank implant: 0.8±0.4 g, FTY implant: 0.65±0.3 g). However, fibrosis that occurs as a result of volumetric muscle injuries may also affect muscle stiffness [161] and thus affect contractility. Further studies will be needed to discern how force generation within injured murine spinotrapezius strips is impacted as a result of time after injury. Though we were unable to detect differences between treatment groups, our ability to detect differences in force generation between healthy and injured spinotrapezius muscle strips represents a sizable leap in method development for *ex vivo* functional testing. This will likely enable the field to assess force generation of other thin muscles such as the diaphragm.

Additionally, this method might be more effective in detecting contractile force differences in studies looking at systemic treatments in which the entirety of the muscle may be affected, rather than localized injury and treatment.

We believe that the value of the spinotrapezius volumetric muscle loss model lies in its capacity to screen therapies for favorable acute cellular responses and in evaluating localized healing outcomes. With confocal imaging, we were able to demonstrate for the first time that CD68+ macrophages closely interact with regenerating muscle fibers (Figure 34). Notably, we observed Thy1+ axons running along vascular structures marked with desmin+ pericytes. (Figure 44). The spatial coupling of axonal regrowth and vasculature provides evidence that regeneration of tissue microcompartments do not occur in isolation, but rather, rely on coordinated interplay between multiple cell types.

Taken together, we have demonstrated that local immunomodulation of innate and adaptive immune responses via FTY720 nanofibers coincide with increased satellite cell numbers after volumetric muscle injury. Animals treated with FTY720 NF displayed improved muscle healing and alignment. Our work highlights the promise of engineering immunomodulatory biomolecules into electrospun biomaterial scaffolds that promote the regeneration of skeletal muscle.

6. CONCLUSIONS AND FUTURE DIRECTIONS

6.1 Overall Summary

In the present work, we expanded our knowledge of the origin of anti-inflammatory CD206+ macrophages within soft tissue injury by demonstrating that non-classical Ly6C^{lo} monocytes are biased towards differentiation into wound-healing macrophages. We utilized this information to design biomaterial therapeutics that selectively recruit non-classical monocytes to a novel model of volumetric skeletal muscle injury and show improved muscle regeneration.

In Aim 1, we identified non-classical monocytes as biased progenitors of CD206+ alternatively-activated macrophages within excisional skin injury. Blood monocytes exist in two primary subpopulations that are broadly characterized as inflammatory (classical) or anti-inflammatory (non-classical). Using latex bead-based labeling techniques, we show that labeled non-classical monocytes preferentially differentiate into alternatively-activated macrophages, whereas labeled classical monocytes do not display this differentiation bias. Depletion of blood non-classical monocytes significantly reduces the generation of CD206+ alternatively-activated macrophages. We compared adoptive transfer of classical versus non-classical monocytes into the circulation of animals undergoing cutaneous injury, and show increased frequency of wound healing macrophages derived from Ly6C^{lo} donor cells compared to Ly6C^{hi} donor cells. Taken together, the results highlight non-classical monocytes as key contributors to the pool of alternatively activated macrophages within skin injury. The *significance* of this work lies in our improved understanding of the relationship between blood-derived monocytes and

injury macrophage subsets and provides a rationale for targeting non-classical monocytes in other models of soft tissue injury where alternatively-activated macrophages are known to exert beneficial roles.

In Aim 2, we demonstrated for the first time that non-classical monocytes are directly recruited to volumetric muscle injury and that their recruitment can be increased by local delivery of the immunomodulatory molecule FTY720. Enrichment of non-classical monocytes within muscle injury coincided with increased CD206+ alternatively-activated macrophages in peri-defect tissue. Assessment of early wound healing parameters revealed that FTY720 increases collagen deposition and vascularization in the defect area. Evaluation of muscle healing at later time points showed increased regenerated muscle fiber diameter and decreased fibrotic collagen deposition with FTY720 treatment. Taken together, these results indicate that local immunomodulation of volumetric skeletal muscle injuries by targeting non-classical monocytes can accelerate muscle healing and attenuate the fibrotic response often seen in clinical VML injuries. The *significance* of this work lies both in the establishment of the spinotrapezius VML model as a tool to investigate mechanisms of *de novo* skeletal muscle regeneration, and in our enhanced understanding of the role that non-classical monocytes play in volumetric muscle defect healing.

In Aim 3, we expanded the spinotrapezius VML model to include a 2mm diameter defect that does not regain full functional recovery over the experimental time course and further explored the mechanisms by which FTY720-encapsulating nanofiber scaffolds impact local immune modulation and muscle healing parameters. We demonstrate that implantation of FTY720 nanofibers over 2mm diameter muscle defects induces acute

lymphopenia and decreases acute CD4+ and CD8+ T lymphocyte accumulation in injured muscle. We hypothesized that the changes in T lymphoid cellular populations early after muscle injury may impact myeloid subset distribution, and indeed, we observed increases in both $Ly6C^{lo}$ non-classical monocytes and CD206+Ly6C- alternatively activated macrophages in response to FTY720 nanofiber treatment. We show for the first time that local immune modulation of adaptive and innate cell subsets coincides with increased numbers of satellite cells within volumetric skeletal muscle injury. Increased alignment of regenerated muscle fibers to the pre-injury fiber axis was observed in animals treated with FTY720 and we demonstrate that this increased alignment relies on the presentation and delivery of FTY720 from a biomaterial scaffold, but not the nano-architecutre. Taken together, these results indicate that FTY720 nanofibers are able to positively impact aspects of muscle regeneration in a non-healing volumetric defect. The *significance* of this work lies in elucidating a connection between lymphoid and myeloid immune cell subset distribution in a non-healing volumetric muscle defect, and demonstrating improved alignment of regenerated muscle fibers along the pre-injury fiber axis. These results highlight the need for additional mechanistic studies to better understand the complex interplay between adaptive and innate immune responses within traumatic muscle injury.

6.2 Identification of regenerative niche components crucial to muscle repair

In the current work, we explored the impact of biomaterial-based delivery of FTY720 on tuning local immune responses to volumetric muscle injury. This was motivated by our identification of non-classical monocytes as biased progenitors of alternatively activated macrophages, and the knowledge that M2-biased injury microenvironments support muscle regeneration, vascularization, and nerve repair. Future

improvements to immunomodulatory biomaterials for the treatment of muscle injuries should focus on 1) identifying components of the regenerative niche that are critical to muscle repair, and 2) incorporation of several cues, whether biological or architectural, to form multi-modal therapies that target more than one regenerative pathway.

Volumetric muscle defects are unique from other models of muscle injury (such as toxin, crush, or cryo-injury) in that all tissue micro compartments must be regenerated *de novo* over large spatial gaps. Studies in toxin-induced muscle injury show that the residual basal lamina ("ghost fibers") that remains after muscle fiber necrosis serves as a structural guide for activated satellite cells to migrate and proliferate along the original fiber axis. Removal of these ghost fibers in volumetric injury results in uncoordinated satellite cell migration, division along diverging axes, and generation of muscle fibers that exhibit chaotic organization [144]. In the current work, we provided a structural surface in the form of nanofiber scaffolds to a large volumetric defect, but did not see an improvement in regenerated fiber alignment due to scaffold alone. Logical next steps in improving the nanofiber therapy platform lies in engineering aligned nanofiber scaffolds that recapitulate the architectural guidance provided by ghost fibers.

Our motivation for targeting the immune response to muscle injury lies in the concept that macrophages are highly sensitive to their microenvironments and adopt functional phenotypes to further orchestrate the behaviors of multiple cell types including vascular cells, satellite cells, and matrix-producing stromal cells. However, stages in myogenesis are tightly coupled to the inflammatory state of the tissue microenvironment. Satellite cell activation and proliferation primarily occurs in the acute pro-inflammatory phase of healing, and satellite cell differentiation occurs in the later, anti-inflammatory

phase of healing, and the failure to undergo each immune state leads to impaired muscle regeneration. In the present work, we aimed to augment the anti-inflammatory, pro-regenerative phase of healing by locally enriching the injury pool of non-classical monocytes and alternatively-activated macrophages. However, the therapy was initiated at the time of injury. Moving forward, an interesting avenue of exploration is the design of biomaterials that release multiple cues that are temporally segregated so as to amplify both the inflammatory phase, and the pro-regenerative phases of healing. Such therapies could employ acute release of recruitment signals such as monocyte chemoattractant protein-1 (MCP-1/CCL2) to attract inflammatory monocytes and macrophages that enhance satellite cell proliferation, and then delayed, sustained release of molecules such as FTY720 or fractalkine that are known to recruit pro-regenerative subsets of monocytes and macrophages to facilitate satellite cell differentiation and tissue remodeling and maturation. Use of other biomaterial platforms such as hydrogel materials enables the tethering of bioactive molecules to the gel via hydrolytically or enzymatically degradable moieties. Selection of the appropriate tethering mechanism per pro- or anti- inflammatory recruitment signal could augment both early and late phases of the immune response with precise temporal regulation.

Other bioactive molecules have been delivered to models of ischemic skeletal muscle injury to promote vascularization (vascular endothelial growth factor – VEGF), to influence the behavior of satellite cells (IGF-1)[162], or to enhance the recruitment of regenerative stem cell populations (SDF-1)[163]. These strategies show varying degrees of success at promoting functional recovery of the muscle, but none have been tested in a

model of volumetric muscle loss. Future studies should test whether these therapies are successful at promoting regeneration of traumatic muscle injuries.

6.3 Improved characterization of innate and adaptive immune cell function in volumetric muscle injury

Much of the knowledge about immune cell subset functions in healing of skeletal muscle injuries have been performed in models of toxin-induced muscle injury. It is increasingly appreciated that immune biology is context dependent. Studies that deplete subpopulations of monocytes/macrophages along the timescale of volumetric muscle defect regeneration (as has been done in toxin induced muscle injury [29]) will elucidate whether particular populations of macrophages are primarily responsible for growth of muscle fibers versus attenuation of fibrosis and fatty infiltration. More detailed studies employing transcriptional profiling of monocyte/macrophage subpopulations present in each stage of muscle repair could reveal gene expression signatures unique to volumetric muscle defect healing. Use of single-cell RNA-sequencing or Mass Cytometry (CyTOF) techniques on immune cells isolated from traumatically-injured skeletal muscle, and downstream bioinformatics analysis could reveal novel subpopulations of muscle-specific wound healing myeloid cells, and additional therapeutic targets.

Though alternatively-activated M2 macrophages (as identified by CD206+ and/or arginase-1 expression) are broadly accepted as pro-regenerative, the heterogeneity in M2 subtypes depending on polarization stimulus (IL-4 vs IL-10) and their subsequent functional effects on tissue regeneration *in vivo* remains unclear. Adoptive transfer of polarized primary macrophages stimulated by either IL-4 or IL-10 into muscle injury and

analysis of satellite cell proliferation and differentiation could answer questions regarding the effects of M2 subtypes on satellite cell behavior in a volumetric muscle defect context.

The role that T lymphocytes, and particularly CD4+CD25+Foxp3+ regulatory T-cells (Treg), play in toxin-induced muscle injury is increasingly appreciated. Apart from directly promoting the growth of muscle fiber via secretion of Amphiregulin (Areg), Tregs are also thought to govern the myeloid phenotype switch from inflammatory to pro-regenerative, however, the mechanisms by which they achieve this switch is unknown. Though CD4+ and CD8+ T-lymphocytes were detected in volumetrically injured skeletal muscle, their roles in the regenerative process are unclear. CD4+/CD8+ T cells have been shown to exacerbate pathophysiology in dystrophic mice[84], whereas ablation of CD8+ T-cells in toxin-injured muscle prevented the accumulation of inflammatory macrophages early after injury, imparing muscle regeneration[83]. Adding another layer of complexity is the understudied impact of lymphoid cell-secreted cytokines on macrophage polarization. Gain or loss of function studies that systematically target T-lymphocyte populations, and analyzing resulting changes in local cytokine profile and macrophage subset distribution would significantly advance our understanding of the relationship between adaptive and innate immunity in muscle regeneration.

6.4 Extension of immunomodulatory therapies to other regenerative medicine applications

The spinotrapezius volumetric muscle loss model that we established in this work lends itself particularly well to the study of cellular responses and examination of healing progress on the microscopic level. However, the small size of the defect and muscle renders

the ability to detect functional differences extremely challenging. Future studies should test the developed immunomodulatory materials in volumetric defects created in larger muscles such as the murine or rat quadriceps. Due to the availability of the femoral nerve in the quadriceps muscle, *in situ* functional testing can be performed[164]. Though polymer films and electrospun nanofibers were utilized in the current studies, they are not themselves void filling. Incorporation of FTY720 into void filling, yet degradable materials (such as hydrogels or extracellular matrix-derived scaffolds) would provide initial structural support for the migration of cells into the defect, and favorably prime the immune microenvironment for regeneration. However, closely engineering the degradation rates of the void filling material is crucial so as to not impede new tissue growth.

In the clinic, muscle flaps are implanted into volumetric injuries but exhibit poor integration into surrounding tissue. Flat biomaterials such as nanofiber strips or sheets could be sandwiched between muscle flap allografts to form a composite construct that fills the muscle defect void. Indeed, the spinotrapezius muscle itself could serve as a model for muscle flaps, by co-implanting an autograft derived from contralateral spinotrapezius muscle with a nanofiber scaffold over a full-thickness defect and assessing integration of the whole construct by imaging techniques that we have extensively developed. This would be particularly interesting in the context of aging muscle that exhibits a severe decline in regenerative capacity after injury.

Because our work was based on the concept of tuning immune responses to soft tissue injury, rather than targeting tissue-specific cells, the findings from our studies can be extended to a multitude of regenerative medicine applications. Any tissue injury is accompanied by an inflammatory response, which provides opportunities for modulating

that response to accelerate or enhance repair. Such applications include using immunomodulatory biomaterials to promote cardiac muscle repair after infarct injury, to promote re-epithelialization of large or chronic cutaneous wounds, or to guide palatal tissue healing after surgical repair of cleft palate abnormalities.

6.5 Conclusions

By tracking and modulating the recruitment of myeloid cells to soft tissue injuries, we have identified non-classical monocytes as a key contributor to the pool of wound healing macrophages. We have demonstrated that locally enriching pro-regenerative monocytes and macrophages via biomaterial based delivery of FTY720 represents a promising strategy for overcoming aspects of clinical challenges faced in treating volumetric muscle loss injuries, such as attenuating fibrosis and improving alignment of regenerated muscle fibers. Taken together, we have gained an improved understand of the role that pro-regenerative subsets of immune cells play in the promotion of endogenous mechanisms of tissue repair after traumatic injuries.

REFERENCES

[1] W.R. Frontera, J. Ochala, Skeletal Muscle: A Brief Review of Structure and Function, Calcified Tissue International 96(3) (2015) 183-195.

[2] R.R. Wolfe, The underappreciated role of muscle in health and disease, The American Journal of Clinical Nutrition 84(3) (2006) 475-482.

[3] G. Begue, U. Raue, B. Jemiolo, S. Trappe, DNA methylation assessment from human slow- and fast-twitch skeletal muscle fibers, Journal of Applied Physiology 122(4) (2017) 952-967.

[4] P. Mishra, G. Varuzhanyan, A.H. Pham, D.C. Chan, Mitochondrial dynamics is a distinguishing feature of skeletal muscle fiber types and regulates organellar compartmentalization, Cell metabolism 22(6) (2015) 1033-44.

[5] H. Yin, F. Price, M.A. Rudnicki, Satellite Cells and the Muscle Stem Cell Niche, Physiological Reviews 93(1) (2013) 23-67.

[6] D. Bosnakovski, Z. Xu, W. Li, S. Thet, O. Cleaver, R.C. Perlingeiro, M. Kyba, Prospective isolation of skeletal muscle stem cells with a Pax7 reporter, Stem Cells 26 (2008).

[7] C.C. Maesner, A.E. Almada, A.J. Wagers, Established cell surface markers efficiently isolate highly overlapping populations of skeletal muscle satellite cells by fluorescence-activated cell sorting, Skeletal Muscle 6(1) (2016) 35.

[8] J.G. Tidball, Regulation of muscle growth and regeneration by the immune system, Nat Rev Immunol 17(3) (2017) 165-178.

[9] C.J. Mann, E. Perdiguero, Y. Kharraz, S. Aguilar, P. Pessina, A.L. Serrano, P. Munoz-Canoves, Aberrant repair and fibrosis development in skeletal muscle, Skelet Muscle 1(1) (2011) 21.

[10] J. Chawla, Stepwise Approach to Myopathy in Systemic Disease, Frontiers in Neurology 2 (2011).

[11] N.C. Chang, F.P. Chevalier, M.A. Rudnicki, Satellite Cells in Muscular Dystrophy – Lost in Polarity, Trends in Molecular Medicine 22(6) 479-496.

[12] C. Auffray, D. Fogg, M. Garfa, G. Elain, O. Join-Lambert, S. Kayal, S. Sarnacki, A. Cumano, G. Lauvau, F. Geissmann, Monitoring of blood vessels and tissues by a population of monocytes with patrolling behavior, Science 317(5838) (2007) 666-70.

[13] C. Jakubzick, E.L. Gautier, S.L. Gibbings, D.K. Sojka, A. Schlitzer, T.E. Johnson, S. Ivanov, Q. Duan, S. Bala, T. Condon, N. van Rooijen, J.R. Grainger, Y. Belkaid, A. Ma'ayan, D.W. Riches, W.M. Yokoyama, F. Ginhoux, P.M. Henson, G.J. Randolph, Minimal differentiation of classical monocytes as they survey steady-state tissues and transport antigen to lymph nodes, Immunity 39(3) (2013) 599-610.

[14] F. Ginhoux, S. Jung, Monocytes and macrophages: developmental pathways and tissue homeostasis, Nature reviews. Immunology 14(6) (2014) 392-404.

[15] F. Ginhoux, M. Greter, M. Leboeuf, S. Nandi, P. See, S. Gokhan, M.F. Mehler, S.J. Conway, L.G. Ng, E.R. Stanley, I.M. Samokhvalov, M. Merad, Fate mapping analysis reveals that adult microglia derive from primitive macrophages, Science (New York, N.Y.) 330(6005) (2010) 841-5.

[16] D. Hashimoto, A. Chow, C. Noizat, P. Teo, M.B. Beasley, M. Leboeuf, C.D. Becker, P. See, J. Price, D. Lucas, M. Greter, A. Mortha, S.W. Boyer, E.C. Forsberg, M. Tanaka, N. van Rooijen, A. Garcia-Sastre, E.R. Stanley, F. Ginhoux, P.S. Frenette, M. Merad, Tissue-resident macrophages self-maintain locally throughout adult life with minimal contribution from circulating monocytes, Immunity 38(4) (2013) 792-804.

[17] S. Yona, K.W. Kim, Y. Wolf, A. Mildner, D. Varol, M. Breker, D. Strauss-Ayali, S. Viukov, M. Guilliams, A. Misharin, D.A. Hume, H. Perlman, B. Malissen, E. Zelzer, S. Jung, Fate mapping reveals origins and dynamics of monocytes and tissue macrophages under homeostasis, Immunity 38(1) (2013) 79-91.

[18] K.J. Lavine, S. Epelman, K. Uchida, K.J. Weber, C.G. Nichols, J.D. Schilling, D.M. Ornitz, G.J. Randolph, D.L. Mann, Distinct macrophage lineages contribute to disparate patterns of cardiac recovery and remodeling in the neonatal and adult heart, Proceedings of the National Academy of Sciences of the United States of America 111(45) (2014) 16029-34.

[19] L.C. Davies, Tissue-resident macrophages, 14(10) (2013) 986-95.

[20] C. Qu, E.W. Edwards, F. Tacke, V. Angeli, J. Llodra, G. Sanchez-Schmitz, A. Garin, N.S. Haque, W. Peters, N. van Rooijen, C. Sanchez-Torres, J. Bromberg, I.F. Charo, S. Jung, S.A. Lira, G.J. Randolph, Role of CCR8 and other chemokine pathways in the migration of monocyte-derived dendritic cells to lymph nodes, The Journal of experimental medicine 200(10) (2004) 1231-41.

[21] K.L. Wong, J.J. Tai, W.C. Wong, H. Han, X. Sem, W.H. Yeap, P. Kourilsky, S.C. Wong, Gene expression profiling reveals the defining features of the classical, intermediate, and nonclassical human monocyte subsets, Blood 118(5) (2011) e16-31.

[22] C. Sunderkotter, T. Nikolic, M.J. Dillon, N. Van Rooijen, M. Stehling, D.A. Drevets, P.J. Leenen, Subpopulations of mouse blood monocytes differ in maturation stage and inflammatory response, J Immunol 172(7) (2004) 4410-7.

[23] D.M. Mosser, J.P. Edwards, Exploring the full spectrum of macrophage activation, Nat Rev Immunol 8(12) (2008) 958-69.

[24] B. Deng, M. Wehling-Henricks, S.A. Villalta, Y. Wang, J.G. Tidball, IL-10 triggers changes in macrophage phenotype that promote muscle growth and regeneration, J Immunol 189(7) (2012) 3669-80.

[25] Y. Okuno, A. Nakamura-Ishizu, K. Kishi, T. Suda, Y. Kubota, Bone marrow-derived cells serve as proangiogenic macrophages but not endothelial cells in wound healing, Blood 117(19) (2011) 5264-72.

[26] Y. Takeda, S. Costa, E. Delamarre, C. Roncal, R. Leite de Oliveira, M.L. Squadrito, V. Finisguerra, S. Deschoemaeker, F. Bruyere, M. Wenes, A. Hamm, J. Serneels, J. Magat, T. Bhattacharyya, A. Anisimov, B.F. Jordan, K. Alitalo, P. Maxwell, B. Gallez, Z.W. Zhuang, Y. Saito, M. Simons, M. De Palma, M. Mazzone, Macrophage skewing by Phd2 haplodeficiency prevents ischaemia by inducing arteriogenesis, Nature 479(7371) (2011) 122-6.

[27] D.H. Madsen, D. Leonard, A. Masedunskas, A. Moyer, H.J. Jurgensen, D.E. Peters, P. Amornphimoltham, A. Selvaraj, S.S. Yamada, D.A. Brenner, S. Burgdorf, L.H. Engelholm, N. Behrendt, K. Holmbeck, R. Weigert, T.H. Bugge, M2-like macrophages are responsible for collagen degradation through a mannose receptor-mediated pathway, J Cell Biol 202(6) (2013) 951-66.

[28] K.A. Kigerl, J.C. Gensel, D.P. Ankeny, J.K. Alexander, D.J. Donnelly, P.G. Popovich, Identification of two distinct macrophage subsets with divergent effects causing either neurotoxicity or regeneration in the injured mouse spinal cord, The Journal of neuroscience : the official journal of the Society for Neuroscience 29(43) (2009) 13435-44.

[29] L. Arnold, A. Henry, F. Poron, Y. Baba-Amer, N. van Rooijen, A. Plonquet, R.K. Gherardi, B. Chazaud, Inflammatory monocytes recruited after skeletal muscle injury switch into antiinflammatory macrophages to support myogenesis, The Journal of experimental medicine 204(5) (2007) 1057-69.

[30] P. Ramachandran, A. Pellicoro, M.A. Vernon, L. Boulter, R.L. Aucott, A. Ali, S.N. Hartland, V.K. Snowdon, A. Cappon, T.T. Gordon-Walker, M.J. Williams, D.R. Dunbar, J.R. Manning, N. van Rooijen, J.A. Fallowfield, S.J. Forbes, J.P. Iredale, Differential Ly-6C expression identifies the recruited macrophage phenotype, which orchestrates the regression of murine liver fibrosis, Proc Natl Acad Sci U S A 109(46) (2012) E3186-95.

[31] N.M. Girgis, U.M. Gundra, L.N. Ward, M. Cabrera, U. Frevert, P. Loke, Ly6C(high) monocytes become alternatively activated macrophages in schistosome granulomas with help from CD4+ cells, PLoS Pathog 10(6) (2014) e1004080.

[32] L. Denney, W.L. Kok, S.L. Cole, S. Sanderson, A.J. McMichael, L.P. Ho, Activation of invariant NKT cells in early phase of experimental autoimmune encephalomyelitis results in differentiation of Ly6Chi inflammatory monocyte to M2 macrophages and improved outcome, J Immunol 189(2) (2012) 551-7.

[33] M. Nahrendorf, F.K. Swirski, E. Aikawa, L. Stangenberg, T. Wurdinger, J.L. Figueiredo, P. Libby, R. Weissleder, M.J. Pittet, The healing myocardium sequentially mobilizes two monocyte subsets with divergent and complementary functions, The Journal of experimental medicine 204(12) (2007) 3037-47.

[34] A.O. Awojoodu, M.E. Ogle, L.S. Sefcik, D.T. Bowers, K. Martin, K.L. Brayman, K.R. Lynch, S.M. Peirce-Cottler, E. Botchwey, Sphingosine 1-phosphate receptor 3 regulates recruitment of anti-inflammatory monocytes to microvessels during implant arteriogenesis, Proceedings of the National Academy of Sciences of the United States of America 110(34) (2013) 13785-90.

[35] A.V. Misharin, C.M. Cuda, R. Saber, J.D. Turner, A.K. Gierut, G.K. Haines, 3rd, S. Berdnikovs, A. Filer, A.R. Clark, C.D. Buckley, G.M. Mutlu, G.R. Budinger, H. Perlman, Nonclassical Ly6C(-) monocytes drive the development of inflammatory arthritis in mice, Cell Rep 9(2) (2014) 591-604.

[36] C.E. Olingy, C.L. San Emeterio, M.E. Ogle, J.R. Krieger, A.C. Bruce, D.D. Pfau, B.T. Jordan, S.M. Peirce, E.A. Botchwey, Non-classical monocytes are biased progenitors of wound healing macrophages during soft tissue injury, Sci Rep 7(1) (2017) 447.

[37] M. Summan, G.L. Warren, R.R. Mercer, R. Chapman, T. Hulderman, N. Van Rooijen, P.P. Simeonova, Macrophages and skeletal muscle regeneration: a clodronate-containing liposome depletion study, American Journal of Physiology - Regulatory, Integrative and Comparative Physiology 290(6) (2006) R1488-R1495.

[38] T. Lucas, A. Waisman, R. Ranjan, J. Roes, T. Krieg, W. Muller, A. Roers, S.A. Eming, Differential roles of macrophages in diverse phases of skin repair, J Immunol 184(7) (2010) 3964-77.

[39] M.J. van Amerongen, M.C. Harmsen, N. van Rooijen, A.H. Petersen, M.J. van Luyn, Macrophage depletion impairs wound healing and increases left ventricular remodeling after myocardial injury in mice, The American journal of pathology 170(3) (2007) 818-29.

[40] S. Li, B. Li, H. Jiang, Y. Wang, M. Qu, H. Duan, Q. Zhou, W. Shi, Macrophage depletion impairs corneal wound healing after autologous transplantation in mice, PloS one 8(4) (2013) e61799.

[41] H. Wang, D.W. Melton, L. Porter, Z.U. Sarwar, L.M. McManus, P.K. Shireman, Altered macrophage phenotype transition impairs skeletal muscle regeneration, The American journal of pathology 184(4) (2014) 1167-84.

[42] M. Saclier, H. Yacoub-Youssef, A.L. Mackey, L. Arnold, H. Ardjoune, M. Magnan, F. Sailhan, J. Chelly, G.K. Pavlath, R. Mounier, M. Kjaer, B. Chazaud, Differentially activated macrophages orchestrate myogenic precursor cell fate during human skeletal muscle regeneration, Stem Cells 31(2) (2013) 384-96.

[43] Y.P. Li, TNF-alpha is a mitogen in skeletal muscle, American journal of physiology. Cell physiology 285(2) (2003) C370-6.

[44] H. Wang, E. Hertlein, N. Bakkar, H. Sun, S. Acharyya, J. Wang, M. Carathers, R. Davuluri, D.C. Guttridge, NF-kappaB regulation of YY1 inhibits skeletal myogenesis through transcriptional silencing of myofibrillar genes, Molecular and Cellular Biology 27(12) (2007) 4374-87.

[45] D.C. Guttridge, M.W. Mayo, L.V. Madrid, C.Y. Wang, A.S. Baldwin, Jr., NF-kappaB-induced loss of MyoD messenger RNA: possible role in muscle decay and cachexia, Science (New York, N.Y.) 289(5488) (2000) 2363-6.

[46] P. Londhe, J.K. Davie, Gamma interferon modulates myogenesis through the major histocompatibility complex class II transactivator, CIITA, Molecular and Cellular Biology 31(14) (2011) 2854-66.

[47] X. Wang, H. Wu, Z. Zhang, S. Liu, J. Yang, X. Chen, M. Fan, X. Wang, Effects of interleukin-6, leukemia inhibitory factor, and ciliary neurotrophic factor on the proliferation and differentiation of adult human myoblasts, Cellular and molecular neurobiology 28(1) (2008) 113-24.

[48] J. Tonkin, L. Temmerman, R.D. Sampson, E. Gallego-Colon, L. Barberi, D. Bilbao, M.D. Schneider, A. Musaro, N. Rosenthal, Monocyte/Macrophage-derived IGF-1 Orchestrates Murine Skeletal Muscle Regeneration and Modulates Autocrine Polarization, Mol Ther 23(7) (2015) 1189-200.

[49] B. Chazaud, C. Sonnet, P. Lafuste, G. Bassez, A.C. Rimaniol, F. Poron, F.J. Authier, P.A. Dreyfus, R.K. Gherardi, Satellite cells attract monocytes and use macrophages as a support to escape apoptosis and enhance muscle growth, J Cell Biol 163(5) (2003) 1133-43.

[50] M. Bencze, E. Negroni, D. Vallese, H. Yacoub-Youssef, S. Chaouch, A. Wolff, A. Aamiri, J.P. Di Santo, B. Chazaud, G. Butler-Browne, W. Savino, V. Mouly, I. Riederer, Proinflammatory macrophages enhance the regenerative capacity of human myoblasts by modifying their kinetics of proliferation and differentiation, Mol Ther 20(11) (2012) 2168-79.

[51] J.J. O'Shea, A. Ma, P. Lipsky, Cytokines and autoimmunity, Nat Rev Immunol 2(1) (2002) 37-45.

[52] G.C. Gurtner, S. Werner, Y. Barrandon, M.T. Longaker, Wound repair and regeneration, Nature 453 (2008).

[53] J.A. Knipper, S. Willenborg, J. Brinckmann, W. Bloch, T. Maass, R. Wagener, T. Krieg, T. Sutherland, A. Munitz, M.E. Rothenberg, A. Niehoff, R. Richardson, M. Hammerschmidt, J.E. Allen, S.A. Eming, Interleukin-4 Receptor alpha Signaling in Myeloid Cells Controls Collagen Fibril Assembly in Skin Repair, Immunity 43(4) (2015) 803-16.

[54] E. Song, N. Ouyang, M. Horbelt, B. Antus, M. Wang, M.S. Exton, Influence of alternatively and classically activated macrophages on fibrogenic activities of human fibroblasts, Cellular immunology 204(1) (2000) 19-28.

[55] D.R. Lemos, F. Babaeijandaghi, M. Low, C.K. Chang, S.T. Lee, D. Fiore, R.H. Zhang, A. Natarajan, S.A. Nedospasov, F.M. Rossi, Nilotinib reduces muscle fibrosis in chronic muscle injury by promoting TNF-mediated apoptosis of fibro/adipogenic progenitors, Nature medicine 21(7) (2015) 786-94.

[56] I. Avraham-Davidi, S. Yona, M. Grunewald, L. Landsman, C. Cochain, J.S. Silvestre, H. Mizrahi, M. Faroja, D. Strauss-Ayali, M. Mack, S. Jung, E. Keshet, On-site education of VEGF-recruited monocytes improves their performance as angiogenic and arteriogenic accessory cells, The Journal of experimental medicine 210(12) (2013) 2611-25.

[57] A. Fantin, J.M. Vieira, G. Gestri, L. Denti, Q. Schwarz, S. Prykhozhij, F. Peri, S.W. Wilson, C. Ruhrberg, Tissue macrophages act as cellular chaperones for vascular anastomosis downstream of VEGF-mediated endothelial tip cell induction, Blood 116(5) (2010) 829-40.

[58] M. Grunewald, I. Avraham, Y. Dor, E. Bachar-Lustig, A. Itin, S. Jung, S. Chimenti, L. Landsman, R. Abramovitch, E. Keshet, VEGF-induced adult neovascularization: recruitment, retention, and role of accessory cells, Cell 124(1) (2006) 175-89.

[59] S. Willenborg, T. Lucas, G. van Loo, J.A. Knipper, T. Krieg, I. Haase, B. Brachvogel, M. Hammerschmidt, A. Nagy, N. Ferrara, M. Pasparakis, S.A. Eming, CCR2 recruits an inflammatory macrophage subpopulation critical for angiogenesis in tissue repair, Blood 120(3) (2012) 613-25.

[60] C.W. Hsu, R.A. Poche, J.E. Saik, S. Ali, S. Wang, N. Yosef, G.A. Calderon, L. Scott, Jr., T.J. Vadakkan, I.V. Larina, J.L. West, M.E. Dickinson, Improved Angiogenesis in Response to Localized Delivery of Macrophage-Recruiting Molecules, PloS one 10(7) (2015) e0131643.

[61] A. Das, C.E. Segar, B.B. Hughley, D.T. Bowers, E.A. Botchwey, The promotion of mandibular defect healing by the targeting of S1P receptors and the recruitment of alternatively activated macrophages, Biomaterials 34(38) (2013) 9853-62.

[62] P.J. Murray, J.E. Allen, S.K. Biswas, E.A. Fisher, D.W. Gilroy, S. Goerdt, S. Gordon, J.A. Hamilton, L.B. Ivashkiv, T. Lawrence, M. Locati, A. Mantovani, F.O. Martinez, J.L. Mege, D.M. Mosser, G. Natoli, J.P. Saeij, J.L. Schultze, K.A. Shirey, A. Sica, J. Suttles, I. Udalova, J.A. van Ginderachter, S.N. Vogel, T.A. Wynn, Macrophage activation and polarization: nomenclature and experimental guidelines, Immunity 41(1) (2014) 14-20.

[63] N. Jetten, S. Verbruggen, M.J. Gijbels, M.J. Post, M.P. De Winther, M.M. Donners, Anti-inflammatory M2, but not pro-inflammatory M1 macrophages promote angiogenesis in vivo, Angiogenesis 17(1) (2014) 109-18.

[64] E. Zajac, B. Schweighofer, T.A. Kupriyanova, A. Juncker-Jensen, P. Minder, J.P. Quigley, E.I. Deryugina, Angiogenic capacity of M1- and M2-polarized macrophages is determined by the levels of TIMP-1 complexed with their secreted proMMP-9, Blood 122(25) (2013) 4054-67.

[65] K.L. Spiller, R.R. Anfang, K.J. Spiller, J. Ng, K.R. Nakazawa, J.W. Daulton, G. Vunjak-Novakovic, The role of macrophage phenotype in vascularization of tissue engineering scaffolds, Biomaterials 35(15) (2014) 4477-88.

[66] K.L. Spiller, S. Nassiri, C.E. Witherel, R.R. Anfang, J. Ng, K.R. Nakazawa, T. Yu, G. Vunjak-Novakovic, Sequential delivery of immunomodulatory cytokines to facilitate the M1-to-M2 transition of macrophages and enhance vascularization of bone scaffolds, Biomaterials 37 (2015) 194-207.

[67] J.R. Krieger, M.E. Ogle, J. McFaline-Figueroa, C.E. Segar, J.S. Temenoff, E.A. Botchwey, Spatially localized recruitment of anti-inflammatory monocytes by SDF-1alpha-releasing hydrogels enhances microvascular network remodeling, Biomaterials 77 (2016) 280-90.

[68] A.C. Bruce, M.R. Kelly-Goss, J.L. Heuslein, J.K. Meisner, R.J. Price, S.M. Peirce, Monocytes are recruited from venules during arteriogenesis in the murine spinotrapezius ligation model, Arteriosclerosis, thrombosis, and vascular biology 34(9) (2014) 2012-22.

[69] K. Stark, A. Eckart, S. Haidari, A. Tirniceriu, M. Lorenz, M.L. von Bruhl, F. Gartner, A.G. Khandoga, K.R. Legate, R. Pless, I. Hepper, K. Lauber, B. Walzog, S. Massberg, Capillary and arteriolar pericytes attract innate leukocytes exiting through venules and 'instruct' them with pattern-recognition and motility programs, Nature immunology 14(1) (2013) 41-51.

[70] H. He, J. Xu, C.M. Warren, D. Duan, X. Li, L. Wu, M.L. Iruela-Arispe, Endothelial cells provide an instructive niche for the differentiation and functional polarization of M2-like macrophages, Blood 120(15) (2012) 3152-62.

[71] A.G. Engel, Chapter 3 The neuromuscular junction, Handbook of Clinical Neurology, Elsevier2008, pp. 103-148.

[72] S. Rotshenker, Wallerian degeneration: the innate-immune response to traumatic nerve injury, Journal of Neuroinflammation 8 (2011) 109-109.

[73] G. Stoll, H.W. Muller, Nerve injury, axonal degeneration and neural regeneration: basic insights, Brain pathology (Zurich, Switzerland) 9(2) (1999) 313-25.

[74] W. Bruck, I. Huitinga, C.D. Dijkstra, Liposome-mediated monocyte depletion during wallerian degeneration defines the role of hematogenous phagocytes in myelin removal, Journal of neuroscience research 46(4) (1996) 477-84.

[75] P. Chen, X. Piao, P. Bonaldo, Role of macrophages in Wallerian degeneration and axonal regeneration after peripheral nerve injury, Acta Neuropathologica 130(5) (2015) 605-618.

[76] N. Mokarram, A. Merchant, V. Mukhatyar, G. Patel, R.V. Bellamkonda, Effect of modulating macrophage phenotype on peripheral nerve repair, Biomaterials 33(34) (2012) 8793-801.

[77] J.R. Potas, F. Haque, F.L. Maclean, D.R. Nisbet, Interleukin-10 conjugated electrospun polycaprolactone (PCL) nanofibre scaffolds for promoting alternatively activated (M2) macrophages around the peripheral nerve in vivo, Journal of immunological methods 420 (2015) 38-49.

[78] S.A. Villalta, A.S. Rosenberg, J.A. Bluestone, The immune system in Duchenne muscular dystrophy: Friend or foe, Rare Diseases 3(1) (2015) e1010966.

[79] M. Wehling, M.J. Spencer, J.G. Tidball, A nitric oxide synthase transgene ameliorates muscular dystrophy in mdx mice, The Journal of Cell Biology 155(1) (2001) 123-132.

[80] Y. Wang, M. Wehling-Henricks, G. Samengo, J.G. Tidball, Increases of M2a macrophages and fibrosis in aging muscle are influenced by bone marrow aging and negatively regulated by muscle-derived nitric oxide, Aging cell 14(4) (2015) 678-88.

[81] D. Burzyn, W. Kuswanto, D. Kolodin, J.L. Shadrach, M. Cerletti, Y. Jang, E. Sefik, T.G. Tan, A.J. Wagers, C. Benoist, D. Mathis, A special population of regulatory T cells potentiates muscle repair, Cell 155(6) (2013) 1282-95.

[82] W. Kuswanto, D. Burzyn, M. Panduro, K.K. Wang, Y.C. Jang, A.J. Wagers, C. Benoist, D. Mathis, Poor Repair of Skeletal Muscle in Aging Mice Reflects a Defect in Local, Interleukin-33-Dependent Accumulation of Regulatory T Cells, Immunity 44(2) (2016) 355-67.

[83] J. Zhang, Z. Xiao, C. Qu, W. Cui, X. Wang, J. Du, CD8 T Cells Are Involved in Skeletal Muscle Regeneration through Facilitating MCP-1 Secretion and Gr1^{high} Macrophage Infiltration, The Journal of Immunology 193 (2014) 5149-5160.

[84] M.J. Spencer, E. Montecino-Rodriguez, K. Dorshkind, J.G. Tidball, Helper (CD4+) and Cytotoxic (CD8+) T Cells Promote the Pathology of Dystrophin-Deficient Muscle, Clinical Immunology 98(2) (2001) 235-243.

[85] F. Geissmann, M.G. Manz, S. Jung, M.H. Sieweke, M. Merad, K. Ley, Development of monocytes, macrophages, and dendritic cells, Science (New York, N.Y.) 327(5966) (2010) 656-61.

[86] J.W. Godwin, A.R. Pinto, N.A. Rosenthal, Macrophages are required for adult salamander limb regeneration, Proceedings of the National Academy of Sciences of the United States of America 110(23) (2013) 9415-20.

[87] T.A. Wynn, K.M. Vannella, Macrophages in Tissue Repair, Regeneration, and Fibrosis, Immunity 44(3) (2016) 450-62.

[88] M.J. Crane, J.M. Daley, O. van Houtte, S.K. Brancato, W.L. Henry, Jr., J.E. Albina, The monocyte to macrophage transition in the murine sterile wound, PloS one 9(1) (2014) e86660.

[89] D. Dal-Secco, J. Wang, Z. Zeng, E. Kolaczkowska, C.H. Wong, B. Petri, R.M. Ransohoff, I.F. Charo, C.N. Jenne, P. Kubes, A dynamic spectrum of monocytes arising from the in situ reprogramming of CCR2+ monocytes at a site of sterile injury, The Journal of experimental medicine 212(4) (2015) 447-56.

[90] E. Zigmond, C. Varol, J. Farache, E. Elmaliah, A.T. Satpathy, G. Friedlander, M. Mack, N. Shpigel, I.G. Boneca, K.M. Murphy, G. Shakhar, Z. Halpern, S. Jung, Ly6C hi monocytes in the inflamed colon give rise to proinflammatory effector cells and migratory antigen-presenting cells, Immunity 37(6) (2012) 1076-90.

[91] S.J. Jenkins, D. Ruckerl, P.C. Cook, L.H. Jones, F.D. Finkelman, N. van Rooijen, A.S. MacDonald, J.E. Allen, Local macrophage proliferation, rather than recruitment from the blood, is a signature of TH2 inflammation, Science 332(6035) (2011) 1284-8.

[92] M.E. Ogle, C.E. Segar, S. Sridhar, E.A. Botchwey, Monocytes and macrophages in tissue repair: Implications for immunoregenerative biomaterial design, Exp Biol Med (Maywood) 241(10) (2016) 1084-97.

[93] F. Tacke, F. Ginhoux, C. Jakubzick, N. van Rooijen, M. Merad, G.J. Randolph, Immature monocytes acquire antigens from other cells in the bone marrow and present them to T cells after maturing in the periphery, The Journal of experimental medicine 203(3) (2006) 583-97.

[94] S. Potteaux, E.L. Gautier, S.B. Hutchison, N. van Rooijen, D.J. Rader, M.J. Thomas, M.G. Sorci-Thomas, G.J. Randolph, Suppressed monocyte recruitment drives macrophage removal from atherosclerotic plaques of Apoe-/- mice during disease regression, J Clin Invest 121(5) (2011) 2025-36.

[95] B. Shook, E. Xiao, Y. Kumamoto, A. Iwasaki, V. Horsley, CD301b+ Macrophages Are Essential for Effective Skin Wound Healing, Journal of Investigative Dermatology 136(9) (2016) 1885-1891.

[96] E.L. Gautier, T. Shay, J. Miller, M. Greter, C. Jakubzick, S. Ivanov, J. Helft, A. Chow, K.G. Elpek, S. Gordonov, A.R. Mazloom, A. Ma'ayan, W.J. Chua, T.H. Hansen, S.J. Turley, M. Merad, G.J. Randolph, C. Immunological Genome, Gene-expression profiles and transcriptional regulatory pathways that underlie the identity and diversity of mouse tissue macrophages, Nature immunology 13(11) (2012) 1118-28.

[97] M.E. Ogle, L.S. Sefcik, A.O. Awojoodu, N.F. Chiappa, K. Lynch, S. Peirce-Cottler, E.A. Botchwey, Engineering in vivo gradients of sphingosine-1-phosphate receptor ligands

for localized microvascular remodeling and inflammatory cell positioning, Acta biomaterialia (2014).

[98] F. Geissmann, S. Jung, D.R. Littman, Blood monocytes consist of two principal subsets with distinct migratory properties, Immunity 19(1) (2003) 71-82.

[99] L.M. Carlin, E.G. Stamatiades, C. Auffray, R.N. Hanna, L. Glover, G. Vizcay-Barrena, C.C. Hedrick, H.T. Cook, S. Diebold, F. Geissmann, Nr4a1-dependent Ly6C(low) monocytes monitor endothelial cells and orchestrate their disposal, Cell 153(2) (2013) 362-75.

[100] M. Stein, S. Keshav, N. Harris, S. Gordon, Interleukin 4 potently enhances murine macrophage mannose receptor activity: a marker of alternative immunologic macrophage activation, The Journal of experimental medicine 176(1) (1992) 287-92.

[101] F. Tacke, D. Alvarez, T.J. Kaplan, C. Jakubzick, R. Spanbroek, J. Llodra, A. Garin, J. Liu, M. Mack, N. van Rooijen, S.A. Lira, A.J. Habenicht, G.J. Randolph, Monocyte subsets differentially employ CCR2, CCR5, and CX3CR1 to accumulate within atherosclerotic plaques, The Journal of clinical investigation 117(1) (2007) 185-94.

[102] A. Das, C.E. Segar, Y. Chu, T.W. Wang, Y. Lin, C. Yang, X. Du, R.C. Ogle, Q. Cui, E.A. Botchwey, Bioactive lipid coating of bone allografts directs engraftment and fate determination of bone marrow-derived cells in rat GFP chimeras, Biomaterials 64 (2015) 98-107.

[103] S. Franz, S. Rammelt, D. Scharnweber, J.C. Simon, Immune responses to implants - a review of the implications for the design of immunomodulatory biomaterials, Biomaterials 32(28) (2011) 6692-709.

[104] A. Rodriguez, S.R. Macewan, H. Meyerson, J.T. Kirk, J.M. Anderson, The foreign body reaction in T-cell-deficient mice, J Biomed Mater Res A 90(1) (2009) 106-13.

[105] C.L. San Emeterio, C.E. Olingy, Y. Chu, E.A. Botchwey, Selective recruitment of non-classical monocytes promotes skeletal muscle repair, Biomaterials 117 (2017) 32-43.

[106] T. Varga, R. Mounier, A. Horvath, S. Cuvellier, F. Dumont, S. Poliska, H. Ardjoune, G. Juban, L. Nagy, B. Chazaud, Highly Dynamic Transcriptional Signature of Distinct Macrophage Subsets during Sterile Inflammation, Resolution, and Tissue Repair, The Journal of Immunology (2016).

[107] J. Sottile, Regulation of angiogenesis by extracellular matrix, Biochimica et biophysica acta 1654(1) (2004) 13-22.

[108] K. Garg, C.L. Ward, B.J. Hurtgen, J.M. Wilken, D.J. Stinner, J.C. Wenke, J.G. Owens, B.T. Corona, Volumetric muscle loss: Persistent functional deficits beyond frank loss of tissue, Journal of Orthopaedic Research 33(1) (2015) 40-46.

[109] Y. Takeda, S. Costa, E. Delamarre, C. Roncal, R. Leite de Oliveira, M.L. Squadrito, V. Finisguerra, S. Deschoemaeker, F. Bruyere, M. Wenes, A. Hamm, J. Serneels, J. Magat, T. Bhattacharyya, A. Anisimov, B.F. Jordan, K. Alitalo, P. Maxwell, B. Gallez, Z.W. Zhuang, Y. Saito, M. Simons, M. De Palma, M. Mazzone, Macrophage skewing by Phd2 haplodeficiency prevents ischaemia by inducing arteriogenesis, Nature 479(7371) (2011) 122-126.

[110] T.A.H. Järvinen, T.L.N. Järvinen, M. Kääriäinen, H. Kalimo, M. Järvinen, Muscle Injuries: Biology and Treatment, The American Journal of Sports Medicine 33(5) (2005) 745-764.

[111] N. Mokarram, A. Merchant, V. Mukhatyar, G. Patel, R.V. Bellamkonda, Effect of modulating macrophage phenotype on peripheral nerve repair, Biomaterials 33(34) (2012) 8793-8801.

[112] J. Rivera, R.L. Proia, A. Olivera, THE ALLIANCE OF SPHINGOSINE-1-PHOSPHATE AND ITS RECEPTORS IN IMMUNITY, Nature reviews. Immunology 8(10) (2008) 753-763.

[113] A.O. Awojoodu, M.E. Ogle, L.S. Sefcik, D.T. Bowers, K. Martin, K.L. Brayman, K.R. Lynch, S.M. Peirce-Cottler, E. Botchwey, Sphingosine 1-phosphate receptor 3 regulates recruitment of anti-inflammatory monocytes to microvessels during implant arteriogenesis, Proceedings of the National Academy of Sciences (2013).

[114] A.M. Guendel, K.S. Martin, J. Cutts, P.L. Foley, A.M. Bailey, F. Mac Gabhann, T.R. Cardinal, S.M. Peirce, Murine spinotrapezius model to assess the impact of arteriolar ligation on microvascular function and remodeling, Journal of visualized experiments : JoVE (73) (2013) e50218.

[115] A.M. Bailey, T.J.t. O'Neill, C.E. Morris, S.M. Peirce, Arteriolar remodeling following ischemic injury extends from capillary to large arteriole in the microcirculation, Microcirculation (New York, N.Y. : 1994) 15(5) (2008) 389-404.

[116] L. Micallef, N. Vedrenne, F. Billet, B. Coulomb, I.A. Darby, A. Desmoulière, The myofibroblast, multiple origins for major roles in normal and pathological tissue repair, Fibrogenesis & Tissue Repair 5(1) (2012) 1-5.

[117] E.L. Gautier, T. Shay, J. Miller, M. Greter, C. Jakubzick, S. Ivanov, J. Helft, A. Chow, K.G. Elpek, S. Gordonov, A.R. Mazloom, A. Ma'ayan, W.J. Chua, T.H. Hansen, S.J. Turley, M. Merad, G.J. Randolph, Gene-expression profiles and transcriptional regulatory pathways that underlie the identity and diversity of mouse tissue macrophages, Nature immunology 13(11) (2012) 1118-28.

[118] D. Pilling, T. Fan, D. Huang, B. Kaul, R.H. Gomer, Identification of Markers that Distinguish Monocyte-Derived Fibrocytes from Monocytes, Macrophages, and Fibroblasts, PloS one 4(10) (2009).

[119] A. Wollenberg, M. Mommaas, T. Oppel, E.M. Schottdorf, S. Gunther, M. Moderer, Expression and function of the mannose receptor CD206 on epidermal dendritic cells in inflammatory skin diseases, J Invest Dermatol 118(2) (2002) 327-34.

[120] S. McDougall, J. Dallon, J. Sherratt, P. Maini, Fibroblast migration and collagen deposition during dermal wound healing: mathematical modelling and clinical implications, Philosophical transactions. Series A, Mathematical, physical, and engineering sciences 364(1843) (2006) 1385-405.

[121] E. Rigamonti, T. Touvier, E. Clementi, A.A. Manfredi, S. Brunelli, P. Rovere-Querini, Requirement of Inducible Nitric Oxide Synthase for Skeletal Muscle Regeneration after Acute Damage, J Immunol 190(4) (2013) 1767-77.

[122] I.R. Dunay, R.A. Damatta, B. Fux, R. Presti, S. Greco, M. Colonna, L.D. Sibley, Gr1(+) inflammatory monocytes are required for mucosal resistance to the pathogen Toxoplasma gondii, Immunity 29(2) (2008) 306-17.

[123] S.L. Lin, A.P. Castano, B.T. Nowlin, M.L. Lupher, Jr., J.S. Duffield, Bone marrow Ly6Chigh monocytes are selectively recruited to injured kidney and differentiate into functionally distinct populations, J Immunol 183(10) (2009) 6733-43.

[124] S. Gordon, P.R. Taylor, Monocyte and macrophage heterogeneity, Nat Rev Immunol 5(12) (2005) 953-64.

[125] J. Kajahn, S. Franz, E. Rueckert, I. Forstreuter, V. Hintze, S. Moeller, J.C. Simon, Artificial extracellular matrices composed of collagen I and high sulfated hyaluronan modulate monocyte to macrophage differentiation under conditions of sterile inflammation, Biomatter 2(4) (2012) 226-73.

[126] V.A. Fadok, D.L. Bratton, A. Konowal, P.W. Freed, J.Y. Westcott, P.M. Henson, Macrophages that have ingested apoptotic cells in vitro inhibit proinflammatory cytokine production through autocrine/paracrine mechanisms involving TGF-beta, PGE2, and PAF, The Journal of clinical investigation 101(4) (1998) 890-8.

[127] C. Auffray, D.K. Fogg, E. Narni-Mancinelli, B. Senechal, C. Trouillet, N. Saederup, J. Leemput, K. Bigot, L. Campisi, M. Abitbol, T. Molina, I. Charo, D.A. Hume, A. Cumano, G. Lauvau, F. Geissmann, CX(3)CR1(+) CD115(+) CD135(+) common macrophage/DC precursors and the role of CX(3)CR1 in their response to inflammation, The Journal of experimental medicine 206(3) (2009) 595-606.

[128] L. Landsman, L. Bar-On, A. Zernecke, K.W. Kim, R. Krauthgamer, E. Shagdarsuren, S.A. Lira, I.L. Weissman, C. Weber, S. Jung, CX3CR1 is required for monocyte homeostasis and atherogenesis by promoting cell survival, Blood 113(4) (2009) 963-72.

[129] S. Jung, J. Aliberti, P. Graemmel, M.J. Sunshine, G.W. Kreutzberg, A. Sher, D.R. Littman, Analysis of Fractalkine Receptor CX(3)CR1 Function by Targeted Deletion and Green Fluorescent Protein Reporter Gene Insertion, Molecular and Cellular Biology 20(11) (2000) 4106-14.

[130] B.N. Brown, J.E. Valentin, A.M. Stewart-Akers, G.P. McCabe, S.F. Badylak, Macrophage phenotype and remodeling outcomes in response to biologic scaffolds with and without a cellular component, Biomaterials 30(8) (2009) 1482-91.

[131] S.F. Badylak, J.E. Valentin, A.K. Ravindra, G.P. McCabe, A.M. Stewart-Akers, Macrophage phenotype as a determinant of biologic scaffold remodeling, Tissue engineering. Part A 14(11) (2008) 1835-42.

[132] U.M. Gundra, N.M. Girgis, D. Ruckerl, S. Jenkins, L.N. Ward, Z.D. Kurtz, K.E. Wiens, M.S. Tang, U. Basu-Roy, A. Mansukhani, J.E. Allen, P. Loke, Alternatively activated macrophages derived from monocytes and tissue macrophages are phenotypically and functionally distinct, Blood 123(20) (2014) e110-22.

[133] V.A. Blaho, T. Hla, An update on the biology of sphingosine 1-phosphate receptors, Journal of Lipid Research (2014).

[134] M.E. Ogle, L.S. Sefcik, A.O. Awojoodu, N.F. Chiappa, K. Lynch, S. Peirce-Cottler, E.A. Botchwey, Engineering in vivo gradients of sphingosine-1-phosphate receptor ligands for localized microvascular remodeling and inflammatory cell positioning, Acta biomaterialia 10(11) (2014) 4704-14.

[135] C. Troidl, G. Jung, K. Troidl, J. Hoffmann, H. Mollmann, H. Nef, W. Schaper, C.W. Hamm, T. Schmitz-Rixen, The temporal and spatial distribution of macrophage subpopulations during arteriogenesis, Current vascular pharmacology 11(1) (2013) 5-12.

[136] D. Danieli-Betto, S. Peron, E. Germinario, M. Zanin, G. Sorci, S. Franzoso, D. Sandonà, R. Betto, Sphingosine 1-phosphate signaling is involved in skeletal muscle regeneration, American Journal of Physiology - Cell Physiology 298(3) (2010) C550-C558.

[137] M. Fortier, N. Figeac, R.B. White, P. Knopp, P.S. Zammit, Sphingosine-1-phosphate receptor 3 influences cell cycle progression in muscle satellite cells, Developmental Biology 382(2) (2013) 504-516.

[138] X. Wu, B.T. Corona, X. Chen, T.J. Walters, A standardized rat model of volumetric muscle loss injury for the development of tissue engineering therapies, BioResearch open access 1(6) (2012) 280-90.

[139] J. Huard, Y. Li, F.H. Fu, Muscle Injuries and Repair: Current Trends in Research, The Journal of Bone & Joint Surgery 84(5) (2002) 822-832.

[140] K. Garg, B.T. Corona, T.J. Walters, Therapeutic strategies for preventing skeletal muscle fibrosis after injury, Frontiers in pharmacology 6 (2015) 87.

[141] B.T. Corona, K. Garg, C.L. Ward, J.S. McDaniel, T.J. Walters, C.R. Rathbone, Autologous minced muscle grafts: a tissue engineering therapy for the volumetric loss of skeletal muscle, American Journal of Physiology - Cell Physiology 305(7) (2013) C761-C775.

[142] B.M. Sicari, V. Agrawal, B.F. Siu, C.J. Medberry, C.L. Dearth, N.J. Turner, S.F. Badylak, A murine model of volumetric muscle loss and a regenerative medicine approach for tissue replacement, Tissue engineering. Part A 18(19-20) (2012) 1941-8.

[143] B.F. Grogan, J.R. Hsu, Volumetric muscle loss, The Journal of the American Academy of Orthopaedic Surgeons 19 Suppl 1 (2011) S35-7.

[144] Micah T. Webster, U. Manor, J. Lippincott-Schwartz, C.-M. Fan, Intravital Imaging Reveals Ghost Fibers as Architectural Units Guiding Myogenic Progenitors during Regeneration, Cell Stem Cell 18(2) 243-252.

[145] J.A. Alberts B, Lewis J, et al., Molecular Biology of the Cell. 4th edition. The Extracellular Matrix of Animals. Available from: https://www.ncbi.nlm.nih.gov/books/NBK26810/. New York: Garland Science; , (2002).

[146] J.L. Dziki, B.M. Sicari, M.T. Wolf, M.C. Cramer, S.F. Badylak, Immunomodulation and Mobilization of Progenitor Cells by Extracellular Matrix Bioscaffolds for Volumetric Muscle Loss Treatment, Tissue engineering. Part A 22(19-20) (2016) 1129-1139.

[147] T.H. Qazi, D.J. Mooney, M. Pumberger, S. Geißler, G.N. Duda, Biomaterials based strategies for skeletal muscle tissue engineering: Existing technologies and future trends, Biomaterials 53(Supplement C) (2015) 502-521.

[148] E.K. Merritt, M.V. Cannon, D.W. Hammers, L.N. Le, R. Gokhale, A. Sarathy, T.J. Song, M.T. Tierney, L.J. Suggs, T.J. Walters, R.P. Farrar, Repair of traumatic skeletal muscle injury with bone-marrow-derived mesenchymal stem cells seeded on extracellular matrix, Tissue engineering. Part A 16(9) (2010) 2871-81.

[149] M.T. Li, M.A. Ruehle, H.Y. Stevens, N. Servies, N.J. Willett, S. Karthikeyakannan, G.L. Warren, R.E. Guldberg, L. Krishnan, * Skeletal Myoblast-Seeded Vascularized Tissue Scaffolds in the Treatment of a Large Volumetric Muscle Defect in the Rat Biceps Femoris Muscle, Tissue engineering. Part A 23(17-18) (2017) 989-1000.

[150] R. M Anthony, L. I Rutitzky, J. F Urban, M. J Stadecker, W. Gause, Protective immune mechanisms in helminth infection, 2008.

[151] K.L. Spiller, E.A. Wrona, S. Romero-Torres, I. Pallotta, P.L. Graney, C.E. Witherel, L.M. Panicker, R.A. Feldman, A.M. Urbanska, L. Santambrogio, G. Vunjak-Novakovic, D.O. Freytes, Differential gene expression in human, murine, and cell line-derived macrophages upon polarization, Exp Cell Res 347(1) (2016) 1-13.

[152] J.R. Schoenborn, C.B. Wilson, Regulation of interferon-gamma during innate and adaptive immune responses, Advances in immunology 96 (2007) 41-101.

[153] M.S. Sakar, J. Eyckmans, R. Pieters, D. Eberli, B.J. Nelson, C.S. Chen, Cellular forces and matrix assembly coordinate fibrous tissue repair, Nature Communications 7 (2016) 11036.

[154] I.C. Liao, J.B. Liu, N. Bursac, K.W. Leong, Effect of Electromechanical Stimulation on the Maturation of Myotubes on Aligned Electrospun Fibers, Cellular and Molecular Bioengineering 1(2) (2008) 133-145.

[155] U. Stachewicz, T. Qiao, S.C.F. Rawlinson, F.V. Almeida, W.-Q. Li, M. Cattell, A.H. Barber, 3D imaging of cell interactions with electrospun PLGA nanofiber membranes for bone regeneration, Acta biomaterialia 27(Supplement C) (2015) 88-100.

[156] G.T. Christopherson, H. Song, H.-Q. Mao, The influence of fiber diameter of electrospun substrates on neural stem cell differentiation and proliferation, Biomaterials 30(4) (2009) 556-564.

[157] M. Chen, P.K. Patra, S.B. Warner, S. Bhowmick, Role of fiber diameter in adhesion and proliferation of NIH 3T3 fibroblast on electrospun polycaprolactone scaffolds, Tissue Eng 13(3) (2007) 579-87.

[158] H. Tom, Y. Xue-Feng, B. Ardeshir, Electrospun silk fibroin fiber diameter influences in vitro dermal fibroblast behavior and promotes healing of ex vivo wound models, Journal of Tissue Engineering 5 (2014) 2041731414551661.

[159] B.M. Carlson, The Biology of Long-Term Denervated Skeletal Muscle, European Journal of Translational Myology 24(1) (2014).

[160] T. Tando, A. Hirayama, M. Furukawa, Y. Sato, T. Kobayashi, A. Funayama, A. Kanaji, W. Hao, R. Watanabe, M. Morita, T. Oike, K. Miyamoto, T. Soga, M. Nomura, A. Yoshimura, M. Tomita, M. Matsumoto, M. Nakamura, Y. Toyama, T. Miyamoto, Smad2/3 Proteins Are Required for Immobilization-induced Skeletal Muscle Atrophy, The Journal of biological chemistry 291(23) (2016) 12184-94.

[161] R.L. Lieber, S.R. Ward, Cellular Mechanisms of Tissue Fibrosis. 4. Structural and functional consequences of skeletal muscle fibrosis, American journal of physiology. Cell physiology 305(3) (2013) C241-52.

[162] C. Borselli, H. Storrie, F. Benesch-Lee, D. Shvartsman, C. Cezar, J.W. Lichtman, H.H. Vandenburgh, D.J. Mooney, Functional muscle regeneration with combined delivery of angiogenesis and myogenesis factors, Proceedings of the National Academy of Sciences 107(8) (2010) 3287-3292.

[163] V.Y. Rybalko, C.B. Pham, P.L. Hsieh, D.W. Hammers, M. Merscham-Banda, L.J. Suggs, R.P. Farrar, Controlled delivery of SDF-1alpha and IGF-1: CXCR4(+) cell recruitment and functional skeletal muscle recovery, Biomaterials science 3(11) (2015) 1475-86.

[164] M.T.A. Li, N.J. Willett, B.A. Uhrig, R.E. Guldberg, G.L. Warren, Functional Analysis of Limb Recovery following Autograft Treatment of Volumetric Muscle Loss in the Quadriceps Femoris, Journal of biomechanics 47(9) (2014) 2013-2021.